Integrating paper fluidic liquid handling and whole blood plasma separation into silicon photonic biosensors.

Zakariya Armstrong Khaleel

A thesis

submitted in partial fulfillment of the

requirements for the degree of

Master of Science

University of Washington

2019

Committee:

Daniel M. Ratner, Chair

Joshua R. Buser

Program Authorized to Offer Degree:

Bioengineering

University of Washington

Abstract

Integrating paper fluidic liquid handling and whole blood plasma separation into silicon photonic biosensors.

Zakariya Armstrong Khaleel

Chair of the Supervisory Committee:
Associate Professor Dr. Daniel M. Ratner
Department of Bioengineering

Abstract:

Silicon photonic biosensors have emerged as a powerful platform for various lab-on-a-chip applications. The technology can miniaturize assays, perform label-free detection, and is capable of rapid multiplexing. These qualities make silicon photonic biosensors a competitive platform to replace conventional clinical tests based on less scalable technologies. Most silicon photonic biosensors rely on external pumps to deliver samples and reagents over the photonic sensors. To increase the clinical viability of this technology, this project seeks to dramatically reduce the complexity of the bio-sensing system by integrating sample processing and fluidics via a capillary driven network. We have previously integrated paper microfluidic liquid handling with our custom silicon photonic test bench. With the work presented in this thesis, we demonstrate the integration of paper microfluidic networks into the Ratner lab's OEM silicon photonic platform and we increase the complexity of the network to incorporate whole blood plasma separation. The Ratner

lab has recently developed an ABO blood typing assay via silicon photonics. Using silicon photonics as the platform has the potential to achieve a higher level of automation than conventional ABO typing agglutination methods, while simultaneously reducing the assay time, and lowering costs. We validated our paper fluidic network with a reverse ABO typing assay based on the patient's serology. In our system, we need to separate the whole blood sample in order to run the sample without running the risk of stopping the flow in the network. Here we demonstrate capillary network liquid handling and paper-based whole blood separation into our OEM silicon photonic system (i.e. the Genalyte Maverick). This integrated plasma separation and paper fluidic network reagent delivery make the system more suitable for point-of-care and rapid diagnostic testing applications. We hope this work helps bring silicon photonic biosensing closer to clinical adoption and more appropriate for clinical settings.

TABLE OF CONTENTS

CONTENTS

LIST OF FIGURES

LIST OF TABLES

ACKNOWLEDGMENTS

I did not have a conventional undergraduate experience. Due to a serious illness, I was forced to skip autumn quarter of my junior year in 2016. I made up the skipped quarter during my senior year and did graduate with my 2017 cohort. This illness was a pivotal event in my life and profoundly changed who I was. The change was not immediate nor was it static and positive. In the beginning, I felt as if I had cheated death and that death had cheated me. I grew bitter, nihilistic and I could not and did not want to see a path forward. While these feelings may have been warranted, I couldn't help but recognize how lucky I was to have the family, friends, and mentors that I do. It was not lost on me that there were those who had it much worse than I did in terms of health, socioeconomic status and social support structure. After time had passed and I went back to school and my frustration morphed into an unyielding passion for change in our world that starts with the health of its citizens and extrapolates to every aspect of human life. It was imprinted on me that I was and am nothing without those who support and surround me. I am a summation of previous experiences, influences and mentorships. None of my achievements throughout my life are solely my own and would not have been possible without the friends, family and mentors that surround me. This thesis and all of my academic work would not have been possible without my family; my dad Abid Khaleel, my mom Tracy Khaleel, my sister Hannah Khaleel, my brother Jakob Khaleel my grandparents Abdul (Ampa), Zahira (Manga), Dexter (Ginger-daddy-Ampa) and Dianne (Amma Bamma), my aunts Yaya and Gaylene; my uncles Jeffery and Todd and my cousins Noah, Sophia, Nick and Alianna. My time here in Seattle was enriched by the Mohammad family; my second cousins aunts and uncles as they supported me with familial comfort and of course, food. I am forever grateful for my friends and mentors both in Washington and across the country. They are, and always will be, one of the greatest points of pride. Particularly, it should come as no surprise that the Chair of my committee Dr. Daniel Ratner helped shape my young adult career path and gave me much of my foundation in science. I am privileged to have gotten where I am in life and will always do my best to improve the conditions around me and leave this world a better place than I found it.

A Special thanks to the following individuals in and related to the Ratner lab:

Ratner Lab:
Pakapreud Khumwan, Jasmin Chen, Shon Schmidt, Gina Hansen, Alexander Wende, Nick Wasserman Elaine Limqueco, Vaishnavi Dhawan, Daniel Ratner

Committee:
Josh R. Buser

BloodWorks Northwest
Dr. Jill Johnsen
Kerry Lannert

Chapter 1. INTRODUCTION

1.1 MOTIVATION AND TECHNOLOGY OVERVIEW

The 21st century has brought with it more data collection and processing than we have seen in all human history. In the context of biotechnology, we are just beginning to scratch the surface of implementing medical and scientific truths derived from access and analysis of these data. A striking example of the power of these tools is demonstrated by Esteva *et. al*. use of deep convolutional neural networks for diagnosing two types of skin cancer with the same competency as 21 board-certified dermatologists.[1] However, these advanced data-enabled techniques require robust sensing modalities that can provide accurate data for subsequent analysis and interpretation. Many of the most common clinical panels run today require large complex clinical laboratory instruments.[2] These systems provide accurate data but most of the instruments are not point-of-care and do not provide continuous sensing or real-time analysis. Point-of-care devices and real-time analytics can provide information faster to clinicians than their lab-based counterparts. Continuous sensing can provide more data for analysis and provide a better representation of the activity and concentration of the analyte. As a result, many in the field are pushing for more lab-on-a-chip realizations to be the future of diagnostics. Two examples of the cutting-edge of this trend are seen in both continuous glucose monitors and continuous biosensing using aptamers.[3, 4] The Ratner lab focuses on leveraging and improving silicon photonics, an optical chip-based biosensing platform. The technology has emerged as a powerful platform for various lab-on-a-chip applications; the chips can miniaturize assays, perform label free detection, and are capable of rapid multiplexing.[5-7] These qualities make silicon photonic biosensors a competitive platform to replace conventional clinical tests based on less scalable technologies.

Most silicon photonic platforms use external microfluidic pumps to sequence reagents across the chip and use a tunable laser and electric or optical readout to keep track of the signal.[8, 9] The bulk of the cost for the system derives from the pumps, the laser, and the electric readout/detectors. Within the field, there has been focus on developing on-chip lasers and detectors/readout for the platform to decrease the cost and complexity.[10-12] The Ratner lab has focused on addressing the cost of the pneumatic pumps by integrating sample processing and fluidics via paper microfluidics into silicon photonic platforms. We have previously integrated paper microfluidic liquid handling with our custom silicon photonic test bench.[13] With the work presented in this thesis, we demonstrate the integration of paper microfluidic networks into the Ratner lab's OEM silicon photonic platform (the Genalyte Maverick) and we increase the complexity of the network to incorporate whole blood plasma separation.

The Ratner lab has focused on optimizing and implementing ABO blood typing assays into silicon photonic biosensor platforms. Leveraging silicon photonics for ABO typing has the potential to achieve a higher level of automation than conventional agglutination methods, while simultaneously reducing the assay time, and lowering costs.[13, 14] We validated our paper network on our custom test bench with a reverse ABO typing assay. To run this assay, we were required to separate the whole blood sample and run the plasma to minimize the risk of clogging flow in the network. In this thesis, we integrate capillary network liquid handling and paper-based whole blood separation into our OEM silicon photonic system. This integrated plasma separation and paper fluidic network reagent delivery show a proof-of-concept illustrating that the OEM system may be more suitable for point-of-care and rapid diagnostic testing applications. We hope this work will bring silicon photonic biosensing closer to clinical adoption.

1.2 CLINICAL SIGNIFICANCE

The current clinical blood typing test is an agglutination assay that relies on human blood's ABO antigen system. Every blood type includes a reverse and forward type. The forward type describes the presence of antigens on the surface of the cell (for example, A, B, AB, O) and the reverse describes the antibodies found in the patient's blood.[15, 16] In addition to agglutination there are polymerized chain reaction methods for sequence-specific typing.[17] However, most of the blood typing for clinical labs occurs via the agglutination assay and even in more advanced microfluidic chips the observation is still an agglutination event.[17, 18] The Ratner lab for the past ~5 years has focused on optimizing and developing silicon photonic ABO reverse and forward typing assays. This work has resulted in the formation of start-up companies one of which is focusing on developing a comprehensive ABO blood typing via silicon photonic platform. We assert that with silicon photonic biosensing as the diagnostic modality for ABO typing, the assay will be more quantitative, faster, and automated while providing higher specificity clinical information.

ABO Blood typing is performed on millions of patients a year and used in many different clinical contexts. These include trauma emergencies, pregnancies, organ transplants, and blood transfusions.[19, 20] Mistyping either donor or recipient for a transfusion can result in an undesirable reaction in the recipient to the donor's blood. The mistyping could be life-threatening, cause back pain, blood in urine and a host of other problems.[15] Additionally, if the patient needs a transfusion right away they will receive units of O-negative blood; the universal donor. Urgent transfusion needs sometimes result in a shortage in O-negative supply. However, this shortage may be mitigated if there were a robust quantitative rapid diagnostic system to type trauma patients on-site. Without the shortage, blood centers would save time and resources that would otherwise be spend in advertising for donations. In the case of a large-scale emergency, the hospital or blood

supplier may not have enough blood for all the patients who need it. But having a point-of-care quantitative test may not be all that is required in order to both minimize the shortage and number of transfusion errors.

Pre and post-analytical errors account for most clinical diagnostic mistakes.[21] These errors may be due to lack of training, mislabeling, or complicated pre-processing techniques that allow for more potential mistakes. Research suggests automated processing can further reduce errors and the need for complex on-the-job training.[22] In the context of transfusion medicine, one long-term study suggests 29% of transfusion errors occur in the blood bank (testing error, wrong unit issued etc.), 56% of errors occurred outside the blood bank and 15% of errors were compounded between the blood bank and non-blood bank entities.[23, 24] The chances of undergoing a fatal hemolytic transfusion are less than 10% and the total chance of a transfusion error is even lower. But when there is an error, this research suggests it happens across the transfusion process. These errors may be alleviated by implementing an ABO typing platform that is more automated and can re-confirm correct type in real time before transfusion events, acting as a failsafe to prevent transfusion errors. One of the challenges to clinical translation of silicon photonic ABO typing is the cost and complexity of fluidics for reagent delivery. The work presented in this thesis focuses on adapting our OEM silicon photonic platform for paper microfluidic reagent delivery and processing via whole blood plasma separation. With these additions, we hope to bring the technology closer to the clinic by decreasing the cost and complexity as well as increasing the automation of the system. We hope this work may lead to a system in which the patient's blood could be typed by drawing a sample; placing the sample in the paper network and reading out the type and other relevant antibodies and antigens in minutes. This innovation would replace the agglutination assay that has been in use for over 100 years.

Chapter 2. BACKGROUND

2.1 SILICON PHOTONICS

Silicon photonic devices generally consist of micron-sized sensors that function using near-infrared light. These devices have been used in a variety of lab-on-chip applications and show promise as highly multiplexed, chip-scale diagnostic sensors capable of detecting various biological or environmental targets.[5-7, 25-29] The silicon photonic chip contains silicon waveguides through which near infrared light (NIR) enters and propagates. The high refractive index contrast between the silicon dioxide cladding below, the silicon waveguide core, and the water/buffer cladding above the core facilitate the confinement of near-infrared light via total internal reflection (shown in figure 1).[13, 30] The monochromatic light propagates through the waveguide and a portion of light exists as an evanescent field outside of it. For biosensing applications, target analytes perturb this exponentially decaying evanescent electric field upon binding to the waveguide's surface. As a result of this perturbation, the effective refractive index of the waveguide mode is altered, causing a measurable change in light propagation.

The silicon photonic sensing we use in the Ratner lab is based on micro-ring resonators. A general schematic of the architecture of the micro-ring resonator is shown in figure 2 (from ref. [7]) where we can see that a laser will input the NIR sweep and the output from the chip will go to an optical detector. The silicon photonic chip we use for this thesis on the Genalyte OEM test bench is shown in figure 3. The millimeter-scale chip in figure 3(a) consists of groups of sensors (figure 3(b)) that can be multiplexed with various capture reagents. Individual ring resonators (figure 3(c)) are aligned next to the waveguide to allow light to couple into the ring.[31] When NIR laser light is swept through the chip this coupling on each one of these ring resonators creates a resonance condition within the ring. This condition generates an evanescent field outside of the ring (figure

3(d)); this field does not propagate as an electromagnetic wave and its energy is confined to the vicinity of the source (i.e. the micro-ring resonator). This evanescent field is sensitive to changes bulk index of refraction around the sensor and changes in refractive index on the sensor's surface. Therefore, if the media that is traveling over the sensor changes or mass is bound to the sensor, the index of refraction will change which will cause the wavelength at which light is resonating in the ring to change. We see a representation of a micro-ring resonator used for biosensing in figure 4. In figure 4(a) the ring is functionalized with a capture agent and when a sample is introduced the target analyte binds to the ring generating a change in the effective refractive index near the sensor's surface. This change in mass, seen as a change in refractive index shifts the resonance wavelength of the ring (figure 4(b)). Resonance is seen as a lower transmission spectrum value displayed by the photodetector as illustrated by the local minimum peaks in figure 4(b). This index of refraction change translates into a change in resonance wavelength of light in the ring resonator and this change in resonance wavelength is what we detect and plot in a sensogram in figure 4(c). In figure 4 the analyte is binding to the sensor and a new bulk media is introduced over the ring. This causes a resonance shift and after the bulk washes away we see a residual shift indicating we had specific binding (figure 4(c)). Generally, when performing an assay with silicon photonic devices the desired analyte is captured by functionalizing the sensors with various capture agents. After the chip is functionalized, a baseline resonance wavelength is established/zeroed with a running buffer. Then a sample is run over the sensors/chip for capture/detection. After this sample is washed away, we look to observe a specific residual binding or high shift with the sensors that we functionalized with our capture antigen and no specific response from the sensors functionalized with a negative control.

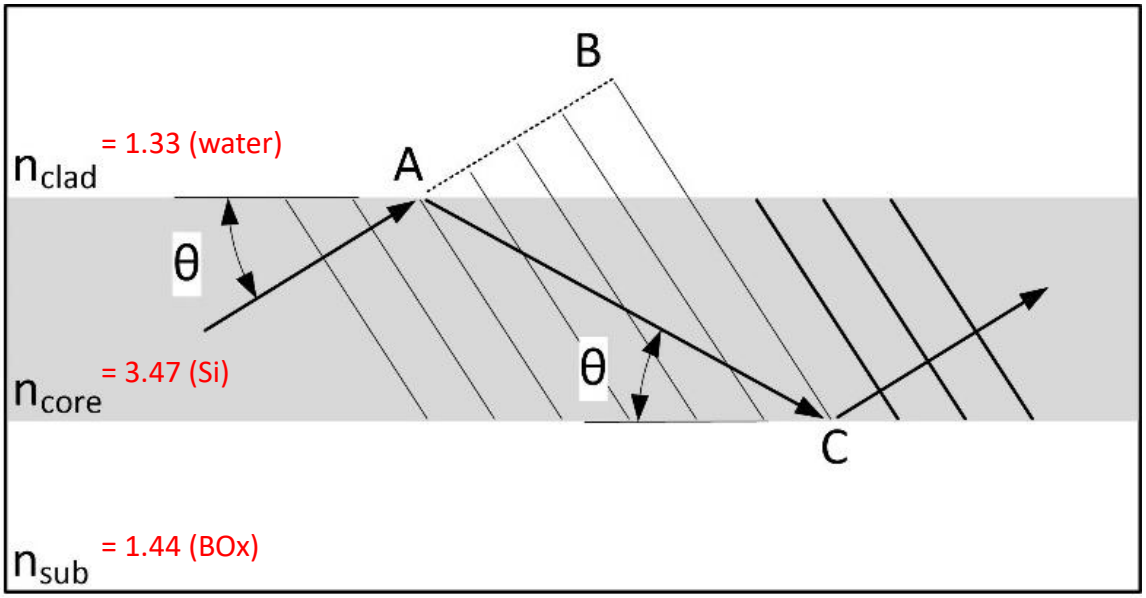

Figure 1: NIR propagating through the waveguide

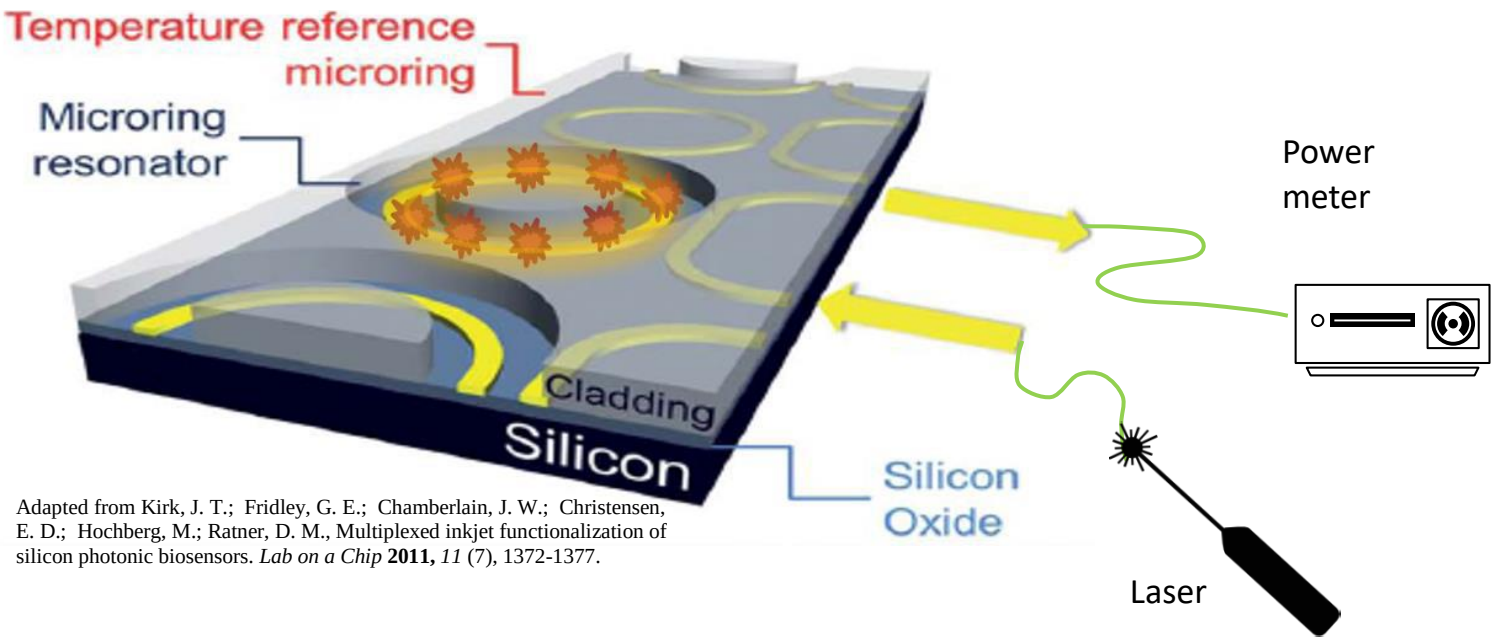

Adapted from Kirk, J. T.; Fridley, G. E.; Chamberlain, J. W.; Christensen, E. D.; Hochberg, M.; Ratner, D. M., Multiplexed inkjet functionalization of silicon photonic biosensors. *Lab on a Chip* **2011,** *11* (7), 1372-1377.

Figure 2: General silicon photonic micro-ring resonator (Adapted from Kirk, J. T.; Fridley, G. E.; Chamberlain, J. W.; Christensen, E. D.; Hochberg, M.; Ratner, D. M., Multiplexed inkjet functionalization of silicon photonic biosensors. *Lab on a Chip* **2011,** *11* (7), 1372-1377))

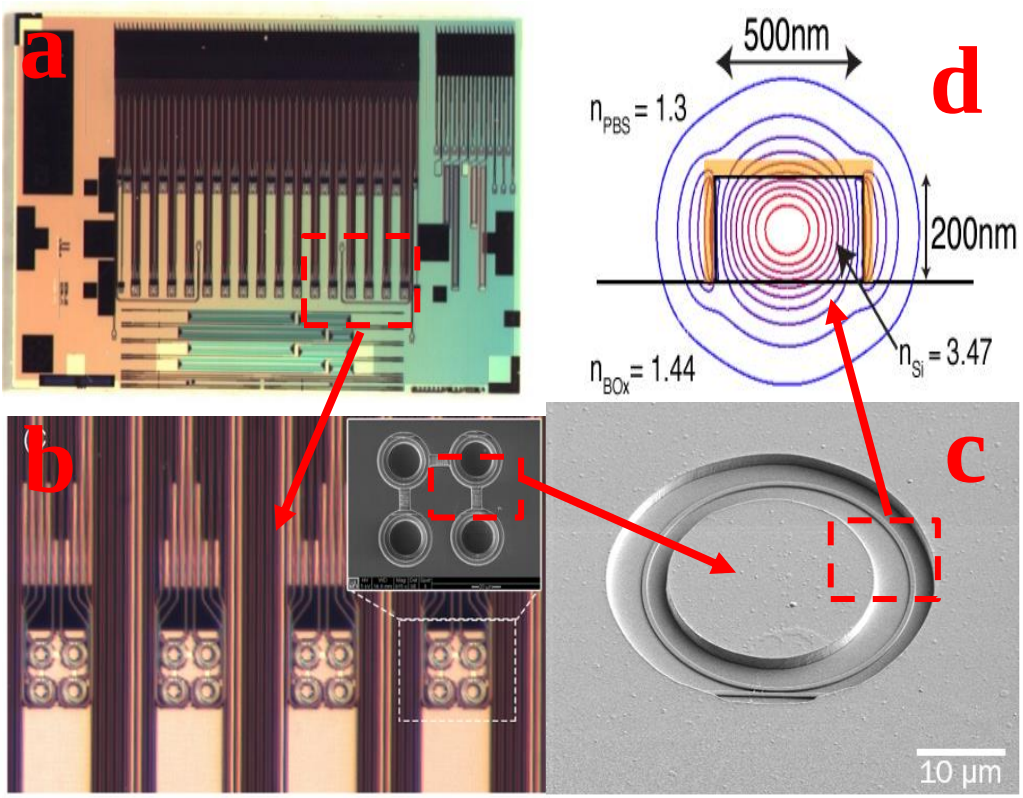

Figure 3: IMEC3 silicon photonic chip used in Genalyte

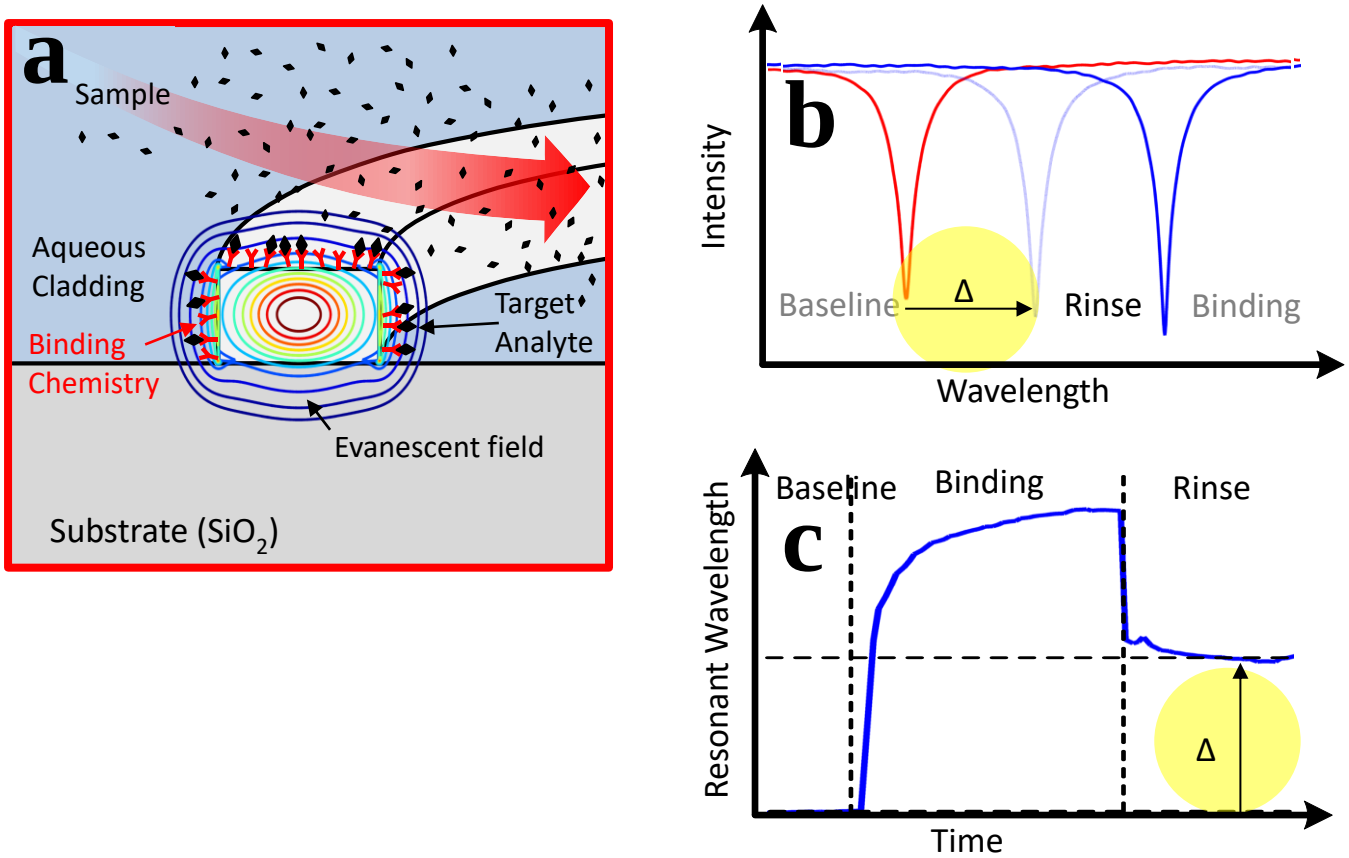

Figure 4: Biosensing with Micro-ring resonators

2.2 CAPILLARY ACTION

This project focuses on integrating capillary action through porous membranes into silicon photonic biosensing. Capillary action allows movement of fluid through a porous membrane (often called "paper") without using external mechanical force such as a pneumatic pump system. The gaps in the porous network allow for surface tension to drive the fluid between the gaps. The ability of the network to continue absorbing fluid is the pressure that drives flow. This is realized by non-fluid-saturated paper or 'dry' paper facilitates a pressure gradient that drives flow.[32-34] Each of the pores uses capillary action to move the fluid along in a process called wicking. A simplified version of this transport is can be modeled by Darcy's Law shown below in Eqn. 2.1 where Q is the volumetric flow rate, κ is the permeability of the paper, w is the width of the membrane, h is the height, μ is the dynamic viscosity, and ΔP is the pressure drop occurring over the length of membrane L.[35] The pressure drop is caused by capillary action and membrane saturation. The volumetric flow rate in paper devices can be controlled by simply varying the fluid path length, L, or the width w.[35, 36] However in our case we create a pseudo-2d network in which the fluid front over the chip is a smaller width than the nitrocellulose wicking pad. This means we can tune the flow rate of the system by varying the width of the nitrocellulose membrane. Additionally, when the nitrocellulose width increases, the area overlap between the nitrocellulose and the absorbent pad will increase which according to Darcy's law, will increase the flow rate.

$$Q = \frac{\kappa w h}{\mu L} \Delta P \tag{2.1}$$

2.3 LATERAL FLOW ASSAYS

In this thesis, we are using components that are used in lateral flow assays which traditionally have an immunochromatographic readout and do not integrate with a quantitative chip-based sensor. A common example of a lateral flow test is a human pregnancy test however today they can detect infectious disease, drugs, glucose levels and a host of other biometrics.[37-40] Most lateral flow immunoassays are modeled after existing formats and use various immune-chromo-graphic chemistries for ease of determining test outcome. The assays tend to follow a consistent format in which the assay begins with a sample pad where the sample is placed followed by a nitrocellulose channel with functionalized test lines within the paper and then the nitrocellulose is attached to an absorbent pad (seen in figure 5).[41] We are not using these paper fluidic components in traditional ways as we are using them to deliver reagents and samples to a sensor as opposed to integrating the sensing modality within the nitrocellulose membrane. There are a few examples of paper fluidic networks integrated with non-traditional sensing modalities as opposed to immunochromatographic. These include the Triage cardiac panel chip; a fluorescence immunoassay that incorporates plasma separation, an electrochemiluminescence μpad based point-of-care assays, and lateral flow assays integrated with electrode readout (e.g. glucose test strips).[42-44] We could not identify a literature example of integration of porous membrane reagent delivery with a silicon photonic chip besides dissertations published by the Ratner lab. The paper fluidic configuration presented in this thesis has the same general structure as a lateral flow test in terms of where the porous membrane components (e.g. a source membrane, a wicking membrane, and an absorbent pad) are placed. However, a silicon photonic chip is in place of the control and test line as the mediator for the bioassay.

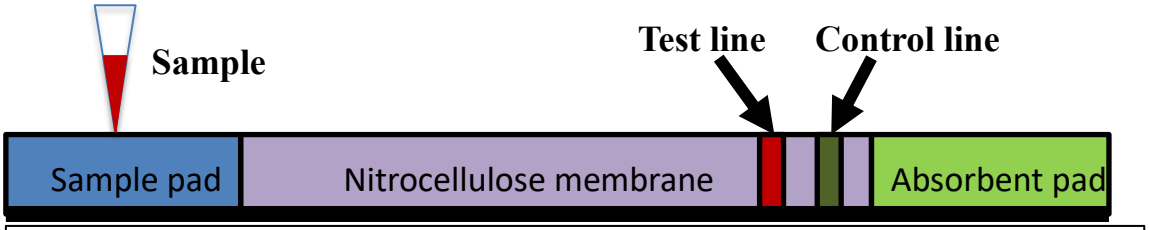

Figure 5: Schematic of traditional lateral flow assay

2.4 PAPER PLASMA SEPARATION

Paper plasma separation membranes leverage both pore size and chemical pre-treatment to separate whole blood from the plasma for serologic assays. The bound glass fiber separators hold the larger sized particles while letting through the plasma.[45] Some separation membranes are pre-treated with either agglutinating agents, reagents to minimize non-specific binding or both. In the commercial realm of plasma separation membranes, there are lateral, vertical and 'hybrid' separators. The lateral separators only work when you allow the blood to wick laterally through the membrane. The vertical separators only operate properly when the whole blood is placed on top of the membrane and separates via gravity, hydrostatic pressure, and capillary action. There are some membranes that claim to be both lateral and vertical plasma separators, but in practice, those are not always reliable and most of the time are not used as the primary separation membrane. Whole blood paper-based plasma separation has been used in various proof-of-concept assays and is currently used in the previously mentioned Triage cardiac panel device.[43] Researchers have demonstrated the power of various separation membranes to linearly separation whole blood.[46] GE blood separation membranes have been used in the wax dipping method (µPADs) for various paper-based lateral flow assays.[41, 47, 48] One of these studies was able to achieve separation of plasma from a single drop of blood within 2 minutes without dilution. While these systems demonstrate efficient plasma separation and point-of-care assays, they do not provide a model for

how to configure the plasma separation membranes within our system. However, they did provide evidence that vertical separation may provide the most flexibility in terms of network design for our paper network silicon photonic integration.

2.5 BLOOD TYPING

The blood typing assay that is used clinically is an agglutination assay that relies on human blood's ABO antigen system shown in figure 6. ABO typing is characterized by individuals with type A blood having anti-B antibodies and A antigens; individuals with type B blood having anti-A antibodies and B antigens; individuals with type O (universal donor) having both anti-A antibodies and anti-B antibodies and neither A or B antigens and finally type AB individuals (universal acceptor) not have antibodies for A or B but having both A and B surface antigens. The blood group antigens can be simplified as carbohydrates and specifically trisaccharides. Both the A and B antigens share a common two sugar groups that makeup what is called an H antigen. A third sugar on this H antigen differentiates A and B. The H antigen is present on O type blood cells. Antibodies against the opposite blood group antigen are present in each of the plasma of each type of blood. [15, 16] Every blood type includes a forward and reverse type. The forward type describes the presence of antigens on the surface of the cell, for example, A, B, AB, O, and the reverse describes the antibodies found in the patient's blood anti-A, anti-B. For a forward typing test, a patient's sample is mixed with antibodies against type A and type B to observe or not observe an agglutination event (A blood will agglutinate with antibodies against type A etc.). A reverse typing test is when a patient's serum is mixed with type A and type B to once again observe an agglutination event (type A patient serum will agglutinate with type B blood etc.). In the context of silicon photonic biosensing blood typing is performed by functionalizing micro-ring resonators with either blood group antigens or blood group antibodies. A sensor functionalized with blood

group antigen is performing a forward typing test and a sensor functionalized with blood group antibody is performing a reverse typing test. Forward typing with silicon photonics seeks to specifically bind the cells to the surface of the chip and reverse typing with silicon photonics seeks to capture the ABO antibodies present within the sample. This concept is illustrated in figure 7. The project presented in this thesis seeks to detect the antibodies within the plasma and therefore perform reverse blood typing.

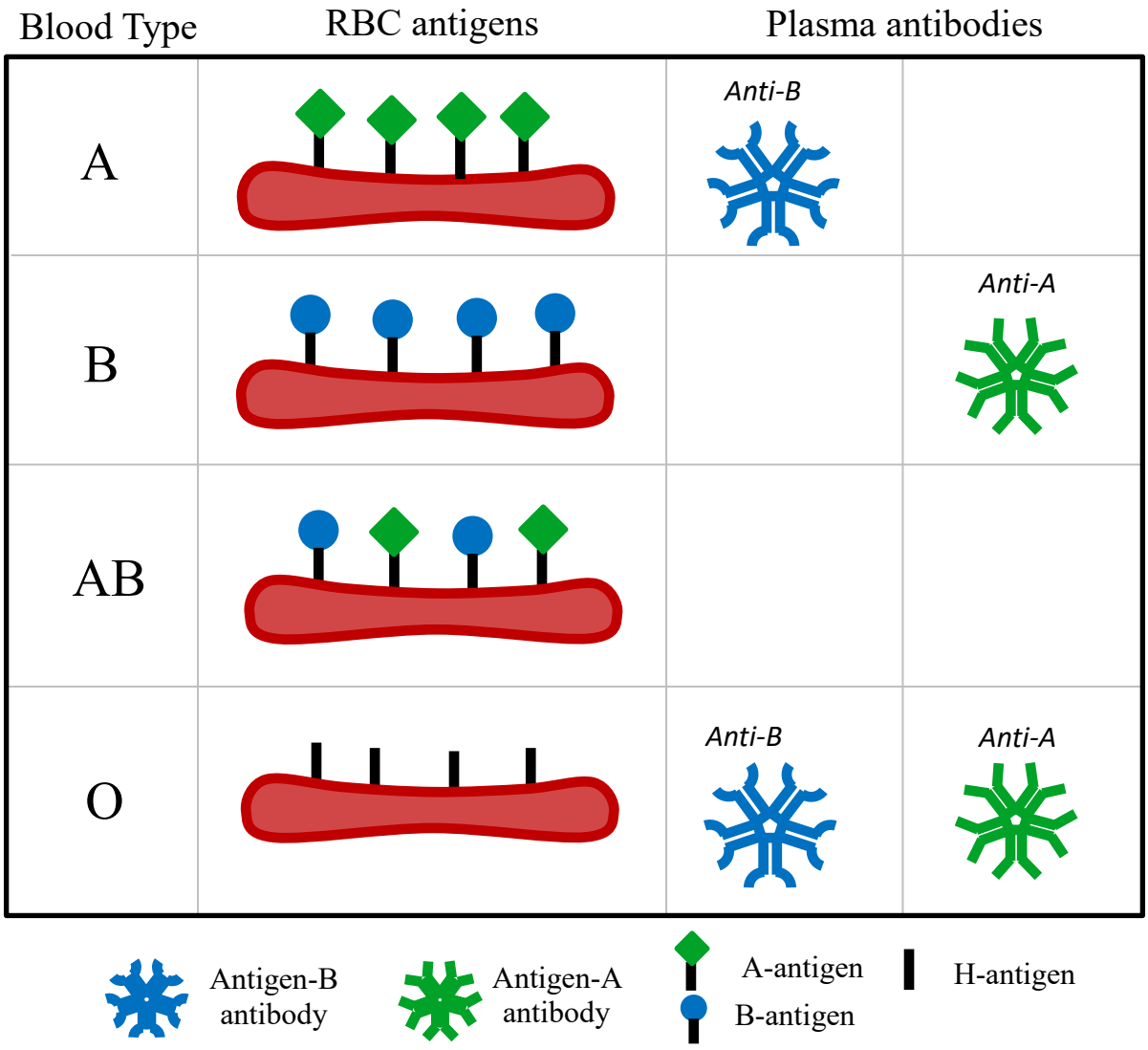

Figure 6: ABO blood typing chart

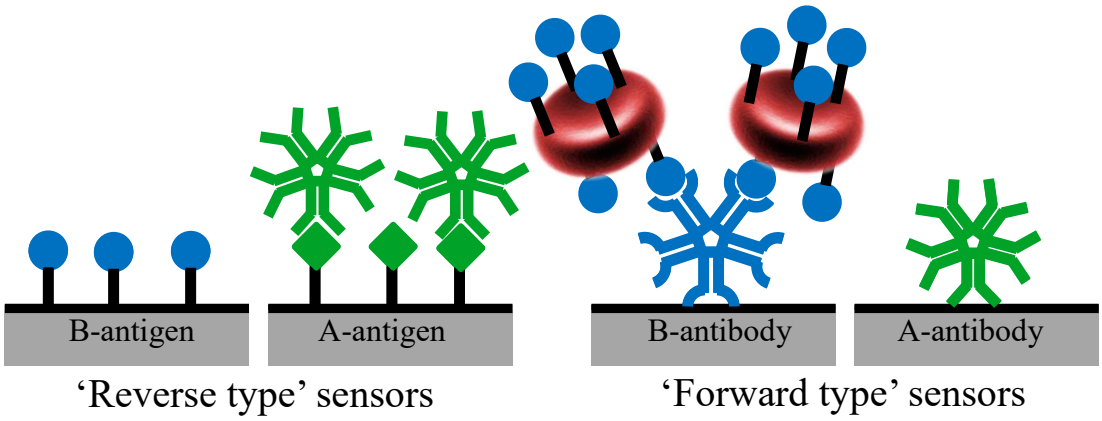

Figure 7: Illustration of blood typing with silicon photonics

2.6 PREVIOUS WORK

Silicon photonic biosensing is leveraged by the Ratner lab and research groups for various diagnostic applications. The platform can be multiplexed and perform semi-automated label-free detection making it a viable competitor in clinical and research diagnostics.[25, 49, 50] Silicon photonic devices have been applied to detect relevant proteins, nucleic acids, viruses, and bacteria.[7, 27, 51-53] The Ratner lab, to the best of our knowledge, is the only lab that is employing silicon photonics for the purposes of blood typing. The patent in reference [50] was granted in 2017 and has not yet been licensed out to other research groups. Therefore, previous work with blood typing on silicon photonics is strictly confined to the dissertations, publications and manuscripts of the Ratner lab group. As stated in previous sections the Ratner lab has integrated paper fluidic liquid handling into our custom silicon photonic platform.[13] The custom silicon photonic test bench is shown in figure 8. In figure 8(a) we see the optical setup mount and well plates used to sequence reagents across sensors using a four-port (two inlets two outlets) PDMS flow cell. In figure 8(b) we have a rear view of the flow cell and in figure 8(c) we have the laser cut silicone gasket that defines the fluid channels that run over the sensors. As with the pump-based delivery, we used silicon gaskets to the establish fluidic channels in which the paper fluidic components were confined. The paper network mounted on the custom test bench is shown in figure 9. Figure 9(a) shows a schematic representation of the porous membrane network. This configuration

created a channel on top of the chip in which fluid could flow via capillary action from the source well over the sensors on the silicon photonic chip to the absorbent pad. The nitrocellulose (NC) strip regulated flow rate, and cellulose absorbent pad to maintained flow. An image of this design is shown in figure 9(b); We see that a test tube is the source well and a delivery window in the silicone gasket in which samples and extra buffer could be placed onto the glass fiber. This window was the region where the sample and reagents were placed when performing the reverse blood typing assay. Note that with this configuration, and with silicon photonics biosensing in general, fluid is always flowing over the chip when an assay is running: A baseline resonance wavelength must be established to see a shift and so phosphate buffered saline (PBS), or DI water first flows over the chip to achieve this baseline in most assays. This buffer maintains a consistent bulk refractive index, delivers reagents to the sensors on the chip, and washes non-specifically bound analytes. If this buffer is disturbed with an air bubble the bulk refractive index will drastically change and the signal will have irrevocable noise and spike beyond a reasonable resonance shift (>10k pm).

We validated the capillary network with a reverse ABO typing serologic assay. The chip was functionalized with streptavidin and biotinylated synthetic blood group antigens to capture the blood group antigen antibodies in the plasma flowed over the network. An example of a reverse typing assay is shown in figure 10. The assay runs as follows: after the zeroed baseline of PBS buffer flows for the first 7 minutes; 20 μL of plasma was placed into the sample window onto the glass fiber and allowed to wick to the chip then; after the bulk plasma washes from the chip 20 μL of an amplification goat anti-human IgG was placed in the sample window. The secondary amplification antibody amplified the signal on the sensors that had specifically bound A or B IgM human antibodies and did not amplify the sensors with no specifically bound antibodies. This is seen in the contrast between the control and the target curves at the end of the assay. The control and target did not return to a zeroed resonance shift and due to protein fouling on surfaces and it is the inherent reason that the secondary amplification step is required. However, with a more sensitive sensor, this label would not be necessary. These results

mimicked those obtained with traditional flow cell/fluidic pump delivery systems. The plasma run through the system was obtained by centrifuging whole blood. Plasma was used not only because we were performing a reverse serologic assay but because the preliminary work showed that whole blood runs the risk of clogging the nitrocellulose membrane and completely stopping flow in the assay. This type of risk cannot be tolerated in a clinical setting and so it was deemed necessary that we use plasma in the system. My project seeks to use whole blood and perform this blood separation in the paper fluidic setup eliminating the need for centrifuging. The work described in this section was imperative to the development of my final design process and innovations.

The preliminary work was done all on the custom photonic setup in the Ratner lab rather than the OEM system called the Genalyte. Each system uses different lasers and silicon chips as well as flow cell pumps. The custom setup is more open but harder to work with and the Genalyte is more of a closed system and much easier to work with. My subsequent capstone project focused on determining whether paper microfluidics could be integrated into the Genalyte OEM silicon photonic platform. During this time, I tried to implement paper fluidic reagent delivery into the system in unconventional ways to determine whether we needed to recreate the solution we arrived at for the custom test bench. After trial and error, I determined that the best configuration was the one we had already implemented on the custom test bench. This rudimentary design is shown in figure 11. In figure 11(a) we have the Genalyte silicon photonic system, in the lower half of the image we see the pump systems and in figure 11(b) we have the mount that is adapted for paper fluidic delivery. The goal of this thesis was to take the work done in my capstone and fabricate reusable and seamless gaskets to run reproducible assays with paper fluidic liquid handling on the Genalyte and integrate plasma separation.

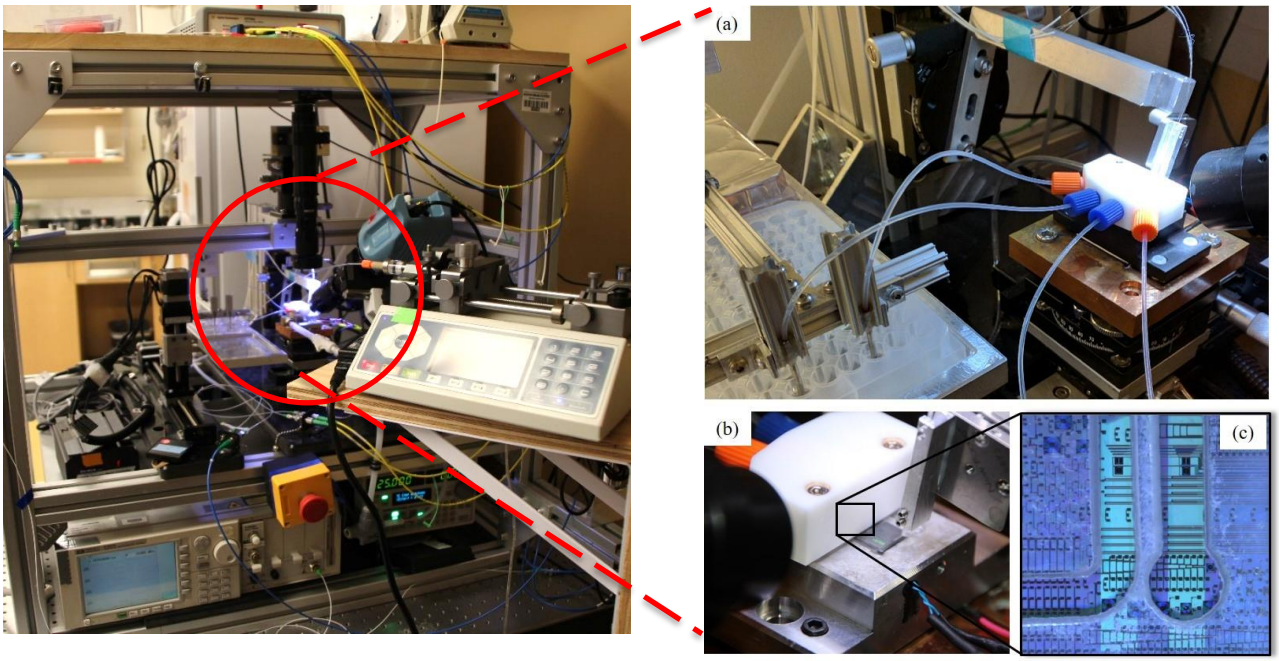

Figure 8: Custom silicon photonic test bench

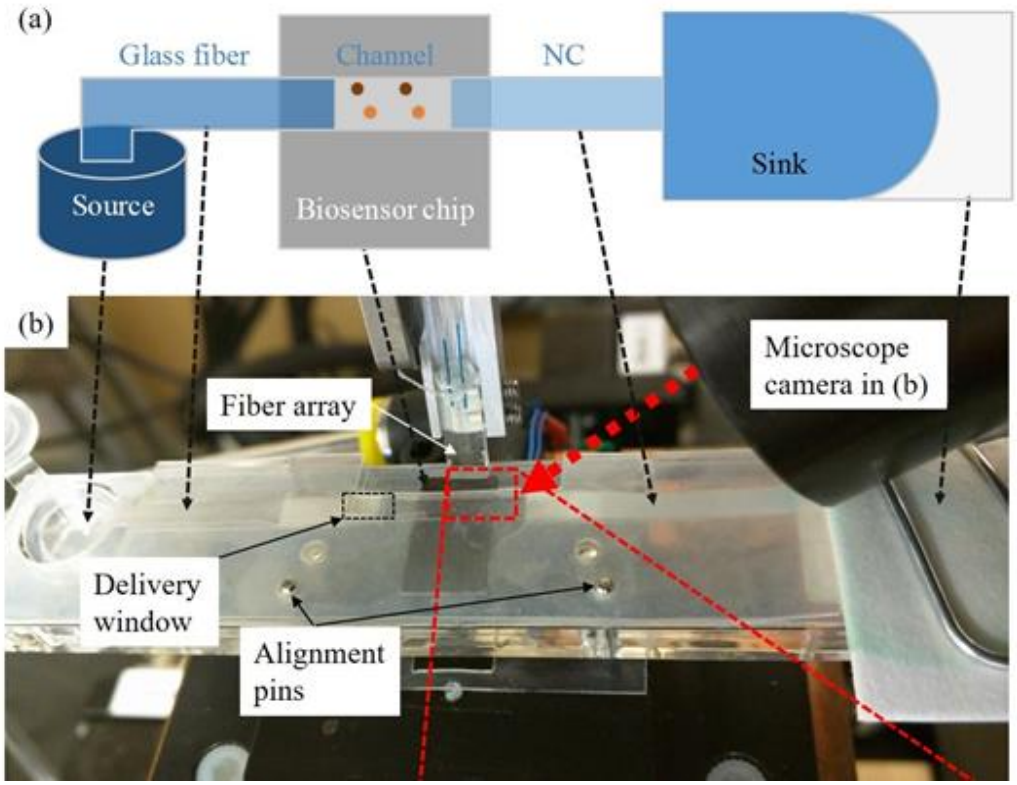

Figure 9: Paper fluidic network mounted on test bench

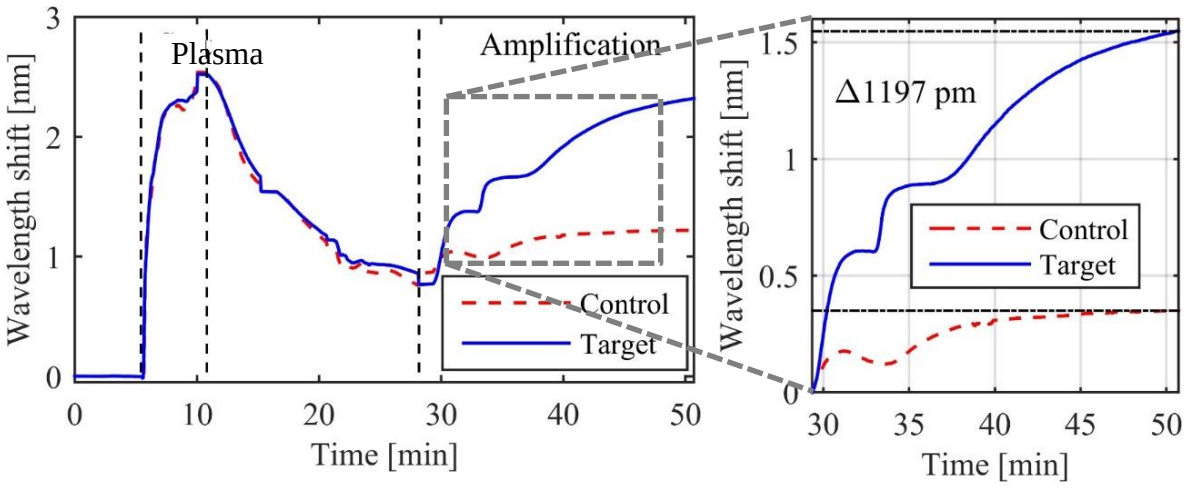

Figure 10: Reverse typing assay using paper fluidic delivery

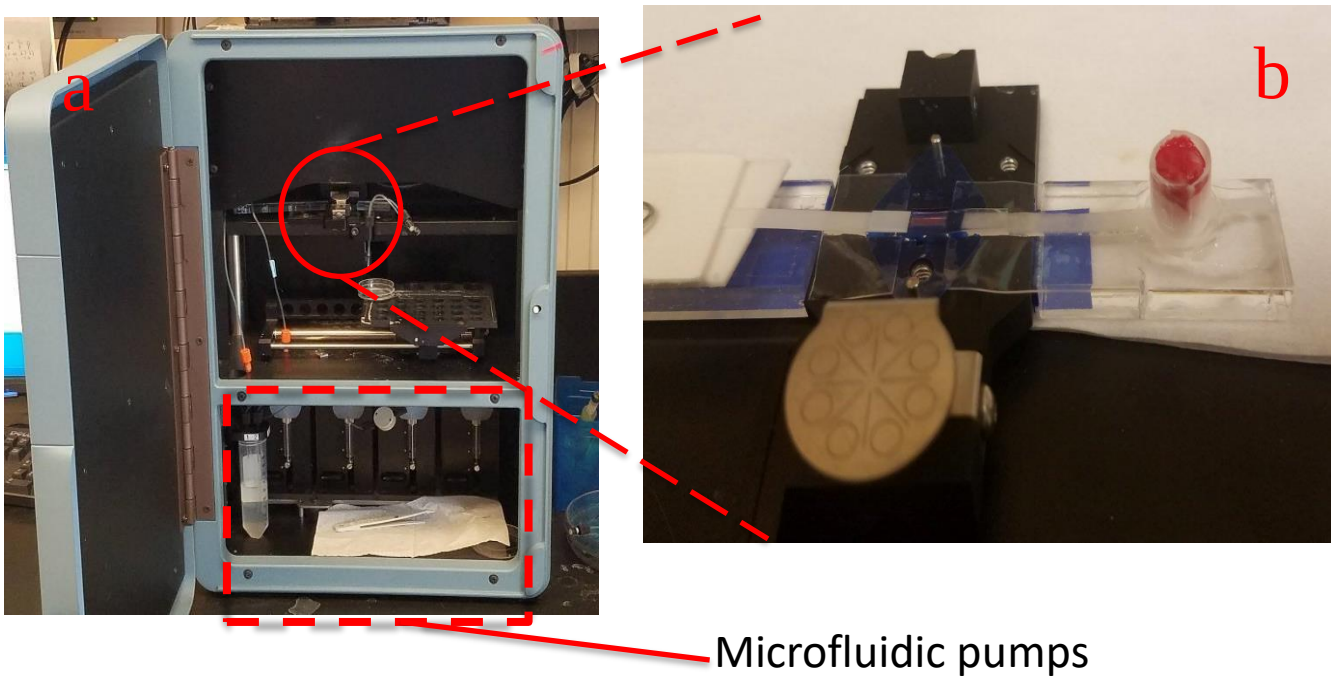

Figure 11: Genalyte system with paper fluidic liquid handling

Chapter 3. MATERIALS AND METHODS

3.1 PAPER NETWORK MATERIALS

The paper fluidic network in our designs comprised of a glass fiber membrane, a nitrocellulose membrane, and an absorbent pad. We fabricated/cut all paper network materials with a VLS4.60 Universal Laser Systems (Scottsdale, AZ) laser cutter. The materials are listed below in table 1 and include the relevant specifications for the purposes of this project. Note that nitrocellulose membranes do not list a water absorption, but we can assume it is relatively high as both the HF240 and HF135 functioned within our designed and were able to handle the amount of fluid running through the system.

Table 1: Paper network materials

Product	Function	Capillary rate (s/4cm)	Thickness (mm)	Water absorption (mg/cm^2)
GE standard 17	Glass fiber/sample pad	34.5	0.37	44.9
Ahlstrom 8964	Glass fiber/sample pad	20	0.43	79
GE CF5	Absorbent pad (cotton)	63.3	0.954	99.2
Millipore Hi-flow plus 135	Polyester Backed Nitrocellulose wicking pad	135	0.150	N/A
Millipore Hi-flow plus 240	Polyester Backed Nitrocellulose wicking pad	240	0.150	N/A

3.2 PAPER NETWORK PERFORMANCE

In order to test both the gaskets and paper fluidic network, we employed both offline and online tests. The offline tests were recorded in MP4 videos using a Samsung Galaxy s7 phone camera mounted on a round bottom flask ring and pointed down towards the paper fluidic adapted mount. The online tests were performed using the Genalyte. In any silicon photonic biosensing assay, buffer is always flowing through the system. Hence, after configuring the gaskets and paper fluidic components in their desired location, we established flow in the system with either DI water or PBS buffer and this flow continued for the entire validation or assay. Initial source buffer volumes (DI water or PBS) ranged from 500-2000 µL depending on the design configuration. For a large portion of the design process we used offline tests to verify the flow profile of the network and following establishing a final gasket design we shifted to online validation.

3.2.1 *Flow rate*

We tested the flow rate online by adding 10-25 µL of 500mM-2M NaCl solution to the delivery inlet windows/wells and estimated the flow rate by dividing the volume by the residence time over the sensors. This is the same method used to validate the flow rate in the custom silicon photonic test bench.[13]

3.2.2 *Salt steps*

To observe the uniformity of the flow profile, we employed salt saline steps to ensure that the profile is not bifurcated and hitting all the sensors uniformly. These experiments were performed online and consisted of running 20 µL of 125 mM, 250 mM, 500 mM, and finally 1 M NaCl saline solutions through the network. We observed the step changes in the bulk refractive index and were able to determine the uniformity of the flow profile.

3.2.3 *Simulated assays*

In order to make sure that the system would perform properly during the reverse typing assay that included whole blood plasma separation, we simulated the assay with NaCl solutions online and dye solutions offline. For the online validation, we placed 25 µL of 250mM-2M NaCl in first port that contained the plasma separation membrane and where, in the reverse typing ABO, assay whole blood is placed. Following this 25 µL flowing over the chip, we placed 20 µL of 250 mM-2M NaCl saline solution in the second inlet port closest to the chip. This application mimics the volume and placement of the secondary amplification antibody that will be run over the sensors following exposure to a sample. For our initial conception of the ABO reverse typing we wanted to separate 25 µL of blood and so all the simulated assays are run with this volume. The 20 µL of secondary remained constant through all the real and simulated assays. When running the offline tests, we performed the same procedure listed in this subsection except instead of 1-2 M NaCl solutions we used visual dye solutions (McCormick Assorted Food Color, Hunt Valley, MD) to observe temporal clearance through the system visually.

3.3 PLASMA SEPARATORS

3.3.1 *Separation materials*

We obtained samples of plasma separators from GE-Whatman and used two of the separation membranes sent. The VF2 is a vertical separation membrane and the MF1 is considered a ‘hybrid’ which in practice we found that it can somewhat separate vertically and laterally. Our primary membrane was the VF2. All the separation membranes were cut using a VLS4.60 Universal Laser Systems (Scottsdale, AZ) laser cutter. Table 2 lists the two separation membranes

and their physical specifications. Note that with other plasma separation membranes, an average blood volume separated per area of membrane specification is given but in the case of the two

membranes we used in this project there was no such specification given by the manufacturer.

Table 2: Plasma separation membranes

Product	Function	Capillary rate (s/4cm)	Thickness (mm)	Water absorption (mg/cm^2)
GE VF2	Vertical plasma separator	23.8	0.785	86.2
GE MF1	Hybrid lateral and vertical plasma separator	29.7	0.367	39.4

3.3.2 *Validation of separation*

As stated above, plasma separation membranes separate whole blood proportional to the area of membrane (e.g. area of membrane per µL of blood). Normally these membranes are dry before separating blood. We tried to do this with our system, but this method was somewhat unreliable. For some assays, a robust fluidic connection between the plasma and the glass fiber was not achieved because of an air bubble blocking flow or an air bubble was pushed through to the glass fiber. Therefore, we chose to pre-wet our membranes with buffer and establish a fluidic connection between the separation membranes and the glass fiber. There needs to be enough hydrostatic pressure to push the plasma through the membrane to the glass fiber.

This means we can either:

1) Add enough blood to push plasma all the way through the membrane
2) Add buffer on top of the membrane to push out the plasma to the glass fiber

We chose the latter to minimize the possibility of RBCs clogging the membrane, fouling the chip and this also ensures more robust separation. With unfunctionalized chips we validated separation membranes (both placement and area of separation membrane) by running the chip on the

Genalyte, adding a select amount of blood to the top of the membrane, allowing the blood to settle into the membrane and finally pushing the plasma through by adding PBS buffer to the top of the membrane.

3.4 GASKET FABRICATION

The gaskets used to support the paper fluidic network were fabricated using the VLS4.60 Universal Laser Systems (Scottsdale, AZ) laser cutter. The gaskets were cut from 250-µm thick, translucent silicone sheets (part#: 664475 Grace Biolabs; Bend, OR). In some of the gaskets, two of the same layers are reversibly bonded with heat (on a hot plate at 60 ℃) in order to obtain a suitable thickness for the application so that the porous membranes were not crushed. The rigid acrylic mount/wings in which the gaskets rested on were fabricated from 4.75 mm thick acrylic sheet (McMaster-Carr part#: 8560K211; Santa Fe Springs, CA). To bond these acrylic components to the black mount we used electrical tape on both the top and the bottom of the black mount and the acrylic component. After much trial and error, this was the most robust solution to keep the acrylic components stable.

3.5 CHIP FUNCTIONALIZATION

3.5.1 *Stripping the new chips*

Each of the new chips were prepared and stripped of their photoresist with the following sequence in 5 different beakers: Beaker 1) Add chips and acetone and place on shaker (ensure speed is high enough to swirl fluid) Beaker 2) transfer chips to another beaker add acetone and place on shaker Beaker 3) transfer chips to another beaker with isopropyl alcohol and place on shaker Beaker 4) transfer chips to another beaker with isopropyl alcohol and place on shaker Beaker 5) transfer chips to another beaker with DI water and place on shaker. Finally wash with

DI water and dry with stream of air. To maximize stripping of photoresist cladding we let the chips incubate in PBS overnight in the 4 ℃ fridge.

3.5.2 *Reagents for reverse ABO typing assay*

Bovine serum albumin (BSA) and streptavidin were from Sigma Aldrich (St. Louis, MO, USA). Murine monoclonal anti-A and anti-B IgM antibodies were from Immucor (Norcross, GA, USA). Biotinylated multivalent polyacrylamides containing blood group A and B antigen trisaccharides (PAA-A and PAA-B) were from GlycoTech (Gaithersburg, MD, USA). Goat anti-human IgG/A/M antibodies were from Thermo Fisher Scientific (Rockford, IL, USA).

3.5.3 *Functionalization for reverse ABO typing assay technique*

To functionalize our chips, we first wash two stripped chips with PBS and dry them with air. We then incubate the chips with 0.1 mg/mL streptavidin in a 1.5 mL Eppendorf tube for 4 hours at room temperature or overnight in the 4 ℃ fridge. Following this we wash the chips with PBS and dry with stream of air. We then put each chip in an individual Petri dish and under a stereo microscope, we add 1 µL of 2 mg/mL of PAA-A on the left side of the chip and 1 µL of 2 mg/mL PAA-B on the right side of the chip. During this process it is important to make sure that the spots do not touch and cover the intended sensors. When hand-spotting I tended to shift both spots to the right as I am right handed and so it is more likely that the spots for PAA-A cover more sensors than PAA-B. An annotated image of the chip is shown in figure 12 and a functionalization map is shown in figure 12(b). After hand-spotting these chips, they are placed in a humidity chamber (a pipette case with a water bath in the bottom) and wrapped with parafilm around the lid and allowed to incubate for 1 hour. After incubation, the chips were washed with PBS and dried with a stream of air. The chips are then blocked with 1 mL of 2 mg/mL BSA solution in PBS for

30 minutes. After the blocking step, the chips are washed with PBS and stored dry in a petri dish wrapped in parafilm in the 4 ℃ fridge. An overview of this functionalization process is shown in figure 13. In 13(a) we see the adsorption of streptavidin, in figure 13(b) we have the binding of the biotinylated reagents and in figure 13(c) we have the BSA blocking step.

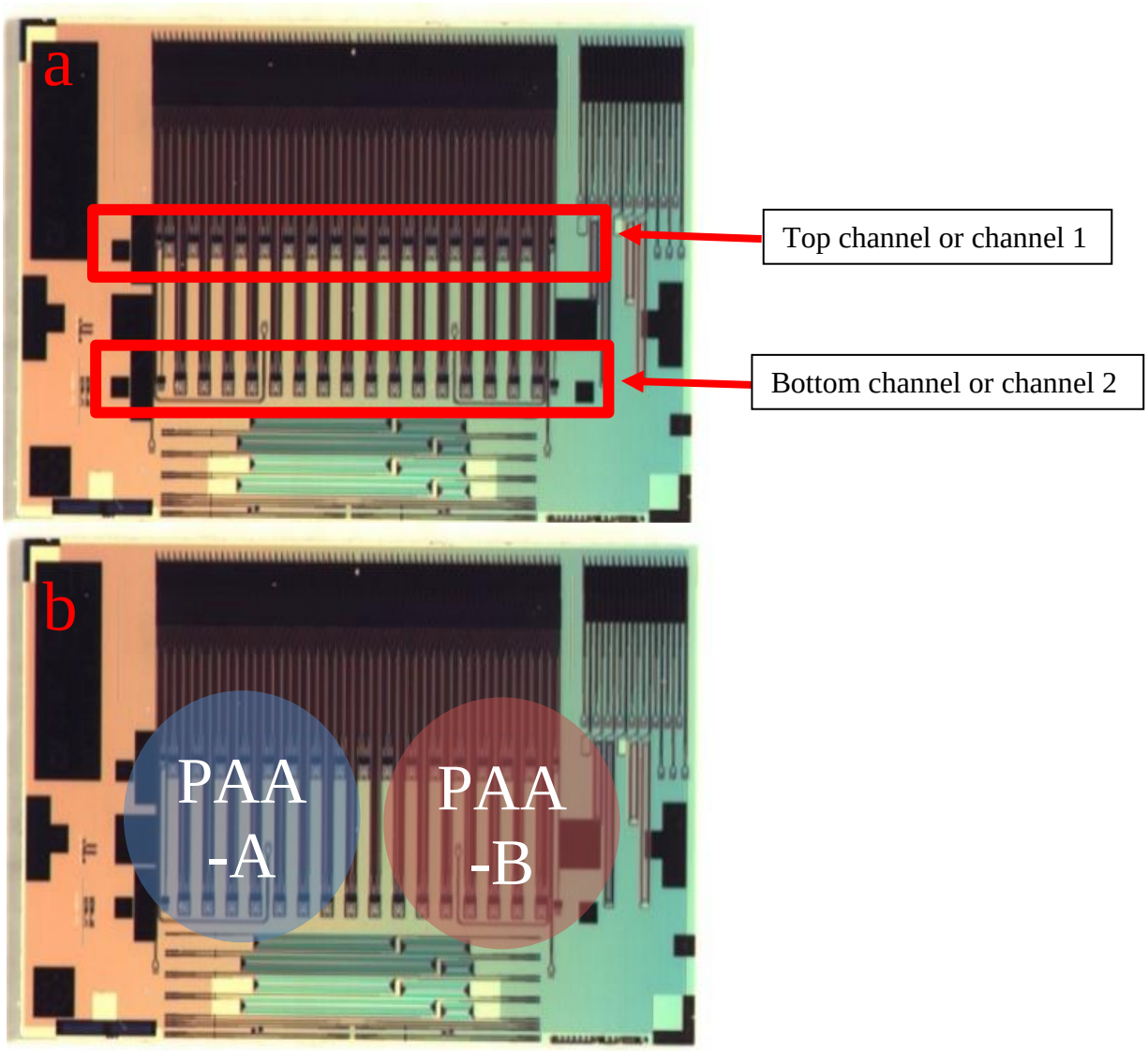

Figure 12: Annotated image of chip and functionalization map

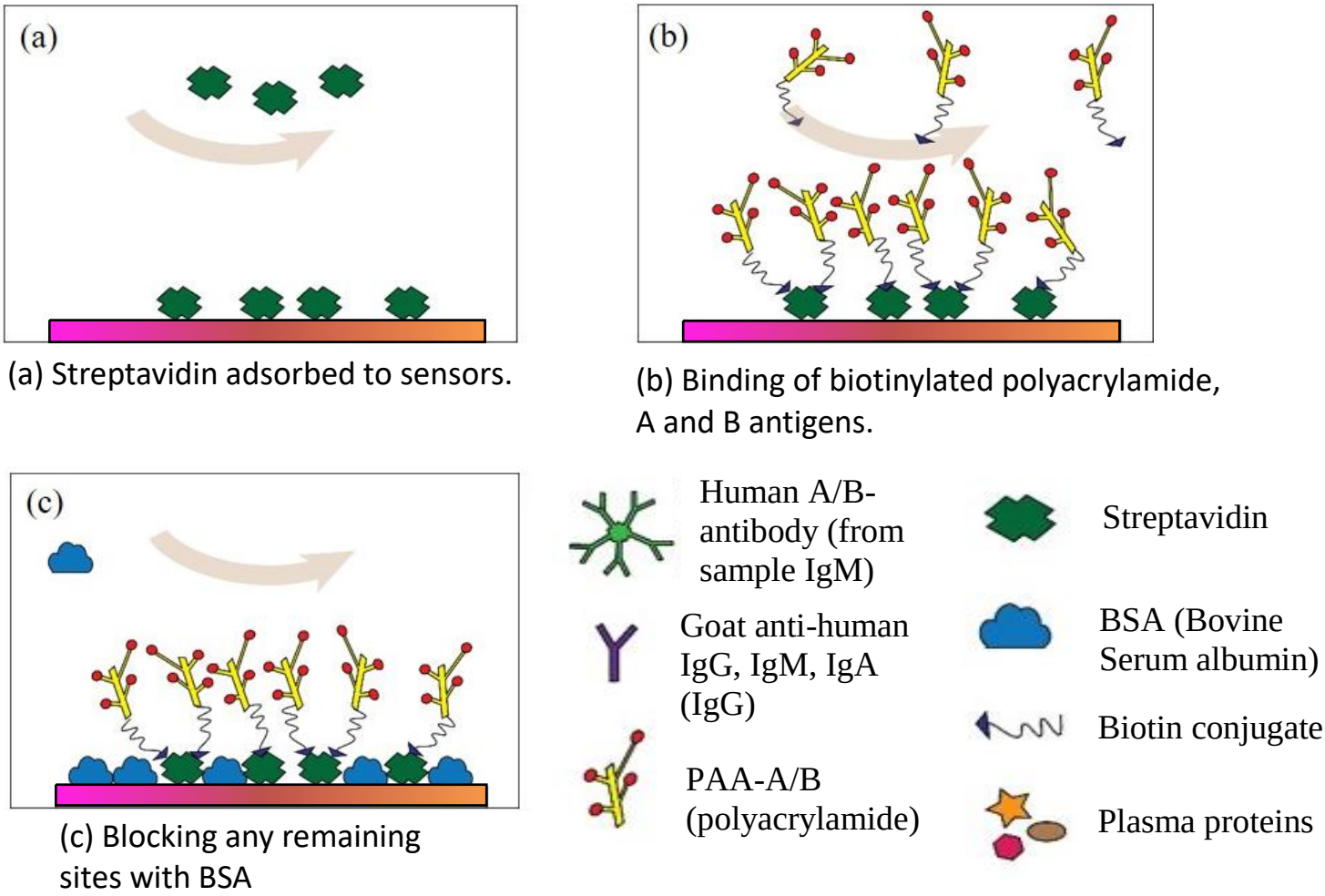

Figure 13: Overview of the functionalization process

3.6 REVERSE TYPING ASSAY

The reverse ABO serologic assay was run with both whole blood (via plasma separation) and with plasma. While the procedure to run the assay for plasma versus whole blood is different the chemistry of the assay remains the same and is illustrated in figure 14. In figure 14(a) the sample is introduced to the chip and in figure 14(b) the secondary amplification antibody binds to the specifically bound human anti B or A antibodies. For all ABO serologic assays, we blocked the glass fiber membrane with 1 mg/mL BSA, then DryCoat Assay Stabilizer (Virusys Corporation;

Taneytown, MD) and we dried it under ambient conditions. We validated the functionalization by flowing over Murine monoclonal anti-A when running the assay with type B blood, and murine monoclonal anti-B when running the assay with type A blood. We only ran one of the validation reagents because if we ran both the murine validation antibody would agglutinate the respective blood type (anti-A antibodies would agglutinate A blood etc.). We also used these validation reagents to ensure the chips were properly functionalized with PAA-A and PAA-B. Note that in our validation the PAA-B did not respond as strongly as PAA-A and we have had trouble in past work obtaining reliable positive results with PAA-B[54] Therefore, for the typing assays run in this thesis we only used B type blood.

3.6.1 *Assay with plasma*

For the assay ran with plasma we allowed baseline PBS to flow in the system and then after 1 minute of buffer flow we placed 20 µL of plasma from a centrifuged whole blood sample in the second inlet port. After the plasma equilibrates over the chip and the new baseline is achieved, we added 20 µL of 1 mg/mL secondary Goat IgG/A/M antibody into the second inlet and observe the specific response just as illustrated in figure 10. However, in our case after the addition of the secondary we added 20 µL of murine validation reagent to the second port and to determine the functional activity of the chip.

3.6.2 *Assay with whole blood*

For the assay with whole blood we would allow PBS to equilibrate and then from minutes 5 to 12 of the assay we would add blood in volumetric increments until we added the desired total volume. We would allow each of these additions to sink into the membrane but not break the surface tension and flow over the membranes instead of through them. Finally, we add PBS to the

top of the separation membrane in the same volumetric increments that we added the blood in order to push the plasma out of the membrane and to the surface of the chip. Following this plasma push we added 20 µL of 1 mg/mL of Goat anti human IgG/A/M secondary antibody to the second inlet. After the secondary response equilibrated, we added 20 µL of validation reagent to the second inlet in order to validate the surface functionalization.

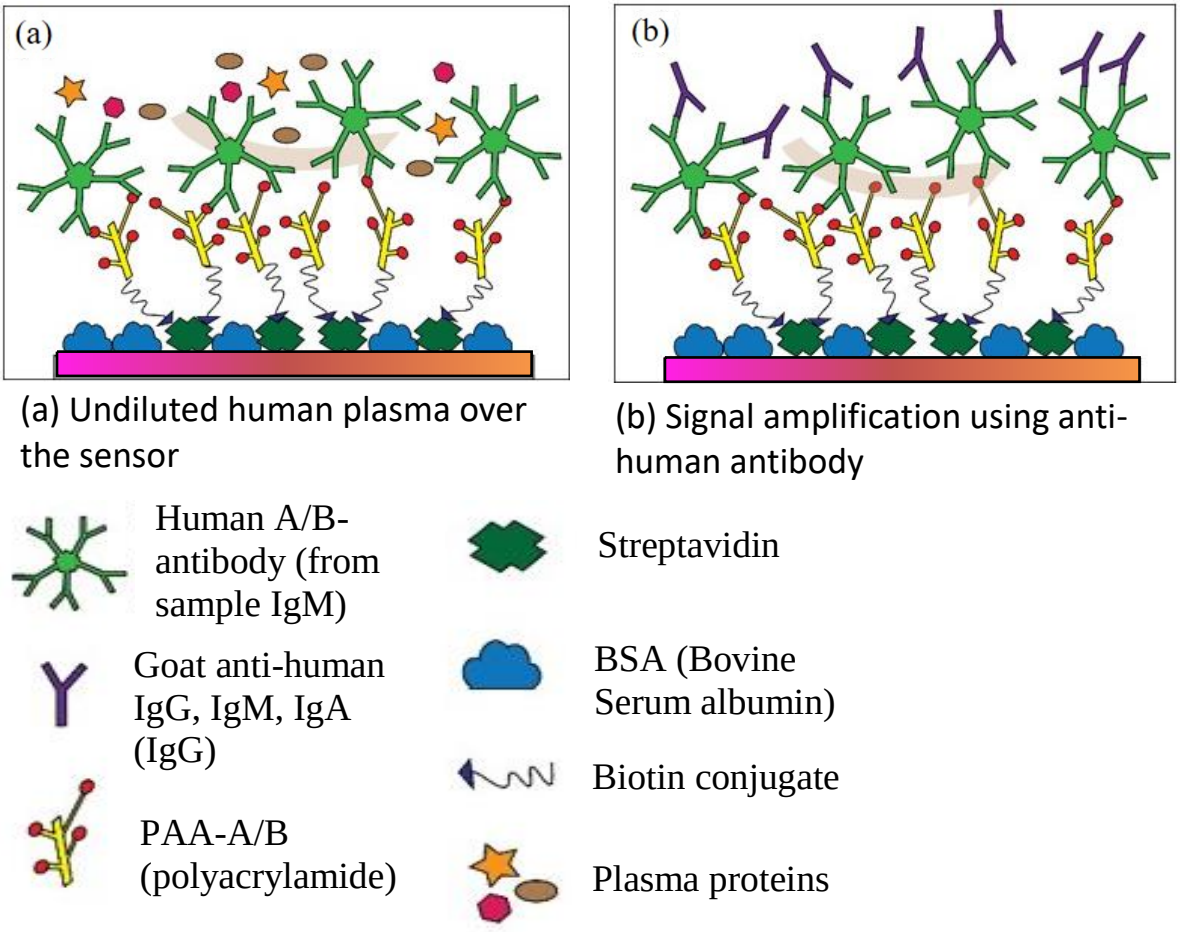

Figure 14: Reverse ABO serologic assay

Chapter 4. DESIGN

4.1 OVERVIEW OF DESIGN: PROCESS AND CONSIDERATIONS

Our gasket design and acrylic components were adapted for the Genalyte mount seen in figure 15. The silicon chip sits in the cavity within the mount (shown in figure 16(a)). When using microfluidic pumps, the blue gasket is placed over the chip to establish the two lateral channels as shown in figure 16(b) and 16(c). The white flow cell is screwed onto the mount and the inlet and outlet channels are on either side of the flow cell (shown in figure 17). In order to adapt the mount for the gaskets we added acrylic 'wings' on the mount on either side (shown in figure 18). To attach these wings, we tried various methods including tape and polyurethane adhesives (clear Gorilla glue and Gorilla clear grip, Sharonville, OH). We found the most efficient solution was to use electric tape on the top and bottom sides of the touching edges of the acrylic and the mount to keep them together and from bending with weight. We based our gasket designs on previous work shown in figure 9 (b) on the custom test bench. Generally, gaskets were designed to level the chip with the mount, establish the channel for the paper fluidic components, and create a place for the separation membranes. In our system the most important design attentions for the mount and gaskets were:

1) The gaskets and needed to minimize leaking around the chip and reversibly bond well together
2) Maintain a uniform flow profile
3) The mount needed to fit efficiently inside the Genalyte

When fabricating and designing these gaskets we needed to measure the dimensions of the mount by hand. We took the measurements with calipers multiple times with different individuals in order to obtain the best estimate. As shown in figure 12 (a) the top and bottom channels on the chip

contain all the sensors. When using the microfluidic pumps, the two channels are facilitated by the blue gasket and can have two different reagents, samples or buffers running over each respective channel. But when using paper fluidic reagent delivery there is only one channel that encompasses all sensors. The minimum width of this single channel needed to be narrow enough to not disturb the optical inputs and outputs at the top of the chip but wide enough to run over all the sensors. We used a stereomicroscope and calipers to determine the minimum width of this channel. The gaskets needed to be fabricated multiple times as some of the measurements were inaccurate. The overall design of the system had largely two variations; they will both be discussed in the next section as well as further nuances of the system.

Figure 15: Genalyte mount

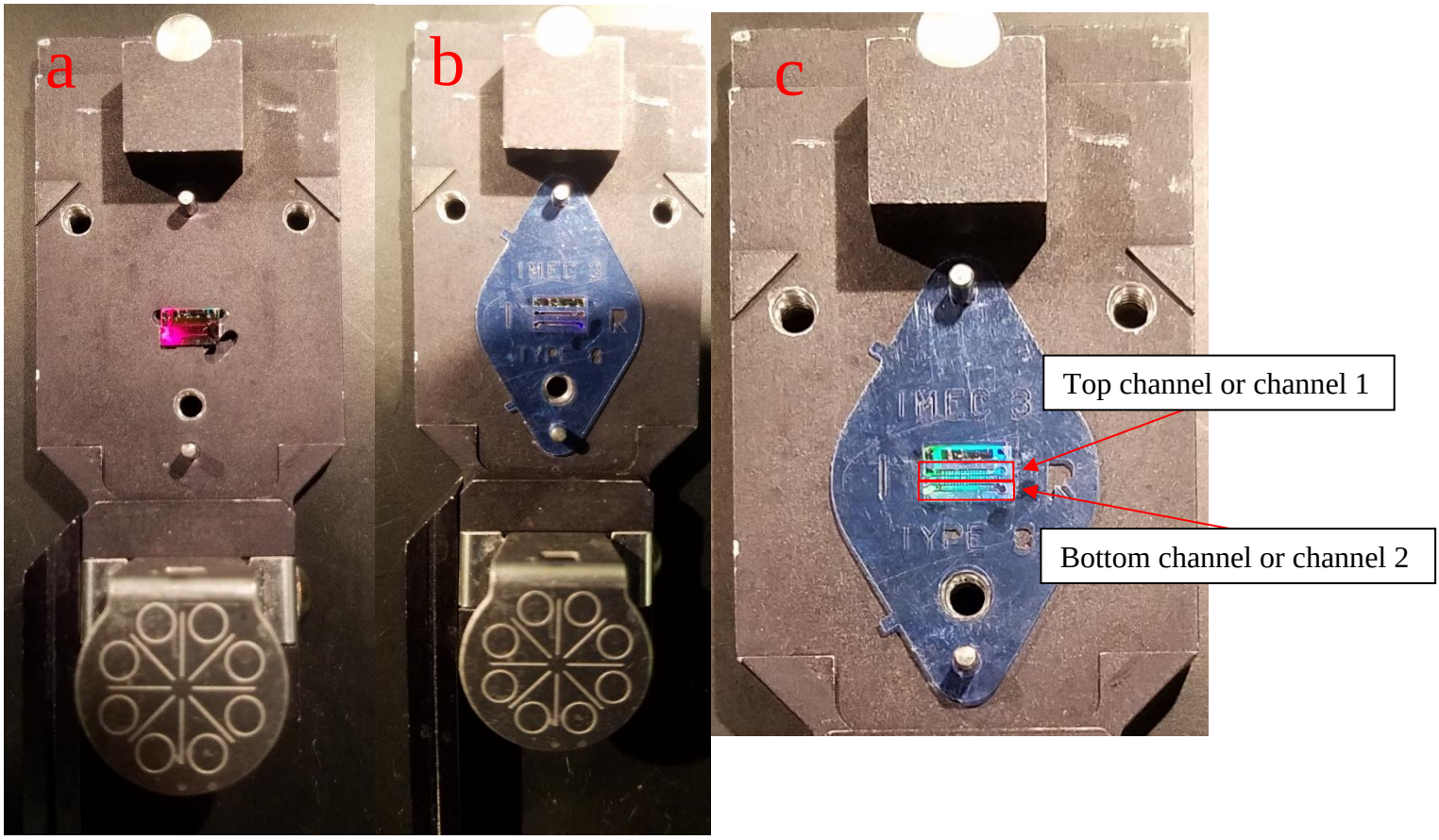

Figure 16: Mount for Genalyte and microfluidic pump gasket

Figure 17: Mount in Genalyte for microfluidic pump delivery

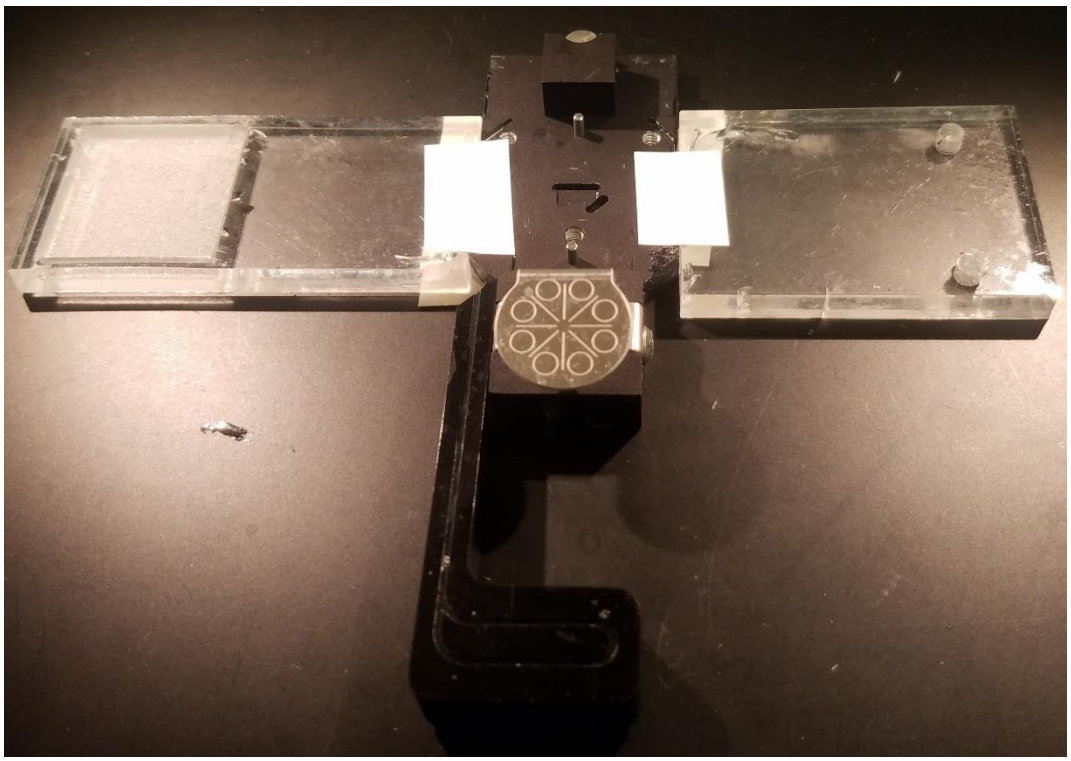

Figure 18: Mount adapted with acrylic for paper fluidic delivery

4.2 DESIGNS

4.2.1 *Positive pressure*

Our first design focused on a system with a source of buffer that provided hydrostatic pressure to the glass fiber via gravity. We identified this system with the name ‘positive pressure’ because the source well was on top of the glass fiber rather than the glass fiber wicking the buffer from a well. As shown in figure 9 the gap over the chip does not contain porous membrane and therefore there will be little capillary pressure wicking the buffer from the glass fiber across the chip to the nitrocellulose. In our previous system, we needed to prime the channel to get buffer to flow over the chip. Therefore, we began our design with this concept to try to create high enough hydrostatic pressure to run buffer across the chip without priming. A schematic of this design is

shown in figure 19. We see from left to right the source well adds the buffer to the top of the glass fiber, and the fiber through capillary action and hydrostatic pressure pushes the buffer over the chip to the nitrocellulose and eventually to the absorbent pad. An image of this system is shown in figure 20. The source well is a 1.5 mL cut Eppendorf tube with 10.43 mm diameter and 16.5 mm height. Inlet well #1 and #2 are 0.5 mL cut Eppendorf tubes with 7.62 mm diameter and 10.5 mm height. In figure 20 the wells adhere to the top gasket with clear Gorilla glue (we found this solution to be best for bonding the wells to the top gasket). Also, note that on the right side of the mount there is an acrylic piece that is screwed into the acrylic wing to maintain pressure on top of the absorbent pad (shown in figure 21). The gasket layers are shown in figure 22; gasket #1 levels the chip with the base, gasket layer #2 defines the channel over the chip, gasket layer #3 defines the space for the plasma separation membrane and layer #4 had the wells adhered on top and defines a small space for the reagents to flow through. Gaskets 2-4 all have the large openings above the chip to allow the chip to optically register with the Genalyte and begin sensing. In gasket layer #3 notice we have two square spaces for plasma separation membrane. During testing, we only used one of these, but we wanted the flexibility to have both depending on the assay we were running.

To test this design, we ran simulated assays offline and recorded videos. As introduced at the beginning of this section we chose to start with the positive pressure design because we did not want to have to prime the system. While we did not have to fully prime the system by adding extra buffer at the beginning of an assay, we did still have to physically cajole the fluid front over the chip. We did this with tweezers and two frames of a video of this process are shown in figure 23. While we recognize this system is not fully automated; we argue that we could have increased the source well volume to increase the likelihood of the system priming itself. We did not pursue this

route of design because it would have required gaskets that are irreversibly bonded as the hydrostatic pressure in the channel would be increased and we wanted to validate the design before we optimized it. We invested much time into developing this system but found that it produced inconsistent fluidics and was not practical to fit into the Genalyte. An example of one such inconsistency is shown in figure 24. As stated in section 3.2.3 to validate our designs we ran offline simulated assays in which we would run buffer through the system and add 25 µL of dye to inlet well 1 and then 20 µL of dye to inlet #2. In order to simulate the fluidics of an assay, we placed a 5 mm by 5mm MF1 separations membrane in gasket #3 just under gasket #4 with the wells on top. In the first frame figure 24(a) (time: 2:15 min) we see there is PBS running buffer in the source well and buffer is flowing across the chip. Following this, we add 25 µL of blue dye to inlet well 1 shown in figure 24(b) (time: 4:07 min). After ~5 minutes we see in figure 24(c) (time: 9:45 min) that the dye begins to flow but note that the source well has almost fully drained and there is no longer an excess of running buffer and in figure 24(d) (time: 16:14 min) the running buffer is fully drained and the dye flows through the system. The fluid in the glass fiber has a high flow rate due to the high hydrostatic pressure generated in the source well. This high flow rate produces a high upward pressure (Bernoulli's principle) on the inlets preventing the dye from immediately flowing into the system. This is especially pronounced in our system because the plasma separation membrane adds more resistance to the diffusion through the system. Although this phenomenon was expected our hope for this design was that diffusion of the dye would overcome the pressure and the dye would slowly flow through the system. The sequential inlet well flow demonstrated by this design is not advantageous for our purposes because it forces the user to continually add buffer to the system as early as 9 minutes into an assay. As well, it intermittently caused leaking in between the gaskets because of the high hydrostatic pressure. Another fluidic inconsistency that

made this design untenable was the occasional air bubble that would not allow flow through the system. This problem is illustrated in the video frames in figure 25; in figure 25(a) buffer is flowing through the system, in figure 25(b) we introduce 300 µL of blue dye into inlet well 1 and the same volume of yellow dye in inlet well 2. We see that in figure 25(c) the dyes do not flow through the system even after ~15 minutes. There is an air bubble in the system and the dye did not begin to flow until we disturbed the bubble with a pipette tip as seen in figures 25(d) and 25(e). This problem would not always occur with this design. We hypothesized that the gaskets may not have been bonded tightly enough, or surface tension could be preventing flow. However, we could not identify the source of this problem as even when we tightly reversibly bonded the wells on gasket #4 with double sided tape, we observed this issue. Between the sequential flow and the occasional bubble that would prevent uniform flow we decided optimizing the positive pressure design would have taken more time than allotted by this thesis and therefore we moved onto another design.

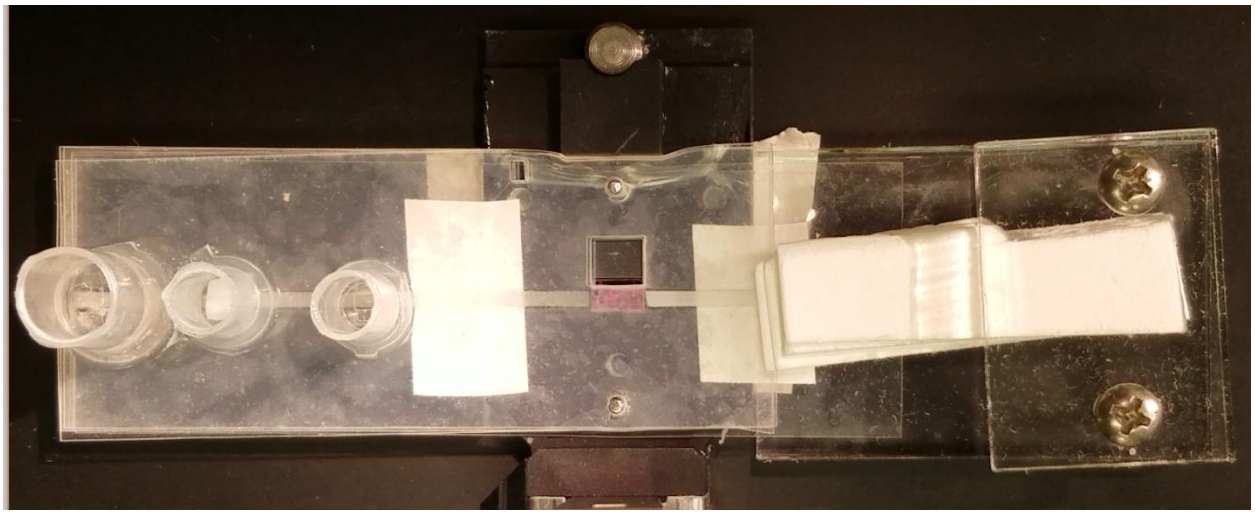

Figure 19: Image of positive pressure design

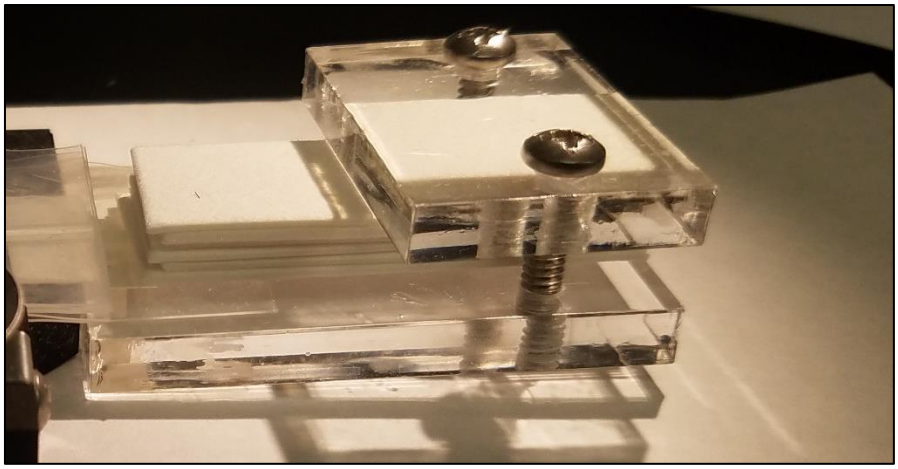

Figure 20: Screwed-in acrylic clamp on absorbent pad

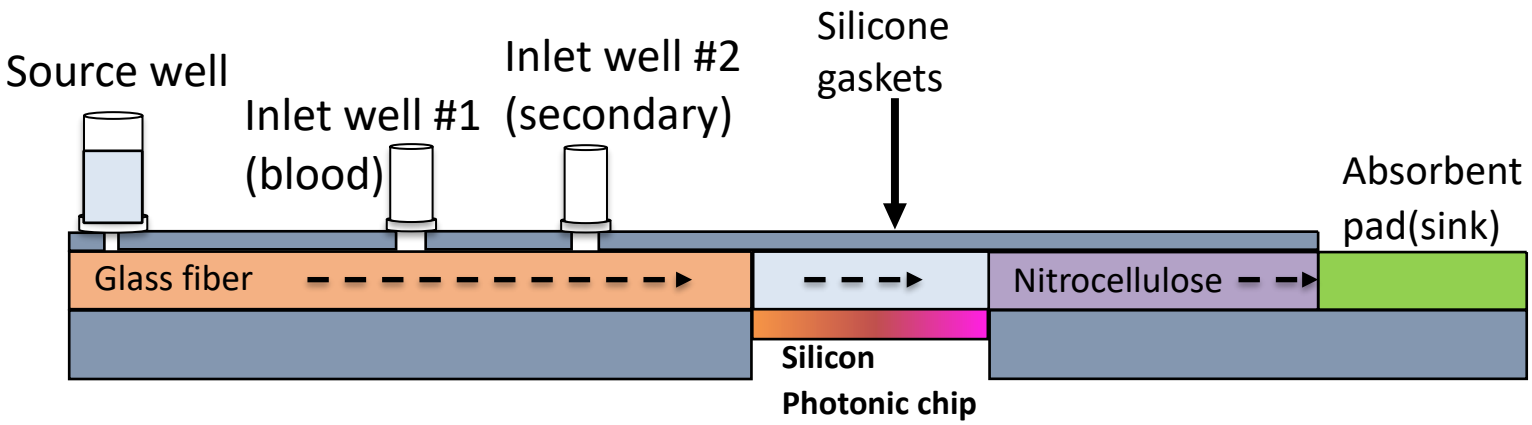

Figure 21: Schematic of positive pressure design

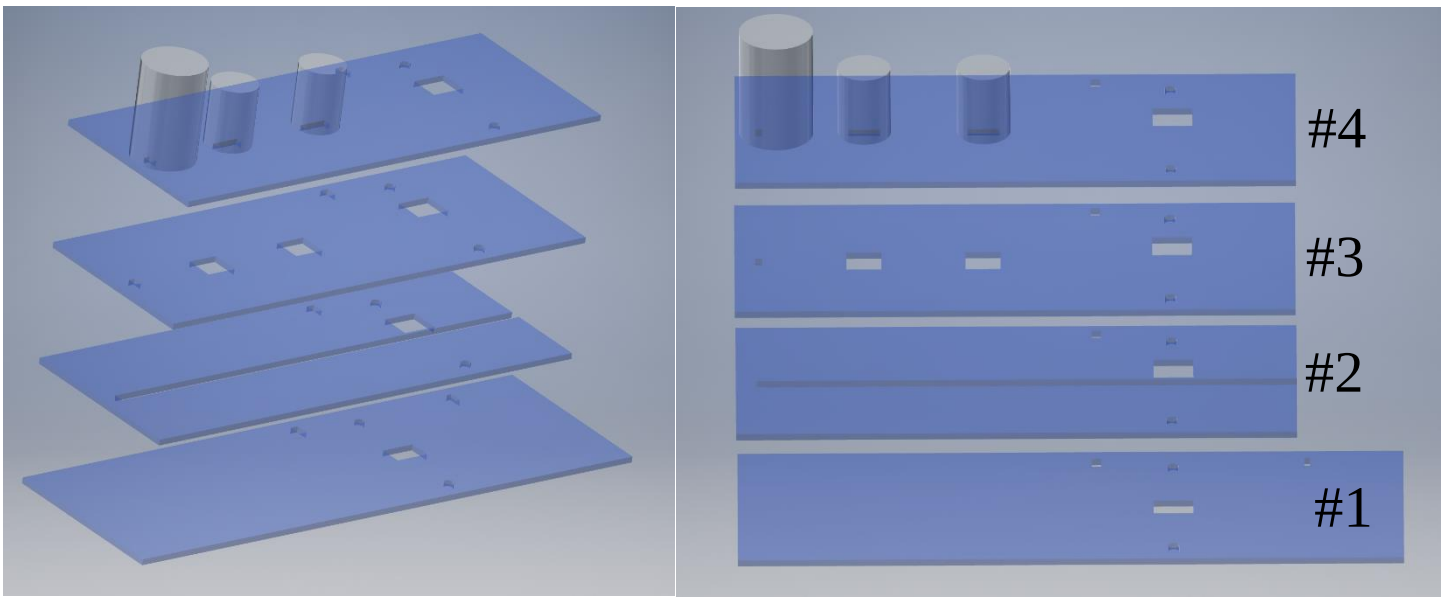

Figure 22: Inventor assembly of positive pressure gaskets

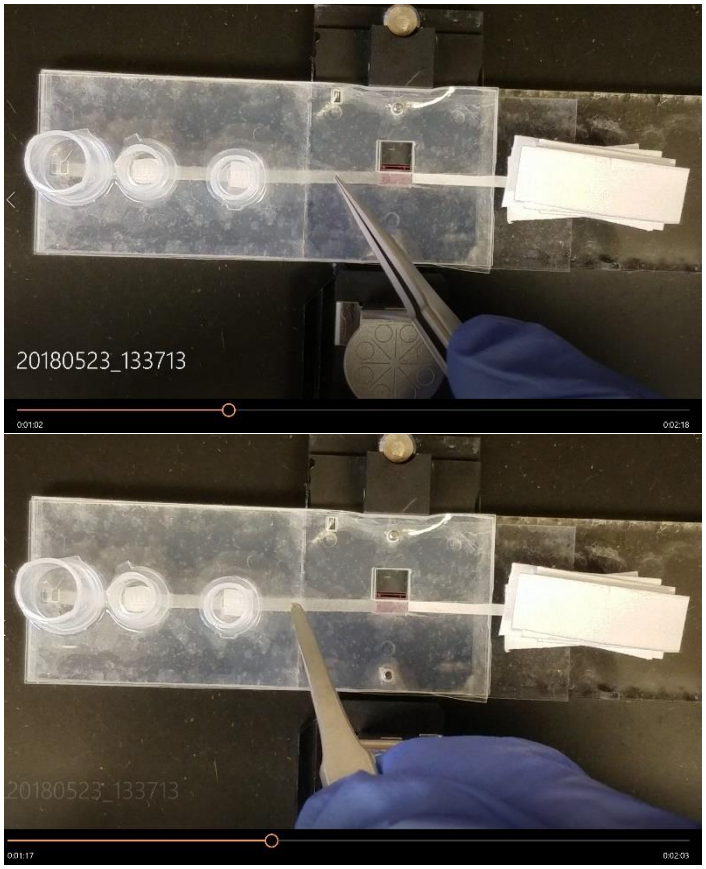

Figure 23: Pushing fluid front through membrane with tweezers

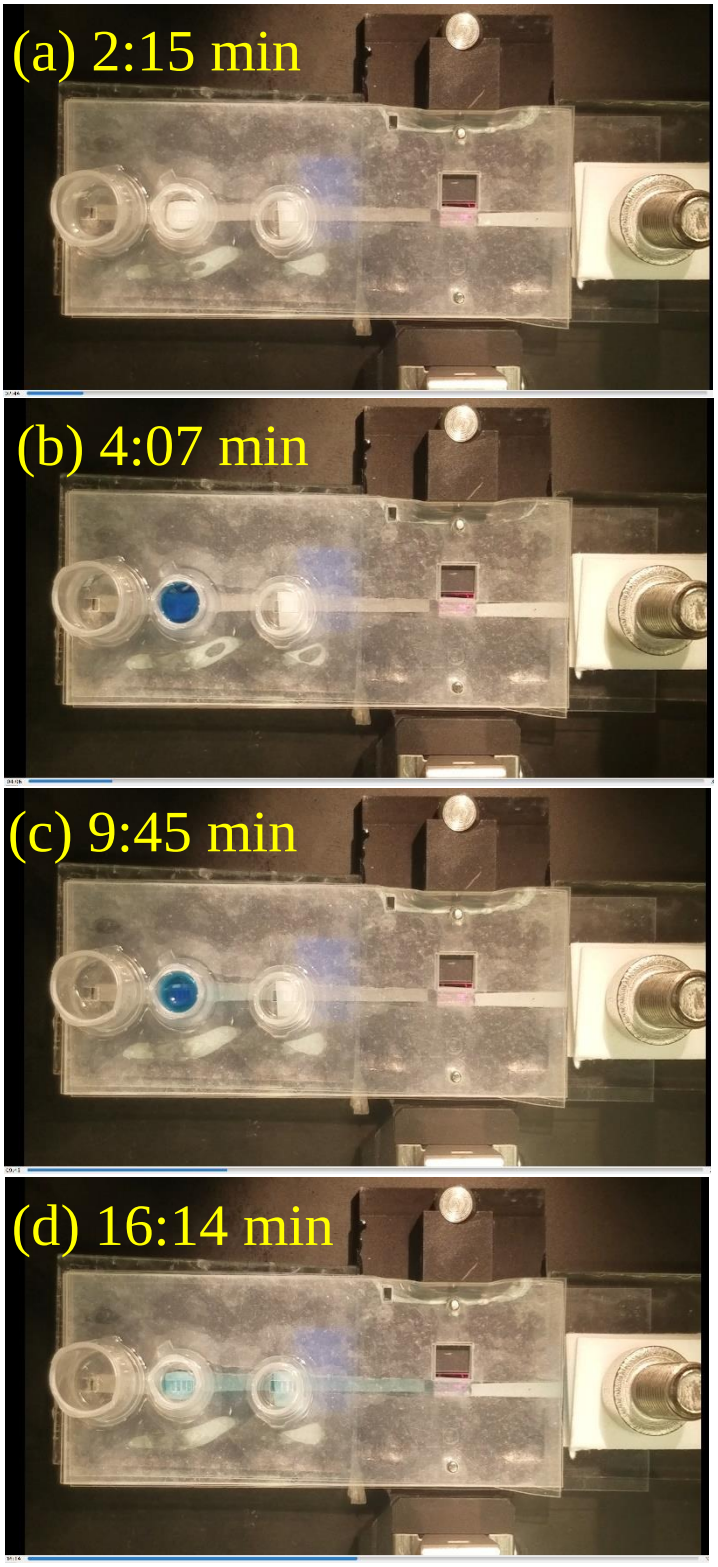

Figure 24: Video frames of sequential flow in positive pressure design

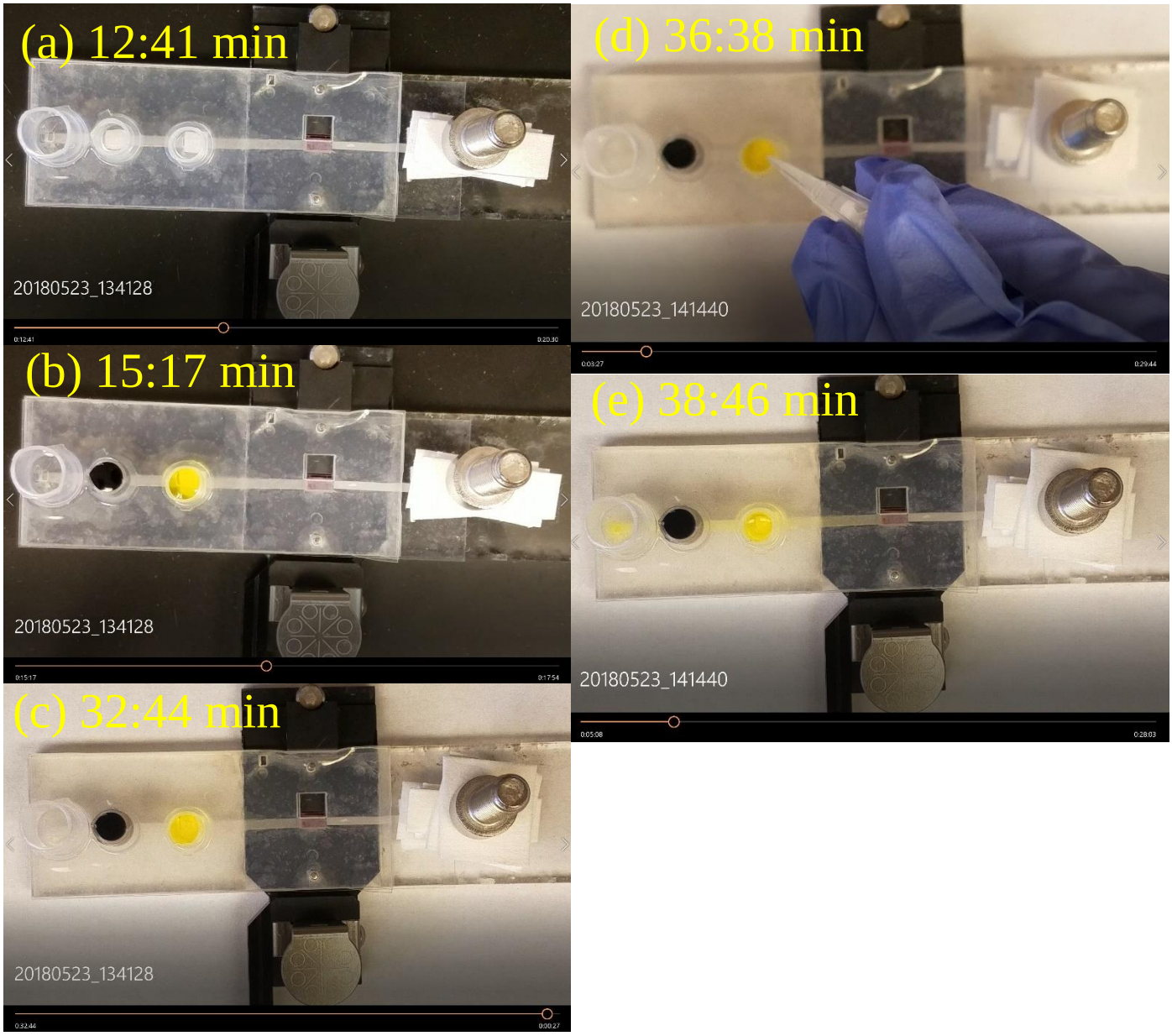

Figure 25: Example of air bubble in positive pressure design

4.2.2 *Negative pressure*

After attempting to troubleshoot the positive pressure design we proceeded to implement a source well like the one shown in figure 9(b). This design was termed ‘Negative pressure’ as the source buffer is at a negative pressure with respect to the glass fiber once the blood and secondary have gone through the network. To conserve resources and save time we chose to use the same gaskets and only change the acrylic to accommodate a source well. A schematic of this design is shown in figure 26. Notice that the source well on the top gasket no longer serves any function in the system. As previously suggested, the source well is replaced by a rastered section in the acrylic that is ~4 mm deep and is a 25 mm by 25 mm square. An image of this system is shown in figure 27. The left acrylic wing is longer than the one used in the ‘positive pressure’ design. We validated this design offline first just as we attempted with the positive pressure design. A frame-by-frame offline simulated assay is shown in figure 28; in figure 28(a) we see that the acrylic source is filled, and PBS buffer is running across the chip. In figure 28(b) we add 25 µL of yellow dye (simulating the blood) to the well #1 and following that, in figure 28(c) we see that the dye begins to flow through the system. This dye wicks through the glass fiber and over the chip in ~15 minutes and in figure 28(d) we add 20 µL of blue dye (simulating the secondary amplification) to well #2 and observe in figure 28(e) that it clears the system in ~14 minutes. This offline simulated assay and other replicates demonstrated that the system was fluidically behaving as intended. We also validated and characterized the fluidics of this design online (on the Genalyte system) and these results will be shown and discussed in the next chapter. Following these validations, we decided to move forward with the negative pressure design, finalize it, and focus on the plasma separation and reverse ABO typing assay.

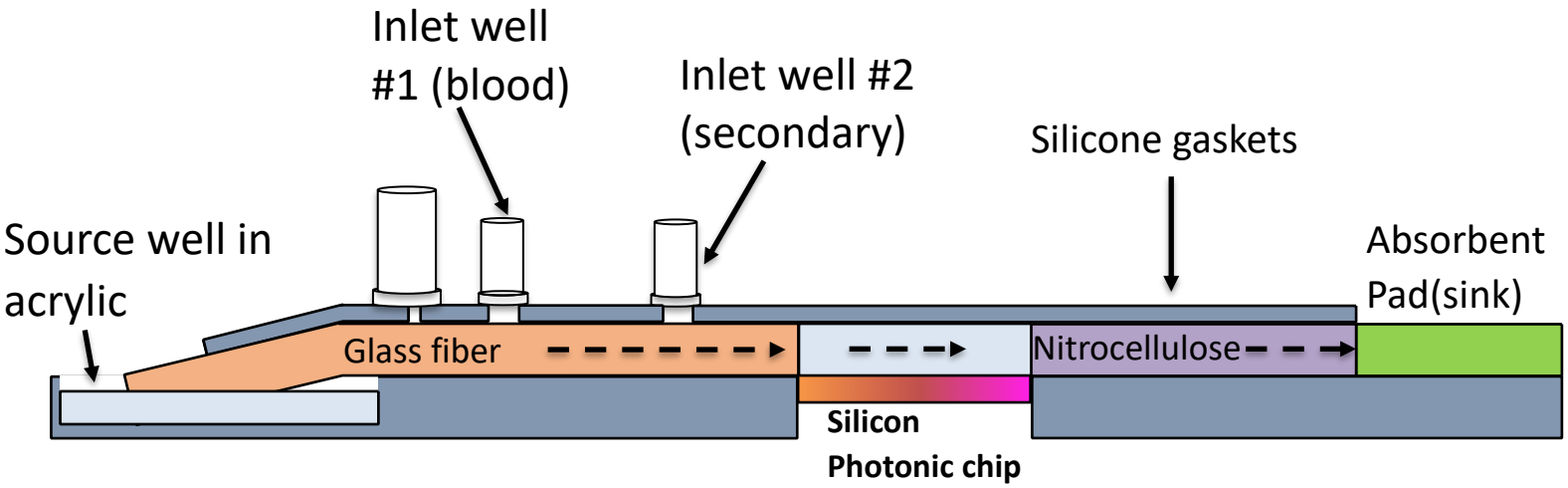

Figure 26: Schematic of negative pressure design

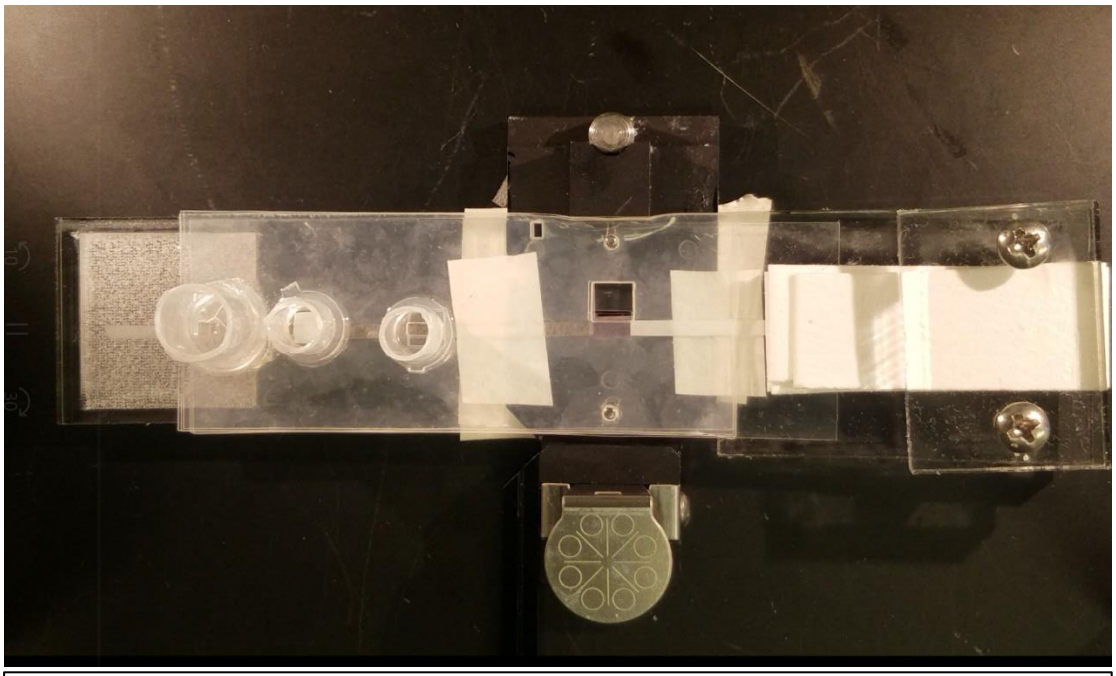

Figure 27: Image of negative pressure design

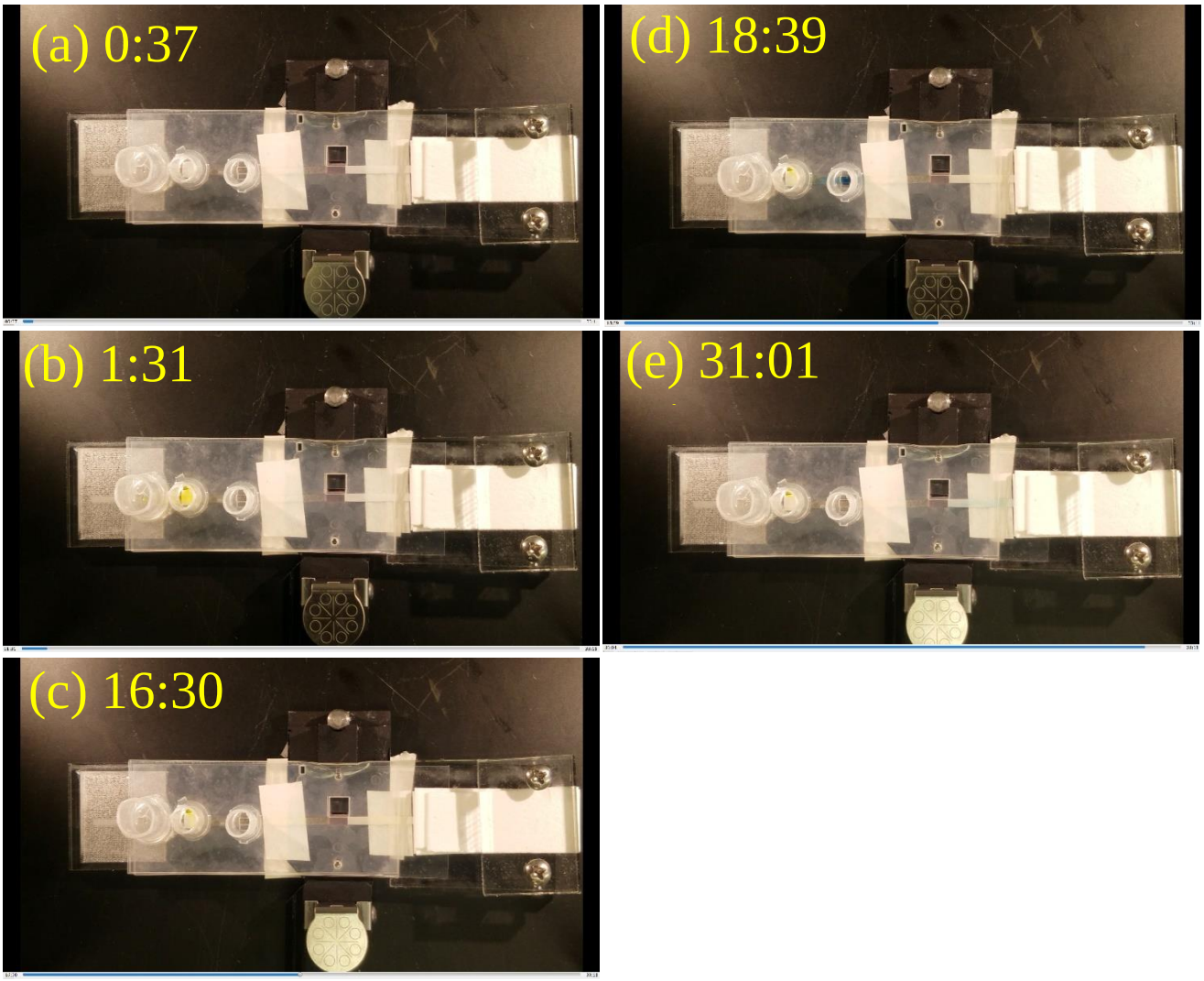

Figure 28: Simulated assay with negative pressure design

4.3 FINAL DESIGN

Our final design was principally derived from the ‘negative pressure’ iteration and composed of four gaskets. For the final design, we no longer used the wells as they are difficult to access within the Genalyte and we are not using high enough volumes of sample or reagent. The dimensions of the gaskets and acrylic are shown in figures 29 and 30 respectively. An exploded view of the gaskets and their order are shown in figure 31. Gasket layer #1 (0.25 mm thick) levels the chip, gasket layer # 2 (0.5 mm thick) defines the channel for the porous membrane. Gasket layer #4 (0.5 mm thick) now contains the square opening for the plasma separation membrane and gasket layer #3 (0.25 mm thick) provides a slit opening for fluid to flow through. We decided to reverse the third and fourth gasket layer (as compared to the previous designs) because we did not want the plasma separation membrane to wick up excess buffer from the glass fiber. The delivery window with slits allows there to be more resistance to fluid moving in and out of the window. This resistance provided an advantage in blood separation because the separation membrane could not oversaturate with buffer making sure the blood went through it and not around it. This final design is optimized for assays with whole blood plasma separation. We determined the required dimensions of the glass fiber, nitrocellulose, and separation membranes by characterizing the flow rate and separation capability; these results will be presented in the next chapter. Images of the assembly process of our final design is shown in figure 32. In figure 32(a) we have the empty mount with the gasket adaptations following this we place the chip in the mount cavity in figure 32(b). We then add gasket layer #1 (figure 32(c)) and gasket layer #2 (figure 32(d)). Following these additions, we add a 2 mm wide and 68 mm long Ahlstrom 8964 glass fiber on the left side of the chip in the channel and to the right side, we add a backed 3mm wide and 42 mm long HF135 nitrocellulose membrane. Note that we tried to align the top edge of the nitrocellulose membrane

with the top edge of the glass fiber to best simulate a sealed integrated channel. Also, notice that the gaskets sink into the well at the leftmost edge; this meant that the glass fiber slotted between gasket #1 and #2 into the source on the left and then on the right the nitrocellulose is level. In figure 32(e) we add gasket layer #3 which defines the two frayed inlet windows and in figure 32(f) we add gasket layer #4 that provides the cavity for the plasma separation membrane. Following this we add 5, 44 mm long by 16mm wide CF6 absorbent pads on top of the nitrocellulose and align the left edge of the absorbent membrane with the white edge of the electrical tape and screw these absorbent pads on with the acrylic drill piece (figure 32(g)). We then add a 5 mm by 5mm MF1 separation membrane to delivery window #1 (figure 32(g)). Finally, depending on how much whole blood we are attempting to separate we add 7.5 mm by 7.5 mm VF2 plasma separation membrane(s) on top of the MF1 membrane (figure 32(h)). This sequence of assembly was the same for all our results however we optimized/varied the dimensions of the porous membrane components (during the online validation); width of the nitrocellulose, glass fiber, and plasma separation membrane.

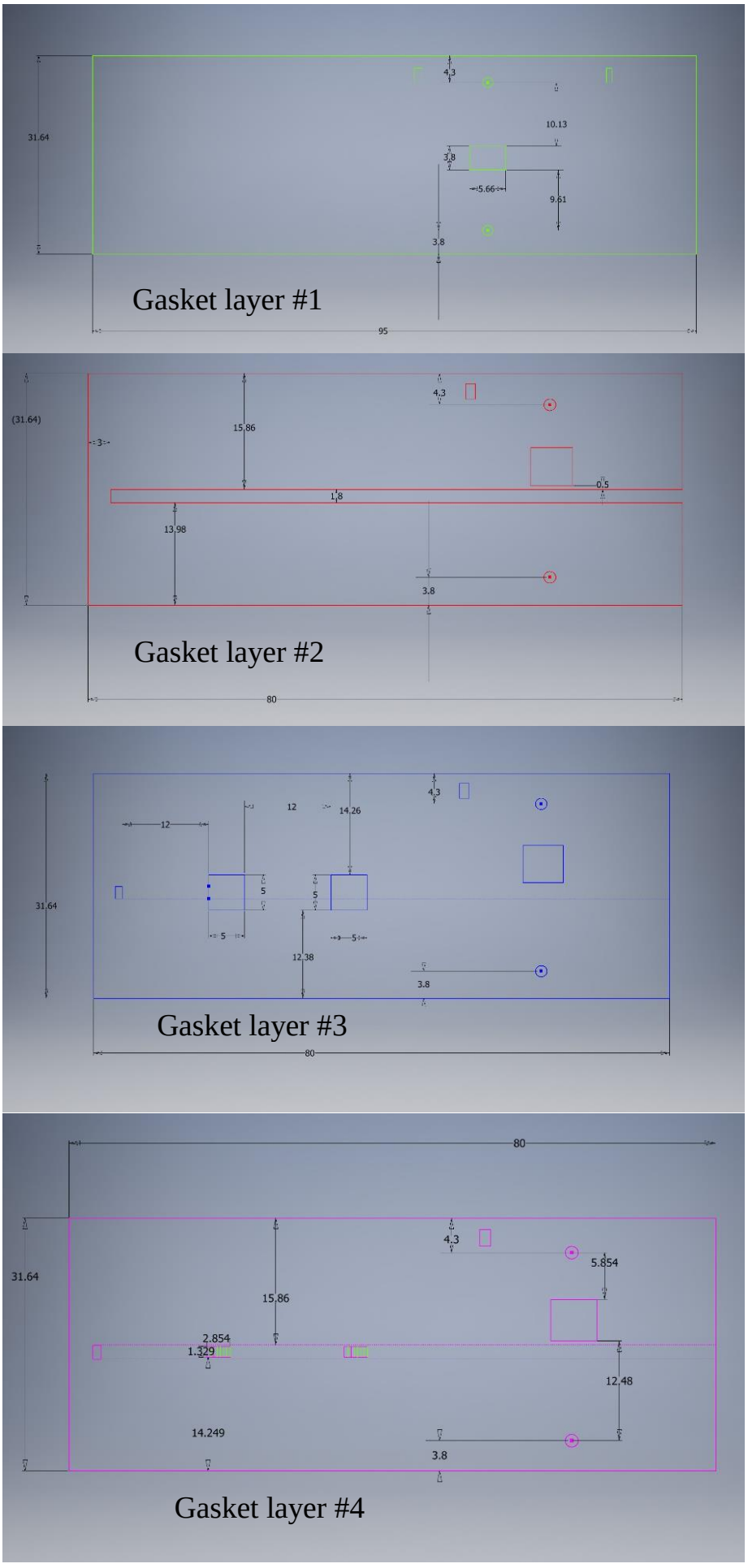

Figure 29: Dimensions of the gaskets

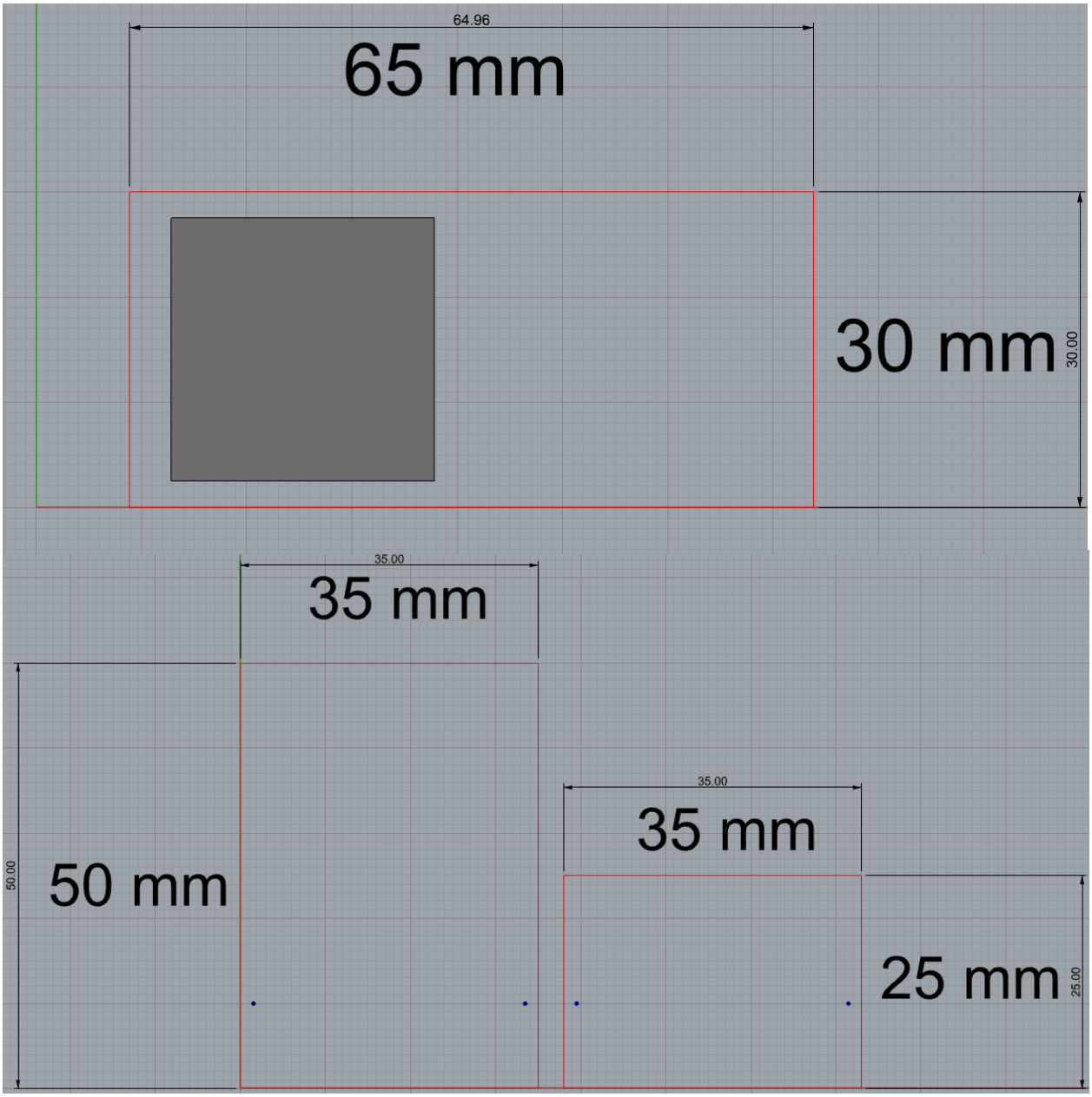

Figure 30: Dimensions of acrylic Top: left acrylic Bottom: right side acrylic

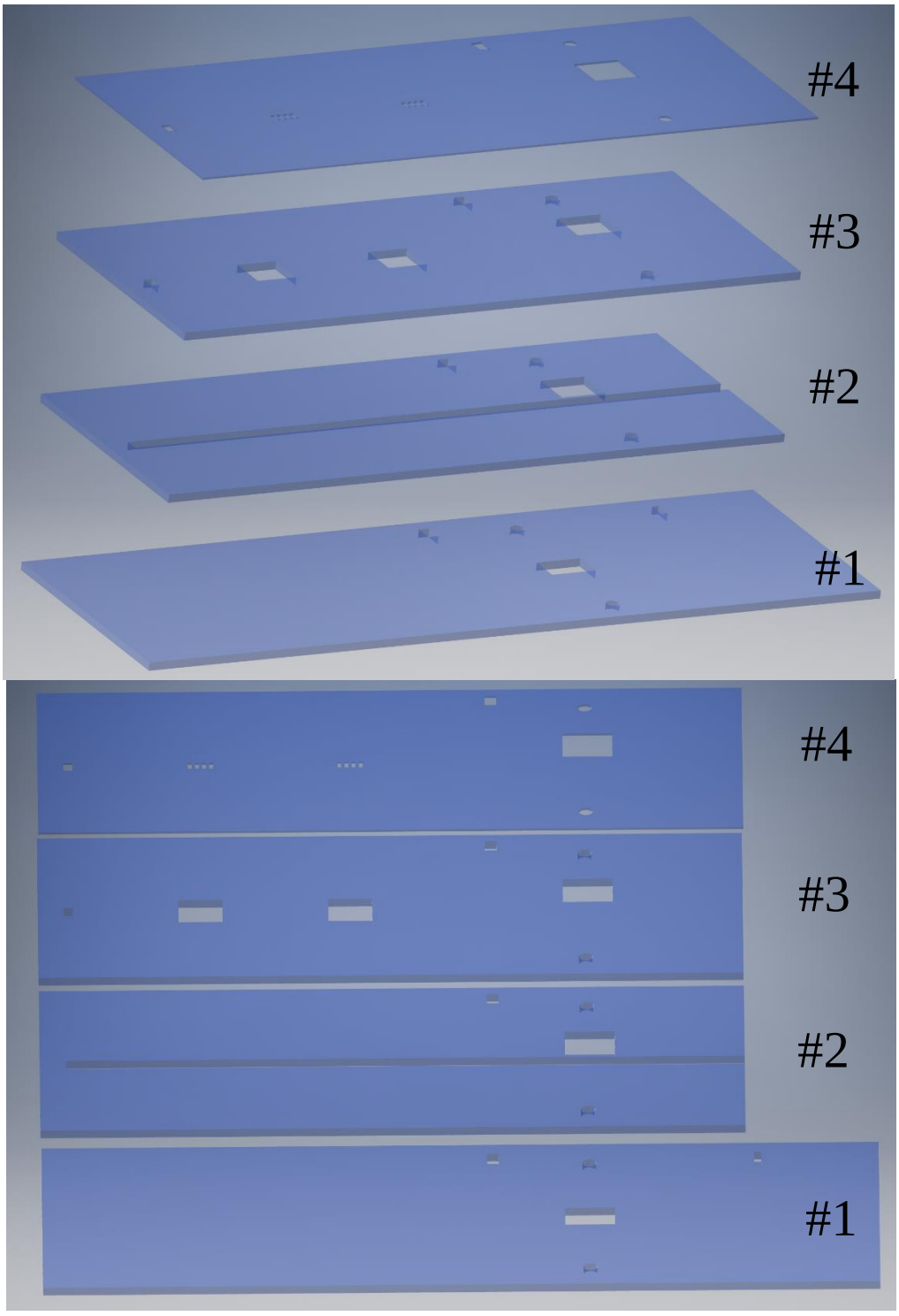

Figure 31: Inventor assembly of final design gaskets

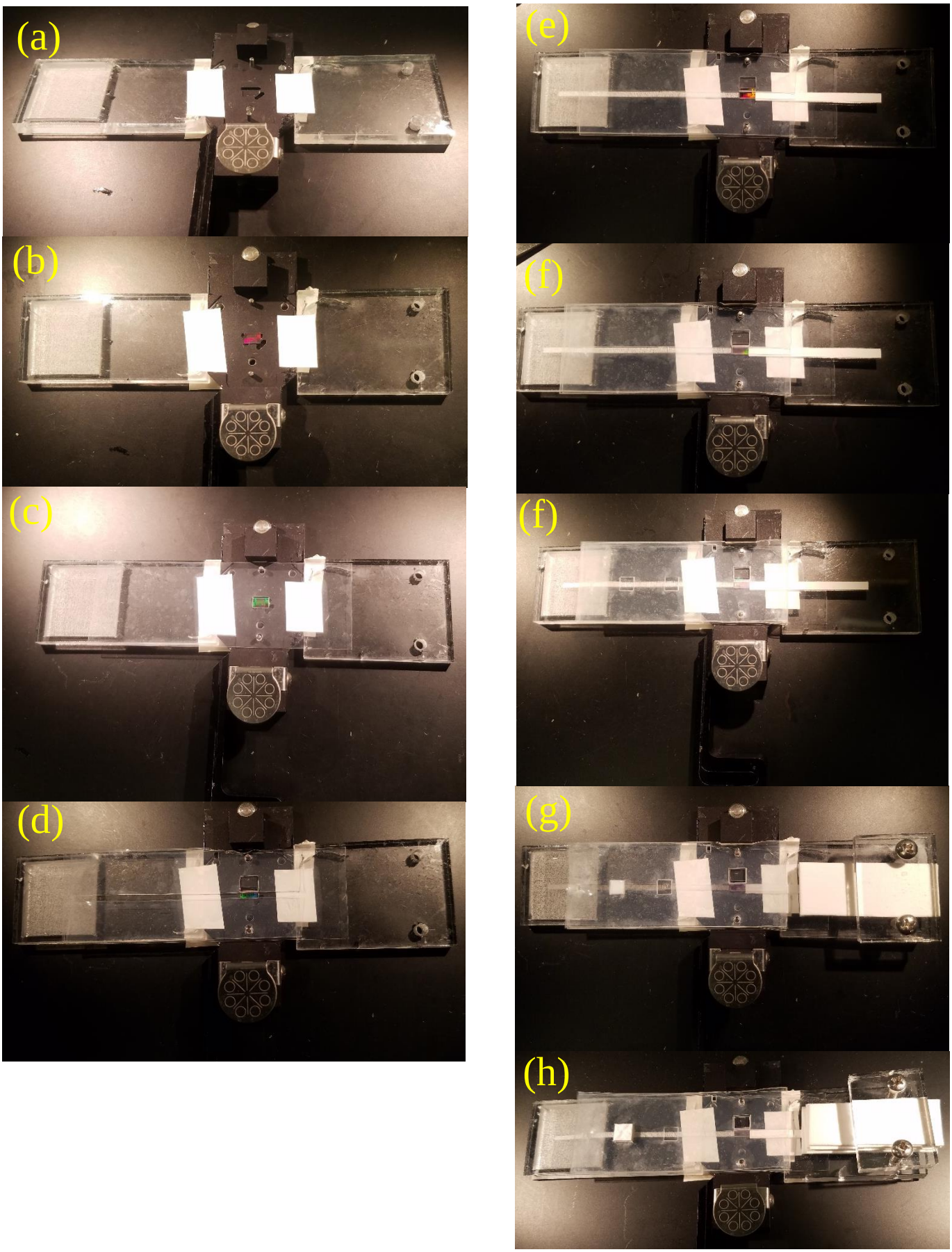

Figure 32: Series of images to assemble design

Chapter 5. RESULTS & DISCUSSION

5.1 FLUIDIC PROFILE

5.1.1 *Salt steps*

We ran salt steps with the final design in which the saline solution (NaCl) was placed in the inlet delivery window #2 with increasing concentrations (figure 33). The DI water running from the source brought the bulk refractive index back down after ~20 minutes. We ran this series to observe the uniformity of the flow profile. As shown in figure 12(a) the chip's sensors are in two rows termed channel 1 and channel 2. We wanted to ensure that the flow over the chip is uniform and not bifurcated or deformed (i.e. both channels respond on similar timescales and similar resonance shift). The results shown in figure 33 validated that we did have bulk uniform as flow with our gaskets. We only ran one replicate of this test because we further validated the flow profile with the flow rate and simulated assay fluidic online tests.

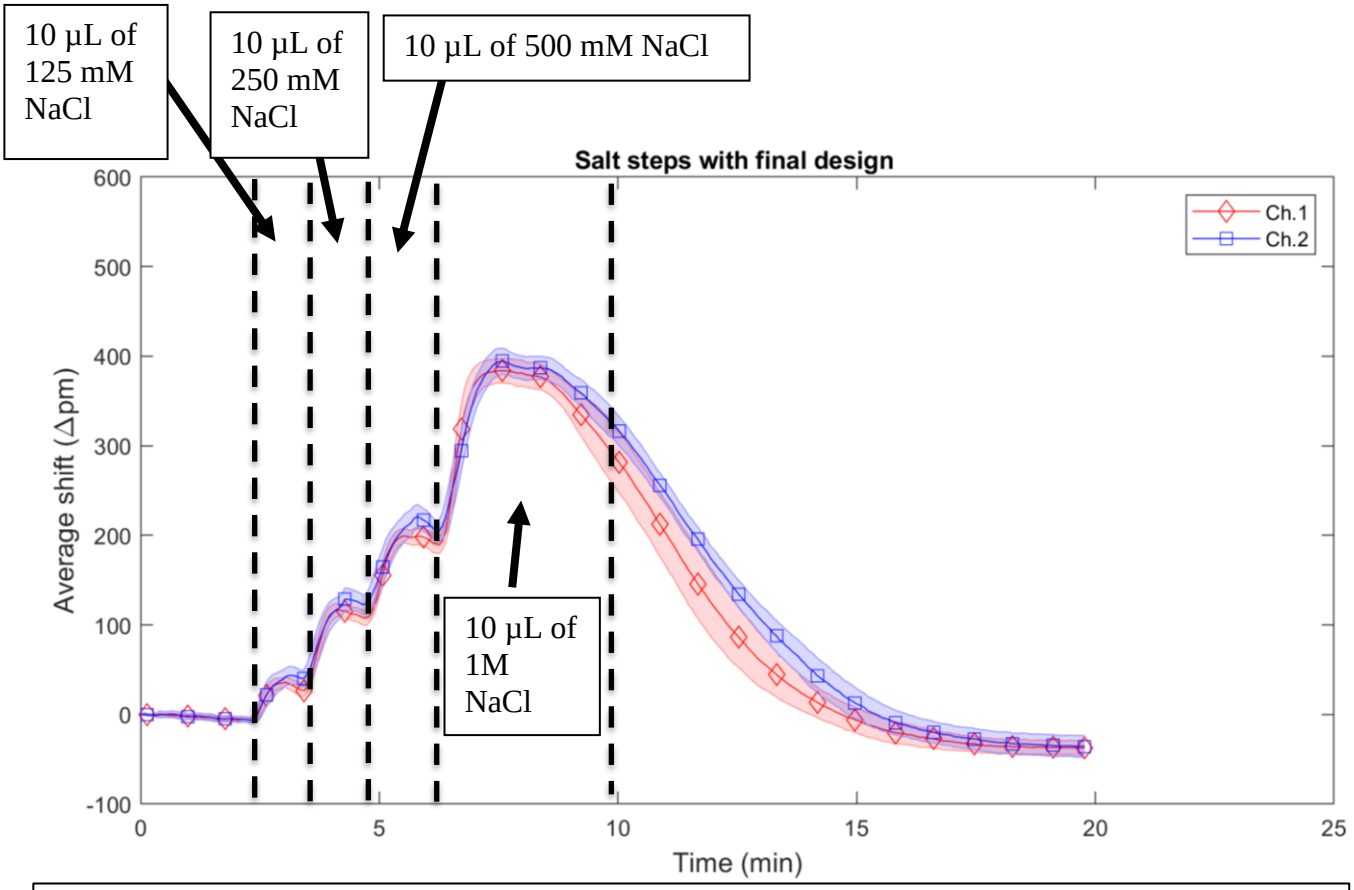

Figure 33: Salt steps with final design

5.1.2 *Flow Rate*

We estimated the flow rate by observing the residence time of 10-25 µL of NaCl saline over the chip and then dividing the volume added by said residence time (as described in 3.2.1). Note that the flow rate estimations are derived from the online simulated assays. The simulated assays comprised of running NaCl saline through the system when it was setup for a reverse ABO typing assay (ensuring we were getting an estimated flow rate relevant to our assay). We tuned this flow rate by changing the width of the nitrocellulose membrane as prescribed by Darcy's law (Eqn. 2.1). In figure 34 we have an example flow rate test with a nitrocellulose membrane that is 2 mm wide and 42 mm long. The estimated flow rate for these dimensions ranged from 0.9-1.31 µL/min for both inlets (more replicates shown in the appendix). We increased the width of the nitrocellulose membrane to 3 mm to increase the flow rate to decrease the overall assay time and to better align with flow rates demonstrated in our previous work.[13] An example of a flow rate test with this 3 mm width nitrocellulose is shown in figure 35. The flow rates for these dimensions varied from 1.5-2.5 µL/min (replicates are shown in the appendix). We were satisfied with this flow rate and used these dimensions in all the results to follow.

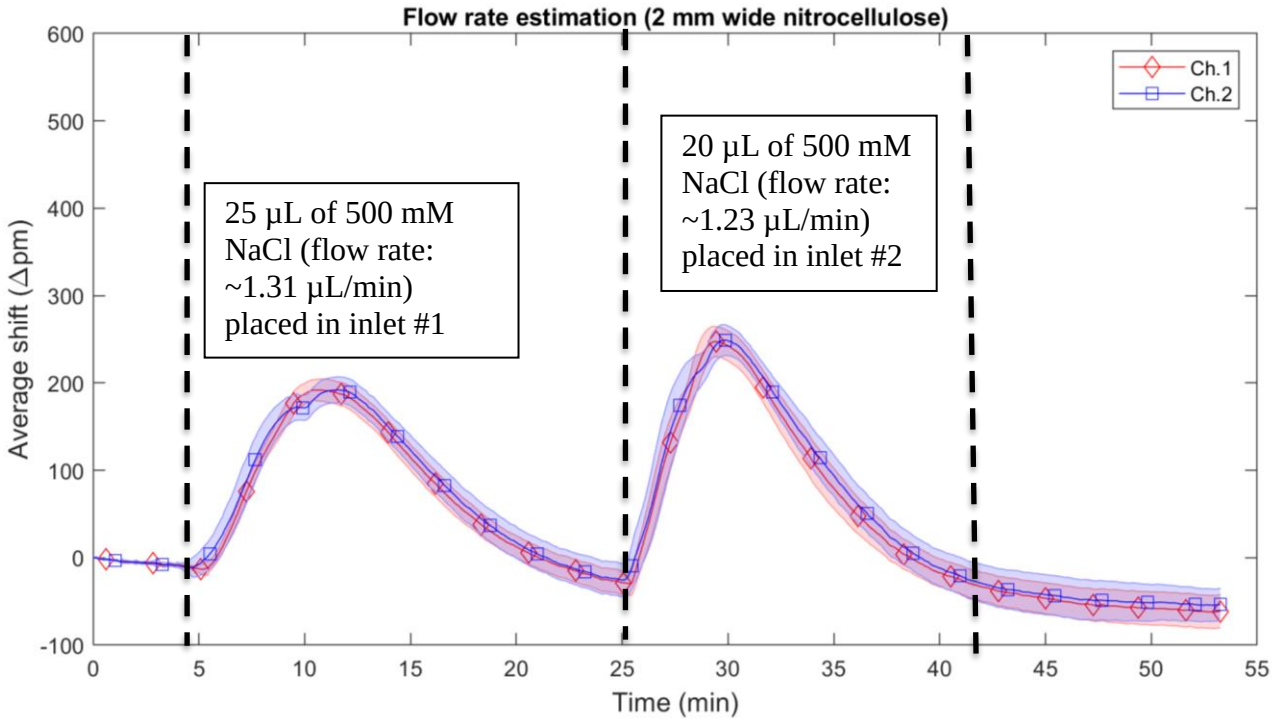

Figure 34: Flow rate test example with 2 mm wide nitrocellulose

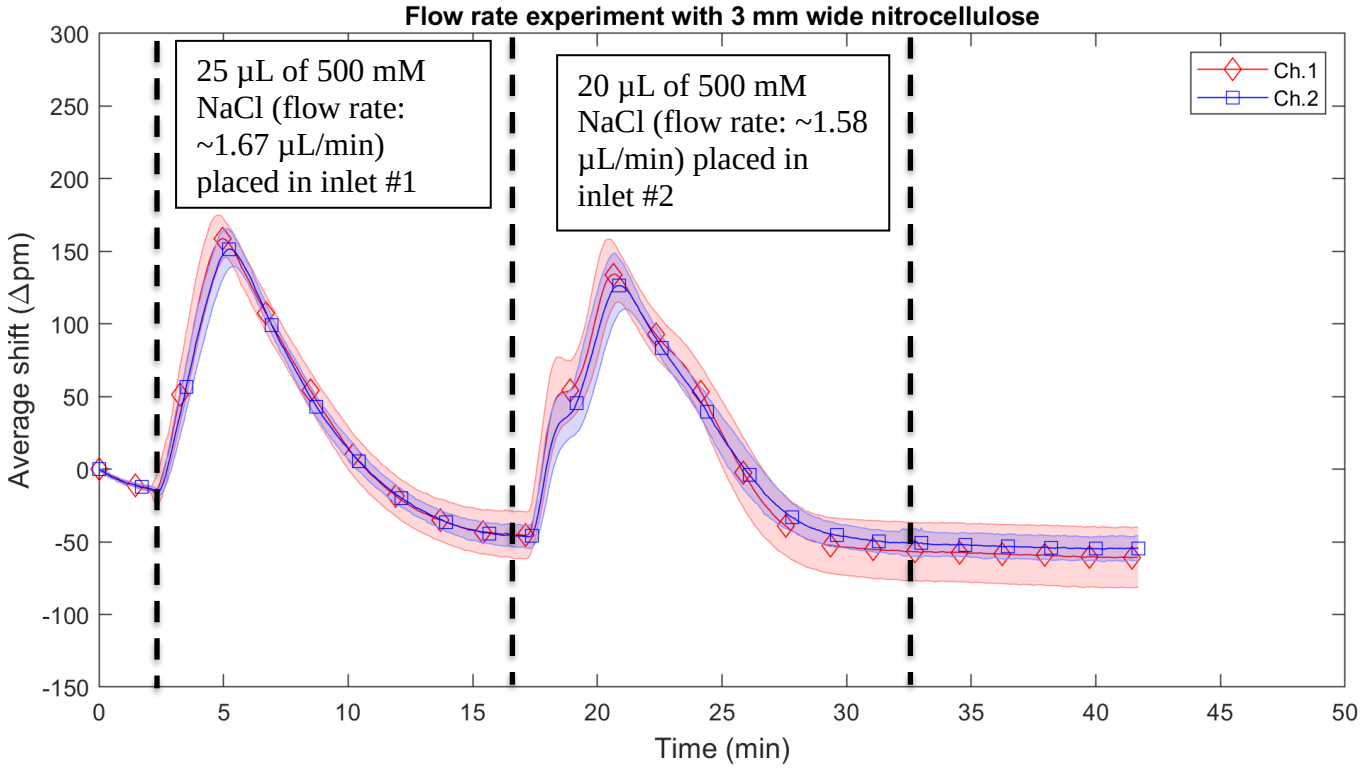

Figure 35: Flow rate test example with 3 mm wide nitrocellulose

5.1.3 *Simulated assays*

The procedure for the ABO typing assay with plasma separation is outlined in 3.6.2 and we simulated this assay by adding equivalent volumes of NaCl saline instead of blood and secondary antibody. We performed these simulated assays offline (as shown in Chapter 4) and online with the Genalyte. Examples of online simulated assays are shown in figure 34, 35 and 36. We used the final design to run these assays and various widths of nitrocellulose membrane (2 and 3 mm) and we show the replicates in the appendix. The simulated assays offline and online (shown in 4.3) showed expected behavior and a relatively uniform profile.

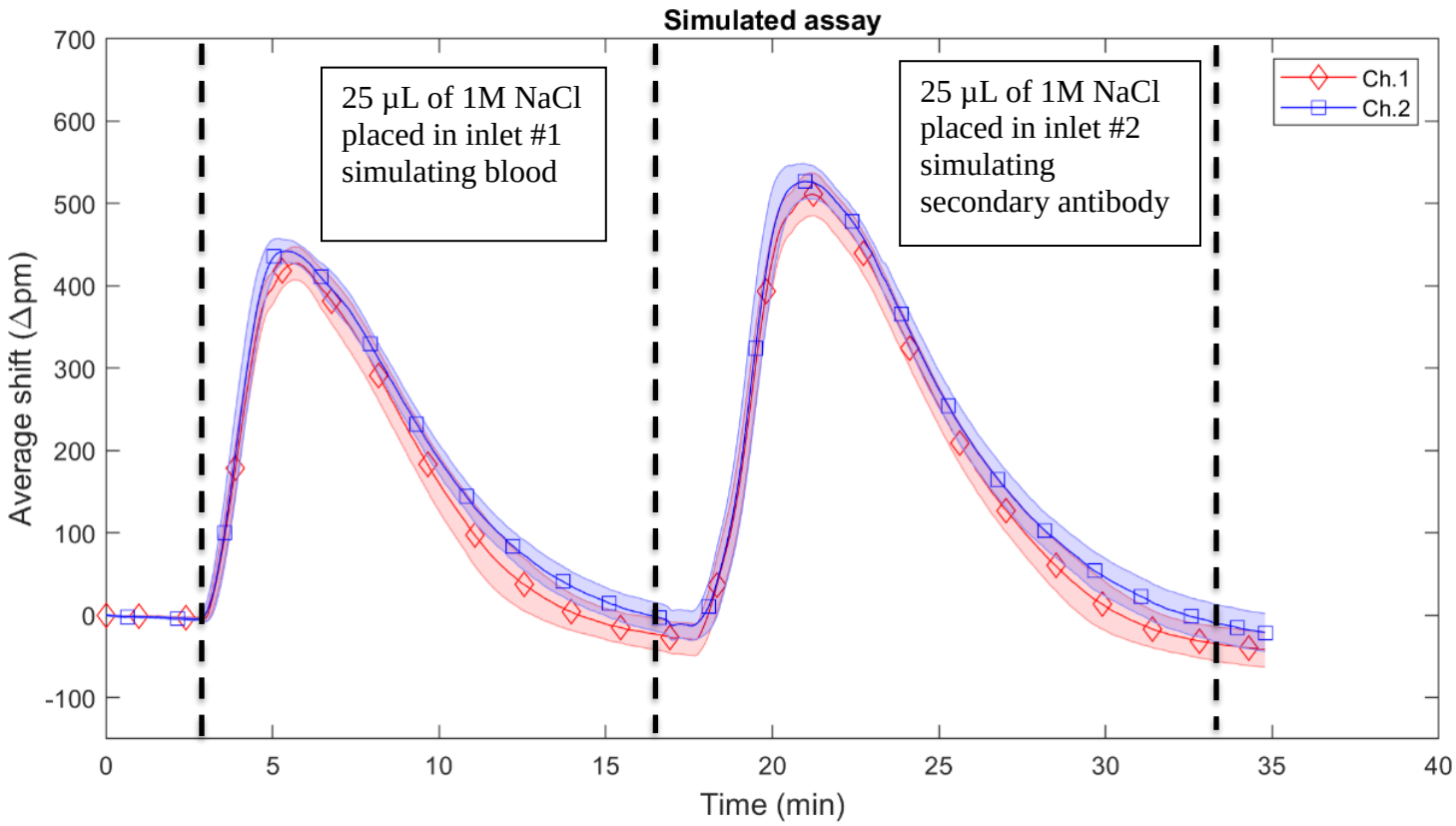

Figure 36: Simulated assay with final design

5.2 PLASMA SEPARATION

With our final design and 3 mm wide nitrocellulose, we began optimizing the plasma separation by running assays without a functionalized chip. We ran all the plasma separation tests online as it was important to see the response of the sensors to understand the effectiveness of the separation. For our separation, we used the MF1 and VF2 plasma separators and added more VF2 membrane depending on how much blood we were trying to separate. As stated in 3.3.2 we ran our plasma separation on pre-wet membranes and pushed the plasma through the membrane with PBS buffer. From previous work, we know that if heme and cellular material are getting to the chip the signal becomes high frequency and generates small noise.[54] We tried to minimize this heme/cell leakage to maintain consistent flow and keep the surface of the chip from fouling.

5.2.1 *25 µL whole blood separation*

In our initial conception of this project, we wanted to separate 25 µL of whole blood and we optimized our system for that volume. Before performing any online tests, brief offline tests were done to observe the rough amount of membrane needed to plausibly separate 25 µL of blood (data not shown). But because plasma is difficult to see travel through the network, we performed the bulk of the optimization online. We first tried to separate the 25 µL with a 5 by 5 mm MF1 membrane in inlet 1 and a 6.5 by 6.5 mm VF2 membrane on top of it. The averaged (with standard dev border shading) and raw results are shown in figure 37. For this test we placed 25 µL of whole blood on top of the VF2 separation membrane at 1 minute and then at 3 minutes we pushed 25 µL of PBS on top of the VF2. The sample was leaking through to the glass fiber before we pushed with buffer and that is why we see a response before the push. This leakage is illustrated by the high frequency in the raw signal. These dimensions of the VF2 plasma separation membrane were not quite enough to prevent initial leakage to the glass fiber and so we increased the area of the

VF2 by 14 mm^2 (all dimensions by 1 mm). The results of this test are shown in figure 38. Note in the raw results there is little high frequency noise until the second push of 25 µL of PBS in which more heme and cell components were flown through the system. This was confirmed by a visual inspection of the mount after this test (image shown in figure 39) as we see there is very little heme within the nitrocellulose. Before moving on to the ABO reverse typing assay, we wanted to push the limits of the system and observe the response of the sensors after adding sequential 25 µL PBS buffer pushes on top of the VF2 membrane. This test is shown in figure 40. Notice that with each successive PBS addition more sample is pushed from the membrane and to the surface of the chip. Also note that with each successive push the high frequency noise increases meaning that more cell and heme components to the surface of the chip. With this test, we saw that even when pushing out much heme and cells from the system we did not stop flow. This test affirmed that we are unlikely to clog the nitrocellulose membrane when using these dimensions of plasma separation membrane. Overall these tests demonstrated that we can separate plasma from whole blood effectively and efficiently in our system. However, these results did not give us any information on the impact that cell and heme leakage have on the ABO reverse typing assay.

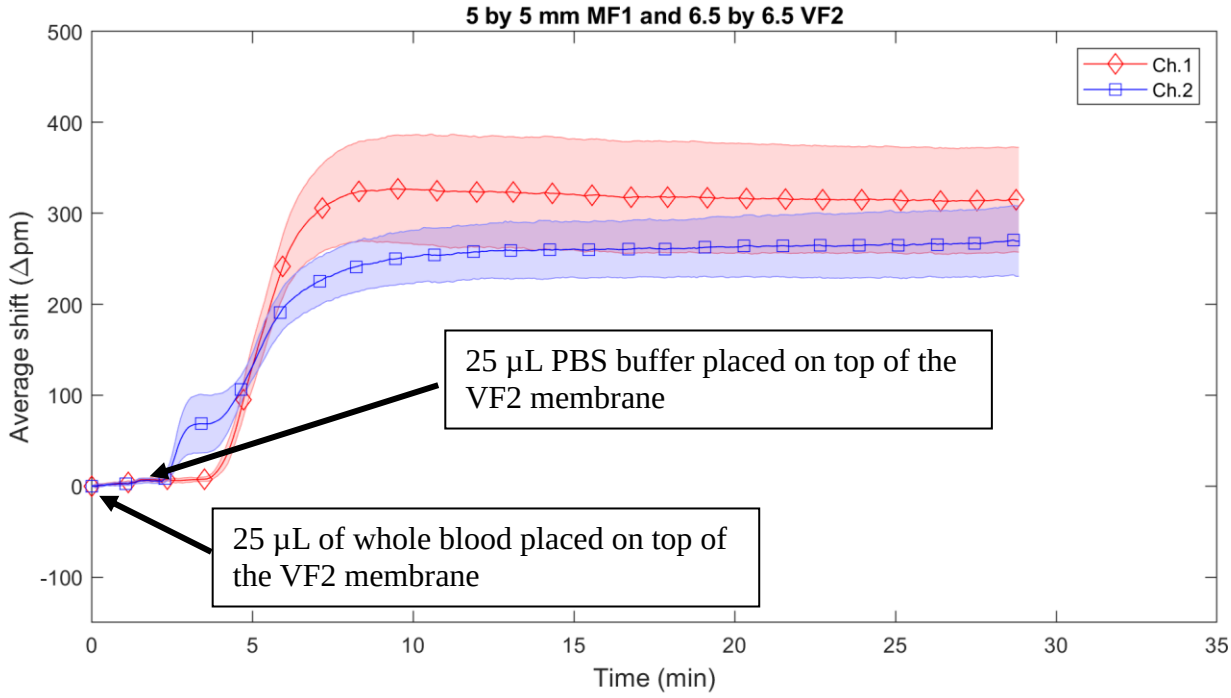

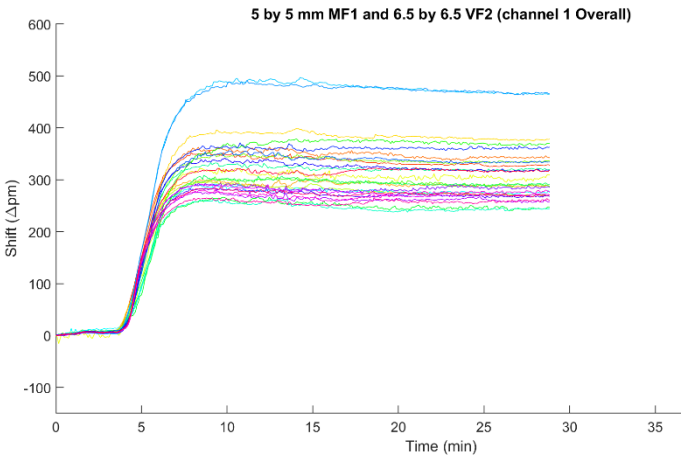

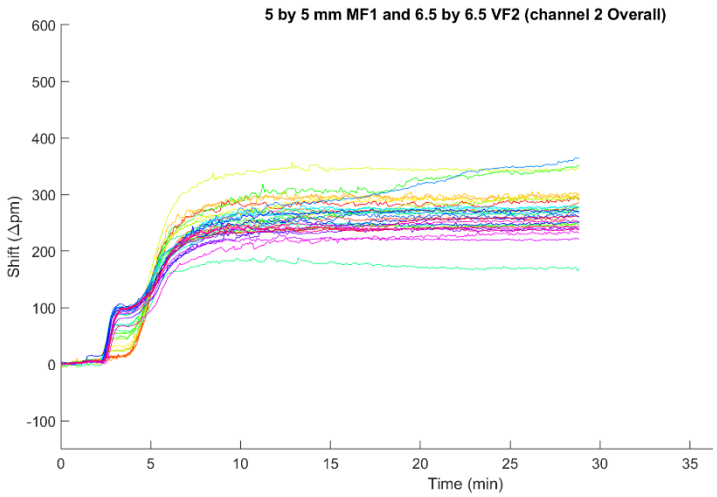

Figure 37: Plasma separation with 5 by 5 mm MF1 and 6.5 by 6.5 VF2

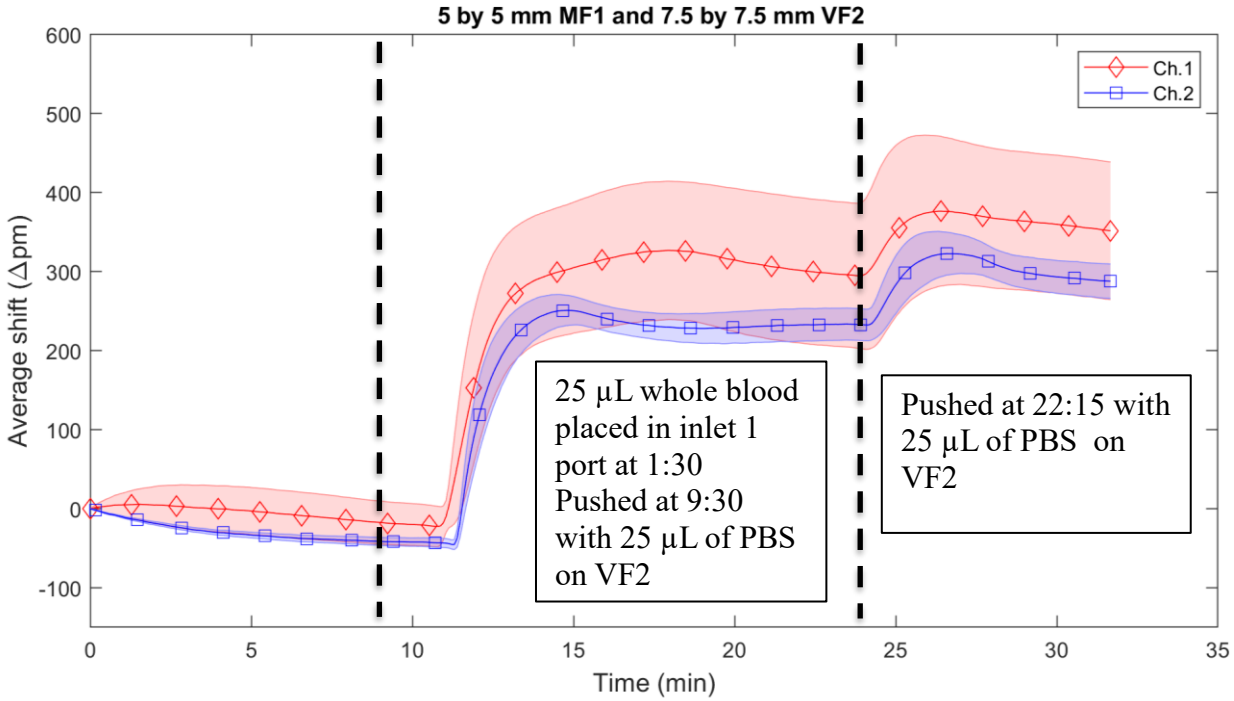

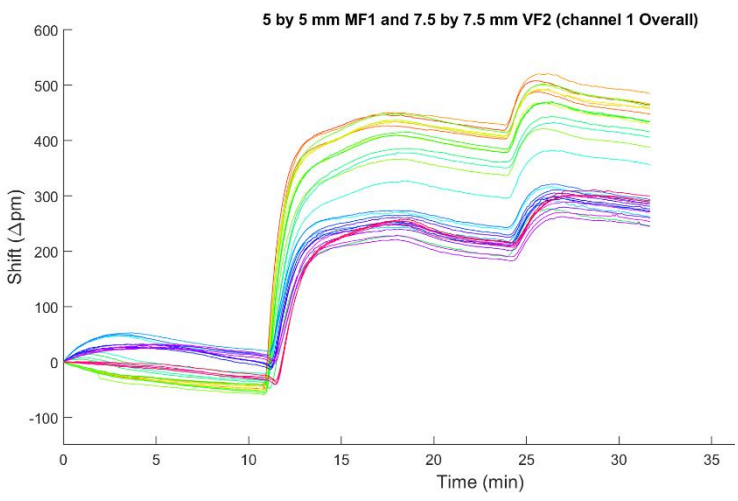

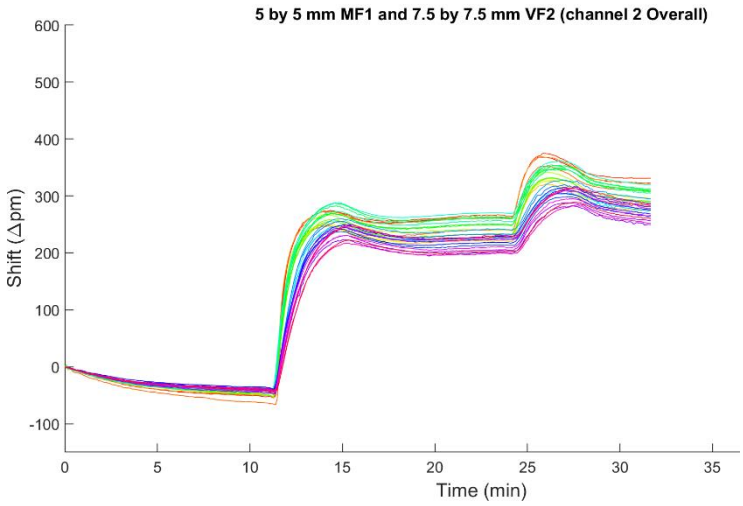

Figure 38: Plasma separation test with 5 by 5 mm MF1 and 7.5 by 7.5 mm VF2

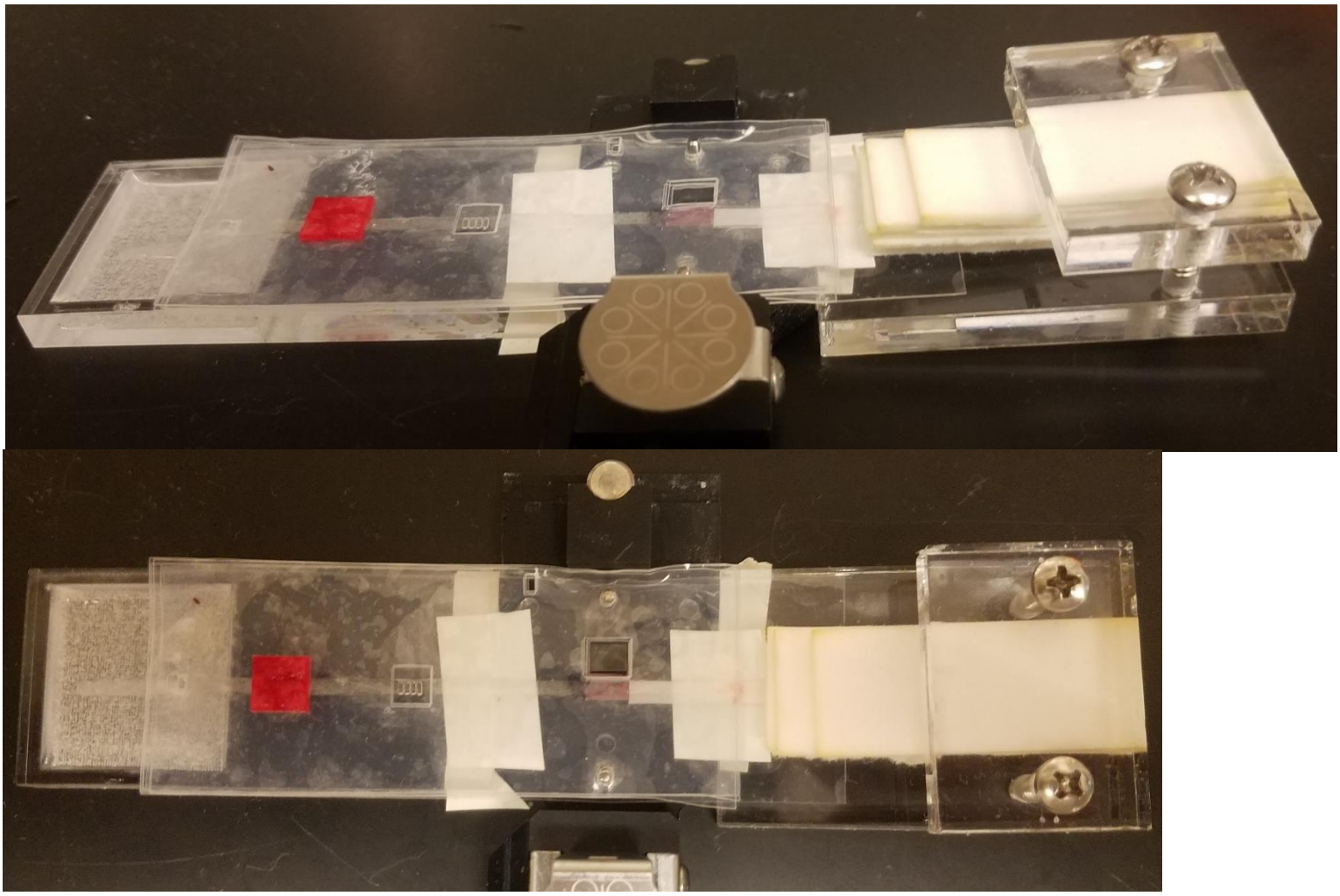

Figure 39: Images of mount post-test in figure 37

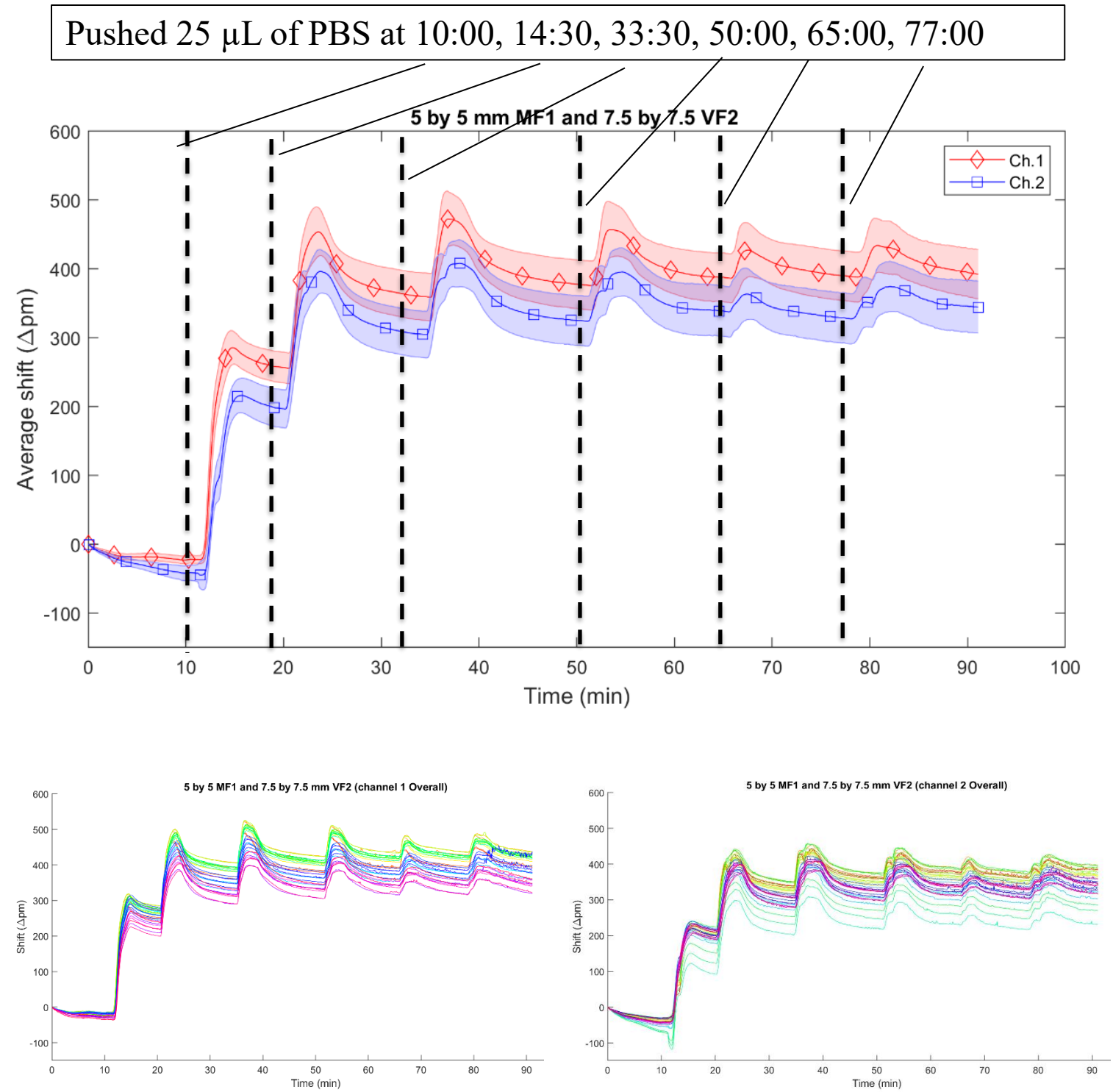

Figure 40: Sequential PBS additions and plasma separation with 5 by 5 mm MF1 and 7.5 by 7.5 mm VF2

5.3 REVERSE ABO SEROLOGIC ASSAY

5.3.1 *Variation in functionalization of the chips*

When running the assays presented in this chapter, we noticed a difference in relative and relevant response between channel 1 and channel 2 (different in figure 12(a)). We also observed a shift of the functionalization to the right side of the chip. This meant that it was more likely for the mid-section of the chip to be functionalized with PAA-A (figure 12(b) shows functionalization scheme). Overall these discrepancies suggest the hand-spotting method used to functionalize the chips was not able to produce consistent functionalization of only certain rings. The Ratner lab encountered this problem in previous work and has demonstrated the solution via inkjet printing reagents to functionalize the chips but this method was not accessible to this project.[7] Due to lack of uniformity system and lack of consistent performance, we only present the relevant data for each result/chip as to not detract from the main findings of each section.

5.3.2 *Validating PAA-A and PAA-B*

We ran a validation assay with anti-A and anti-B murine monoclonal IgM antibodies with the pump system over the Genalyte. The chip was functionalized in the same way it is for all typing assays in this project (PAA-A on left side PAA-B on right shown in figure 12(b)). The results are shown in figure 41. We see that the PAA-A has a specific response, but the PAA-B is not active and does not robustly respond to anti-B. There is a differential response between the synthetic antigens (left and right) when anti-A validation reagent is flowed over the chip, indicating the left sensors are functionalized. The shift on the right sensors when the anti-B validation reagent is flowed through does not have a noticeably higher average response than the left PAA-A side.

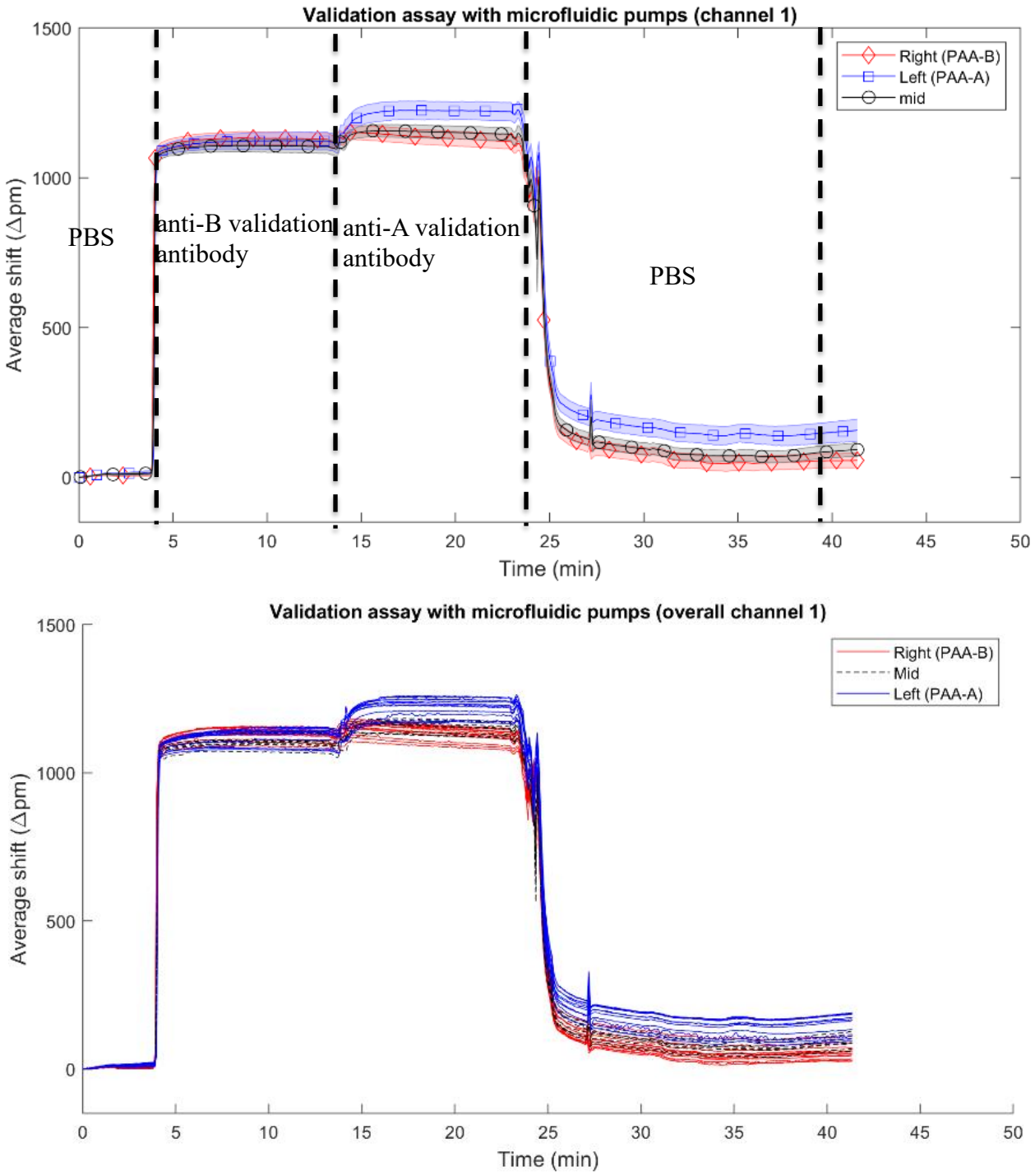

Figure 41: Validation assay with microfluidic pumps

5.3.3 *ABO reverse typing assay with plasma*

We ran reverse typing assays with 20 µL of plasma spun down from type BPOS whole blood at 2000 g for 5 minutes. Two runs with positive typing responses are shown in figures 42 and 43 these assays were run not using microfluidic pumps but with the paper fluidic mount design. After the addition of the plasma observe a positive response from only the left side of the chip as we would expect to from a B-type plasma sample (anti-A antibodies bound to PAA-A). We notice that the positive response is more pronounced and specific in the overall results. In figure 42 we see after the secondary the left side responds robustly but the right does not respond at all. Not all the chips run with this plasma typing assay produced a positive response and those replicates are shown in the appendix.

20 µL of Type-B plasma added to inlet 2 at 1:00

1 mg/mL secondary (goat anti-human IgG/A/M) placed at inlet 2 at 22:20

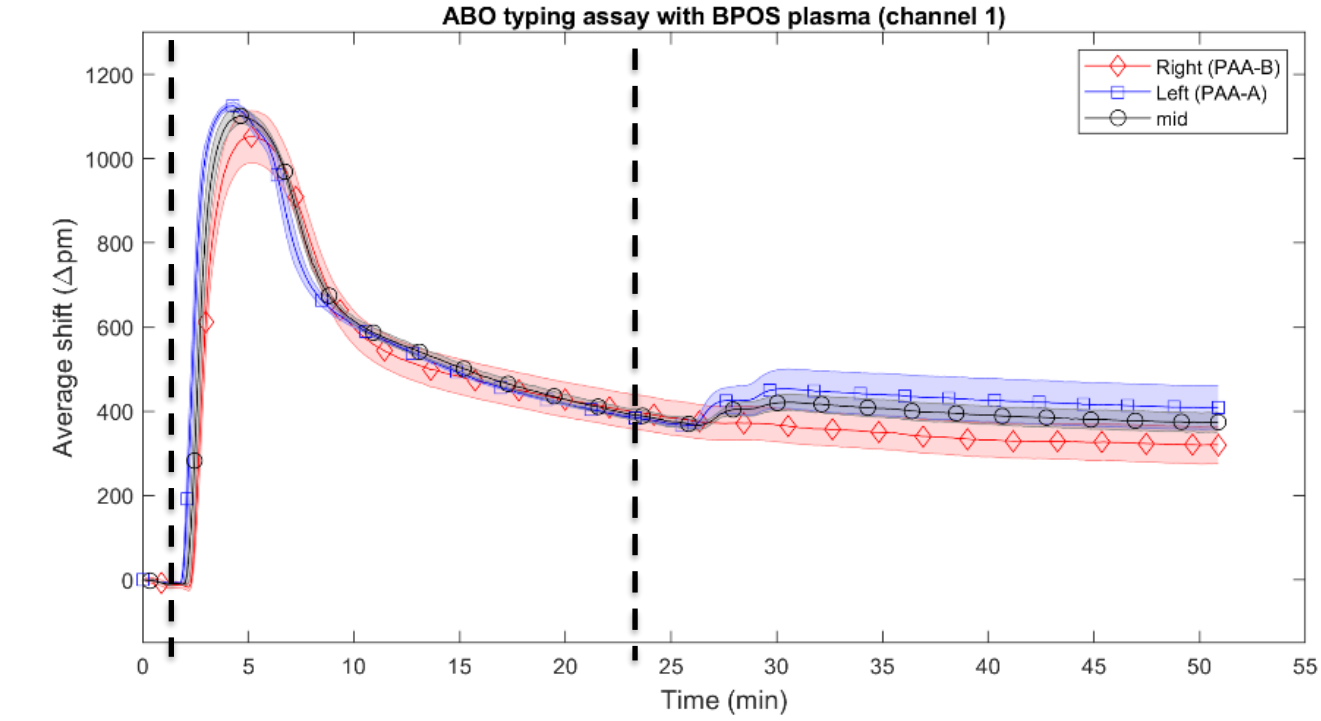

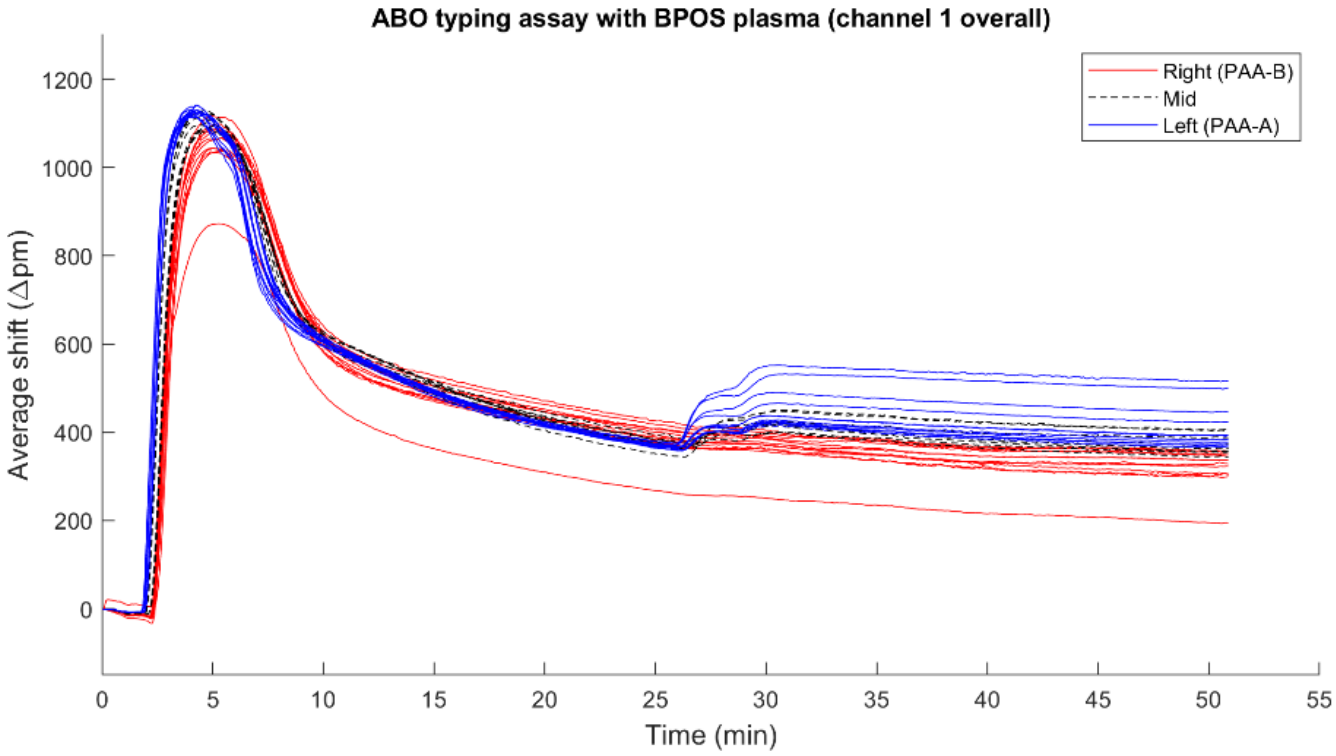

Figure 42: ABO reverse typing assay with type B plasma

20 µL of Type-B plasma added to inlet 2 at 1:00

20 µL 1 mg/mL secondary (goat anti-human IgG/A/M) placed at inlet 2 at 21:10

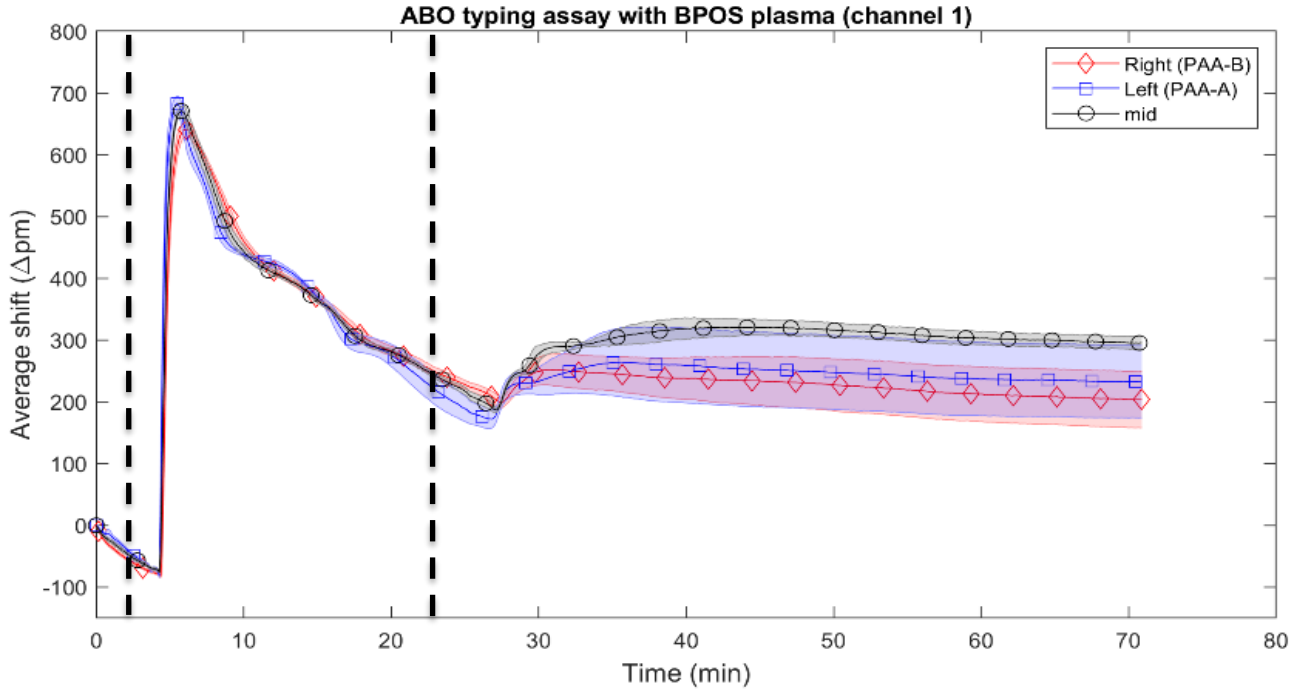

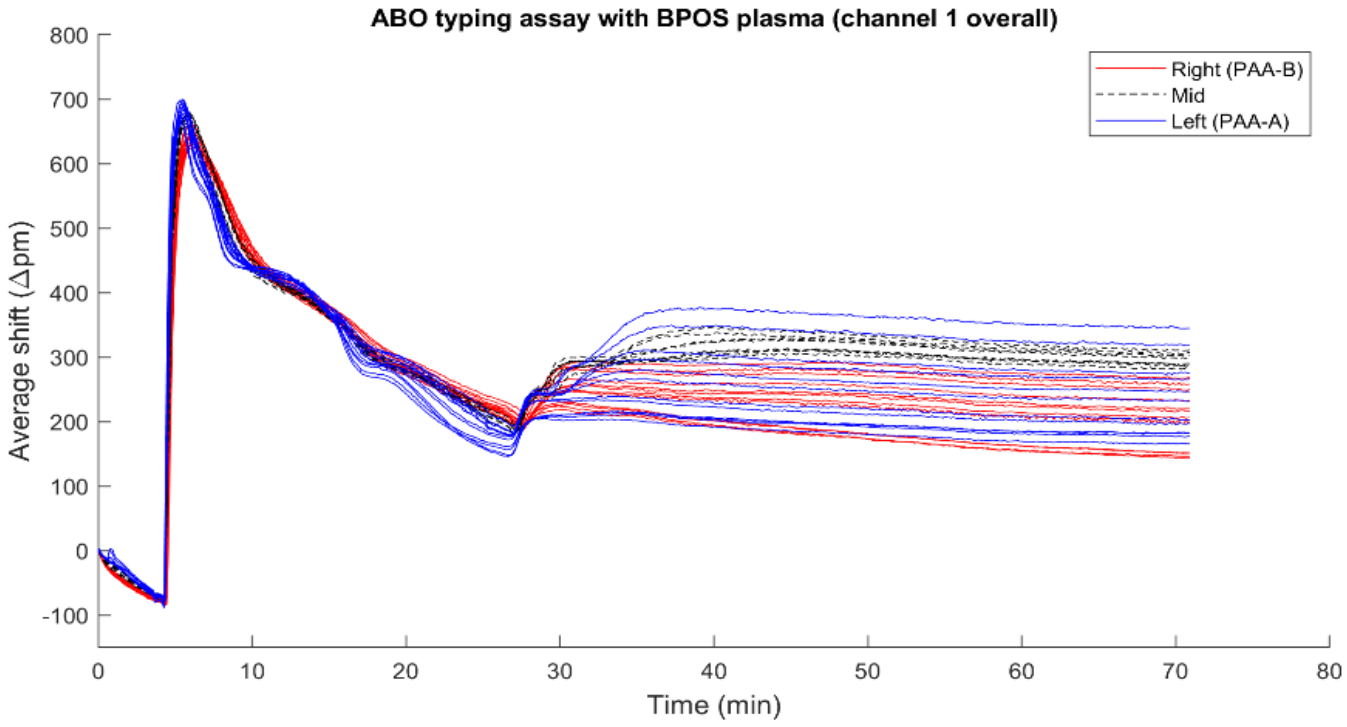

Figure 43: ABO reverse typing assay with type B plasma (replicate 2)

5.3.4 *ABO reverse typing assay with whole blood (25 µL)*

Examples of attempted ABO reverse typing assays with 25 µL of whole blood are shown in figures 44 and 45. In both figures, we were using type APOS blood which contains anti-B IgM antibody. Therefore, we would expect a higher and specific response from the right side of the chip. With both assays, we do not see this and instead observe the left side does not differentially behave when compared to the right when the secondary antibody is added both times. We cannot determine if these negative results were caused by the inactivity of the PAA-B (shown not to be functional in figure 41), or the low antibody titer in only 25 µL of whole blood.

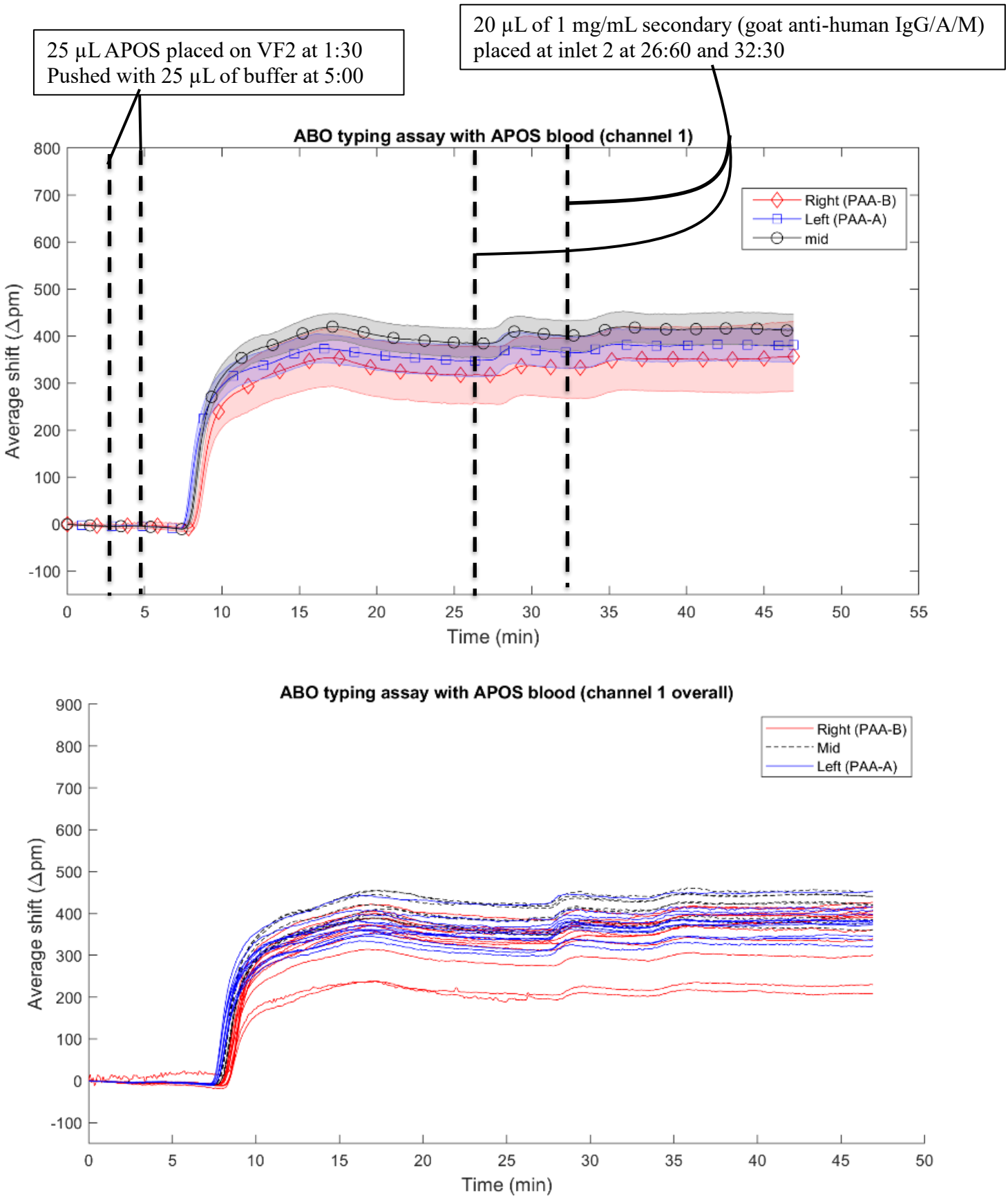

Figure 44: ABO reverse typing assay with 25 microliters of whole blood

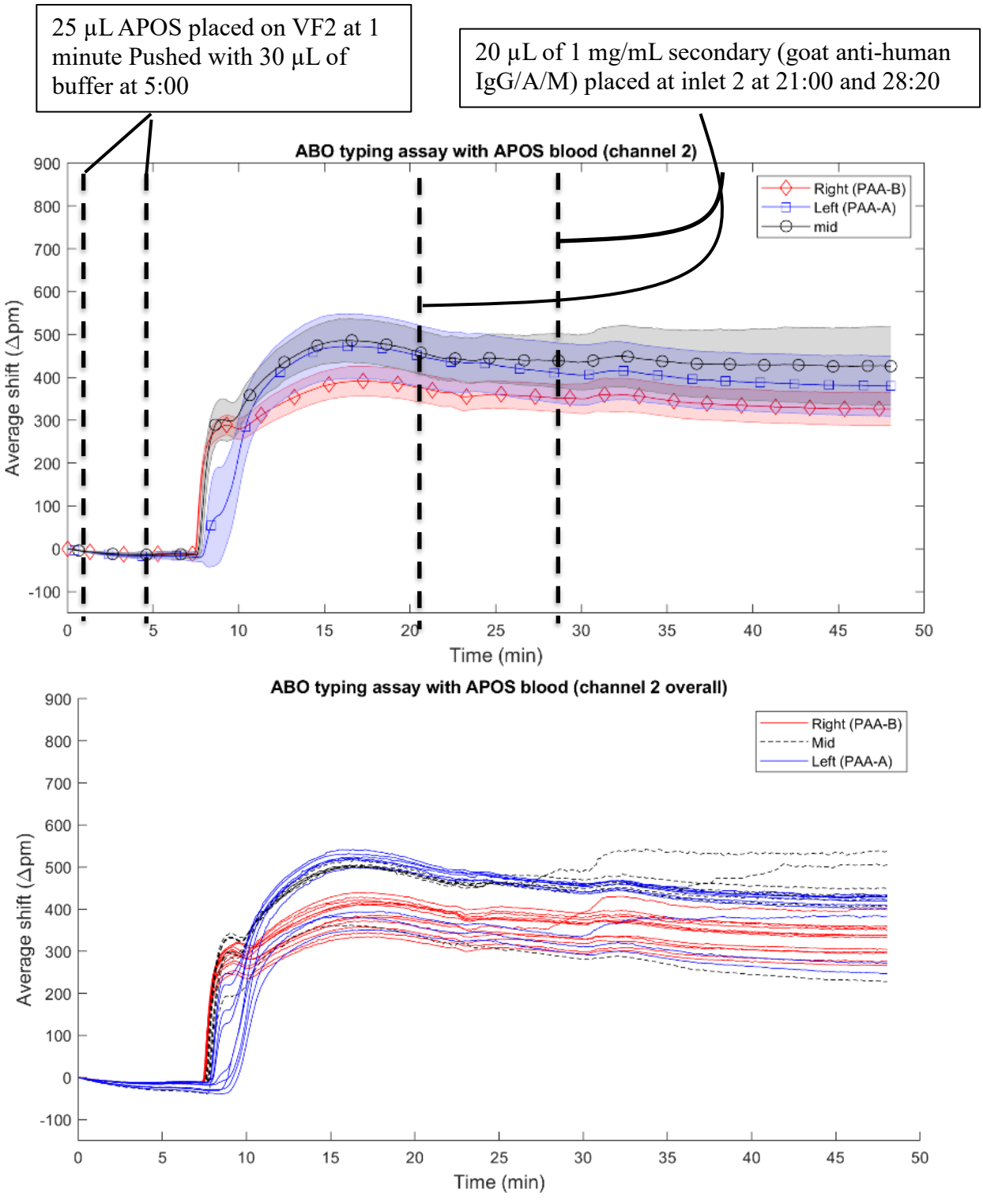

Figure 45:ABO reverse typing assay with 25 microliters of whole blood (replicate 2)

5.3.5 *ABO reverse typing assay with whole blood (50 µL)*

In order to increase the antibody titer in the sample passing over the chip, we increased the volume of blood in the assay. To separate out 20 µL of plasma, the same volume used in the assays shown in figures 42 and 43 (assuming a hematocrit of ~45%), we would require ~50 µL of whole blood. In order to perform an assay with this volume of plasma separation, we added two 7.5 by 7.5 mm VF2 membranes over the 5 by 5 MF1 (in inlet #1); this setup is shown in figure 46. Two examples of typing assays with 50 µL of BPOS whole blood are shown in figures 47 and 48. In both figures/runs we see that the secondary antibody only showed a partially positive response after the addition of the secondary. The type BPOS blood contains anti-A antibodies and we would expect that after the secondary is added the left side would have a higher shift/response as there should be more human anti-A antibodies bound to the left side of the chip. For both assays, we ran a validation step to ensure that that the chip was functionalized and so we ran over anti-A murine antibodies with the expectation that the left side of the chip will have a higher specific signal than the right side (after the buffer brings it back to baseline). The response we observe for the left side of the chip after the secondary for the overall and average results is higher and more specific for the left side than the right indicating the chips were functionalized. This difference between the left and the right after validation is more pronounced in figure 47 indicating that the chip in 47 may have been more robustly functionalized than in figure 48; but overall, they both showed a positive validation step. We note there is less of an offset between the left and the right side of the chip in figure 48 before the secondary is added as compared to the offset in figure 47. This indicates the differential increase in response after the secondary is more likely to be specific in figure 48. However, we do concede that these results only suggest a partial positive response and only demonstrates a proof of concept. Also note that there was heme and cell material leaked through

the membrane and system as we see the high-frequency signal after we push the sample through with PBS. While these results were encouraging, we wanted to try to separate a higher volume of blood to even further increase the titer and chance of a higher positive response. We ran blood volumes from 75-100 µL but none of these assays succeeded and are shown in the appendix. When trying to separate these high volumes the VF2 membrane seemed to clog and indicate we could not just stack more VF2 to separate more volume of whole blood. This clogging would cause a build of surface tension and the blood sample would overflow and leak into the channel. To prevent this from happening we would need to increase the area of the membrane for each specific volume of blood. With this leakage of heme and cells, the chip had more visible fouling and did not respond well to the secondary amplification antibody.

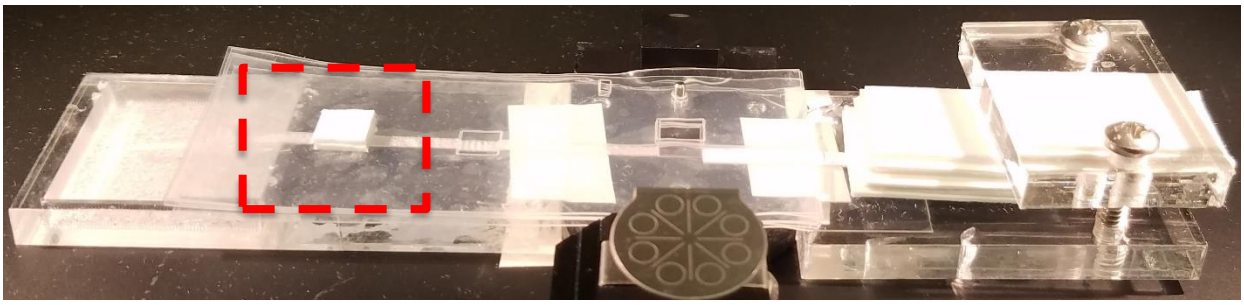

Figure 46: Image of mount with two 7.5 by 7.5 mm VF2 membranes

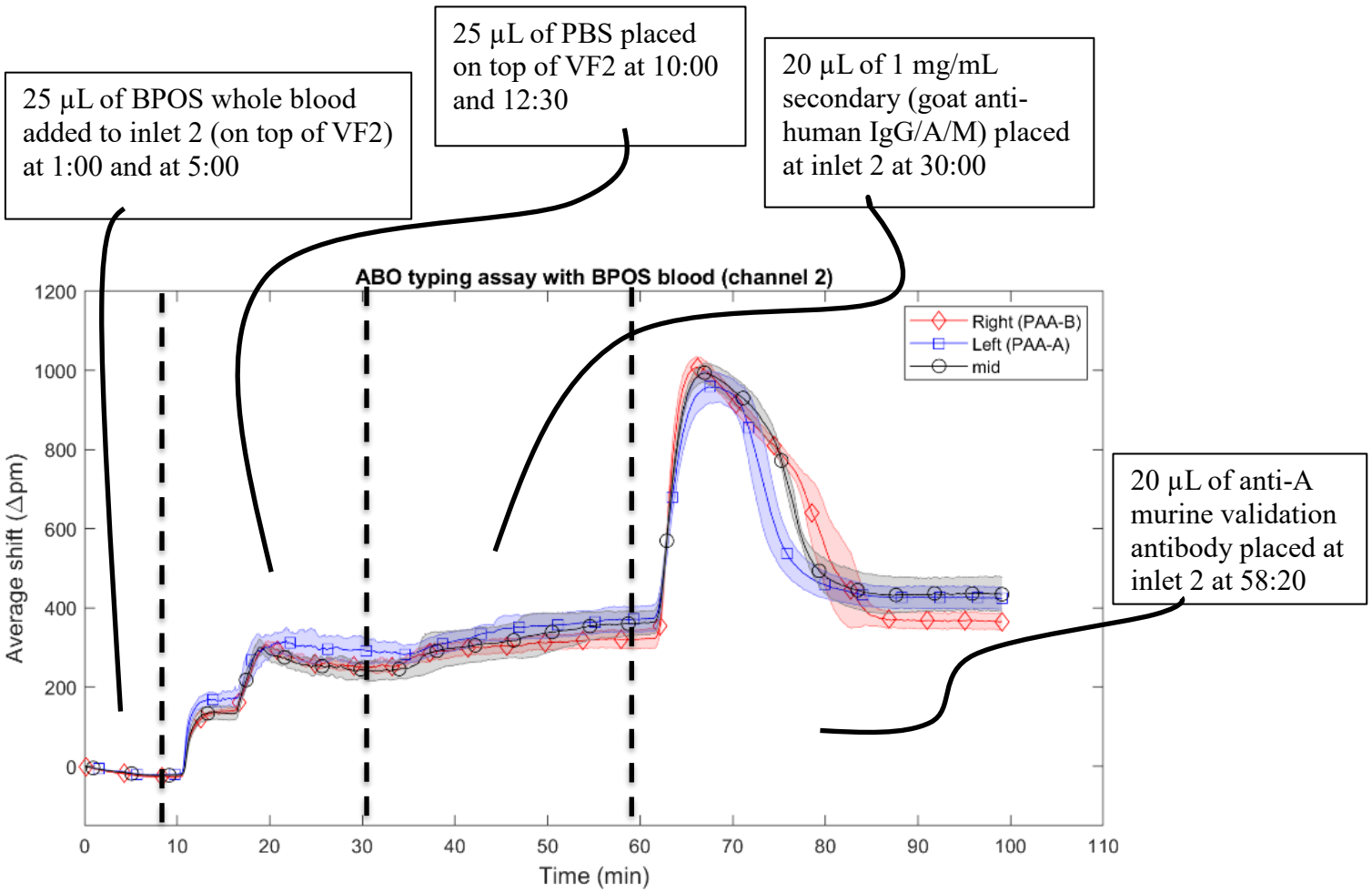

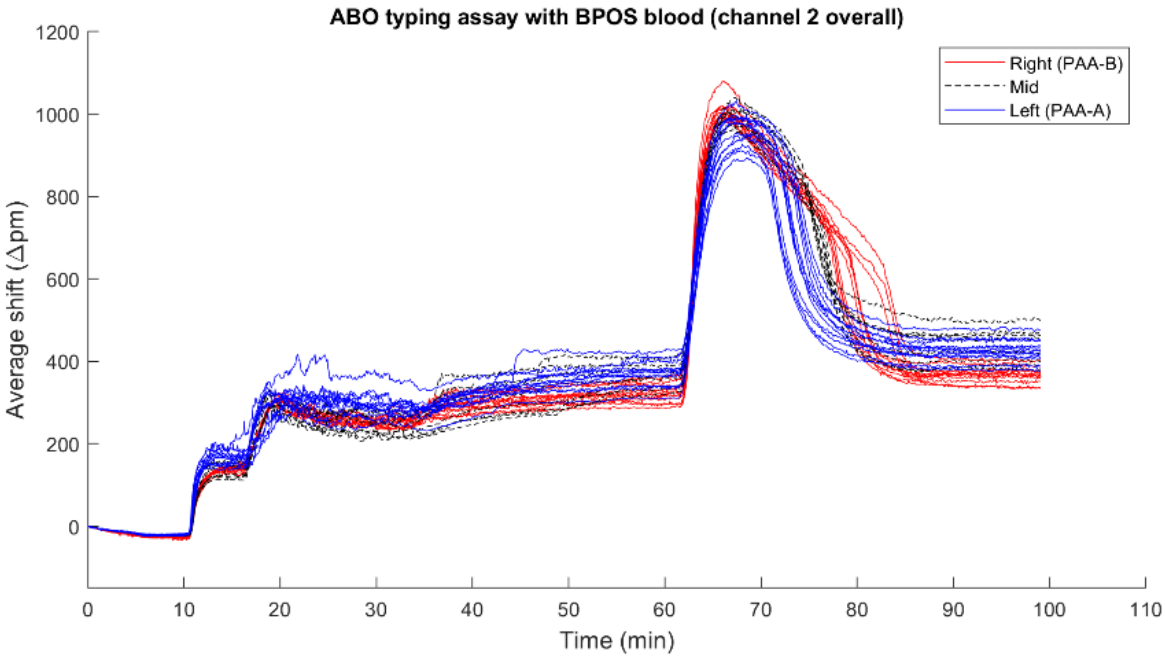

Figure 47: ABO reverse typing assay with BPOS whole blood

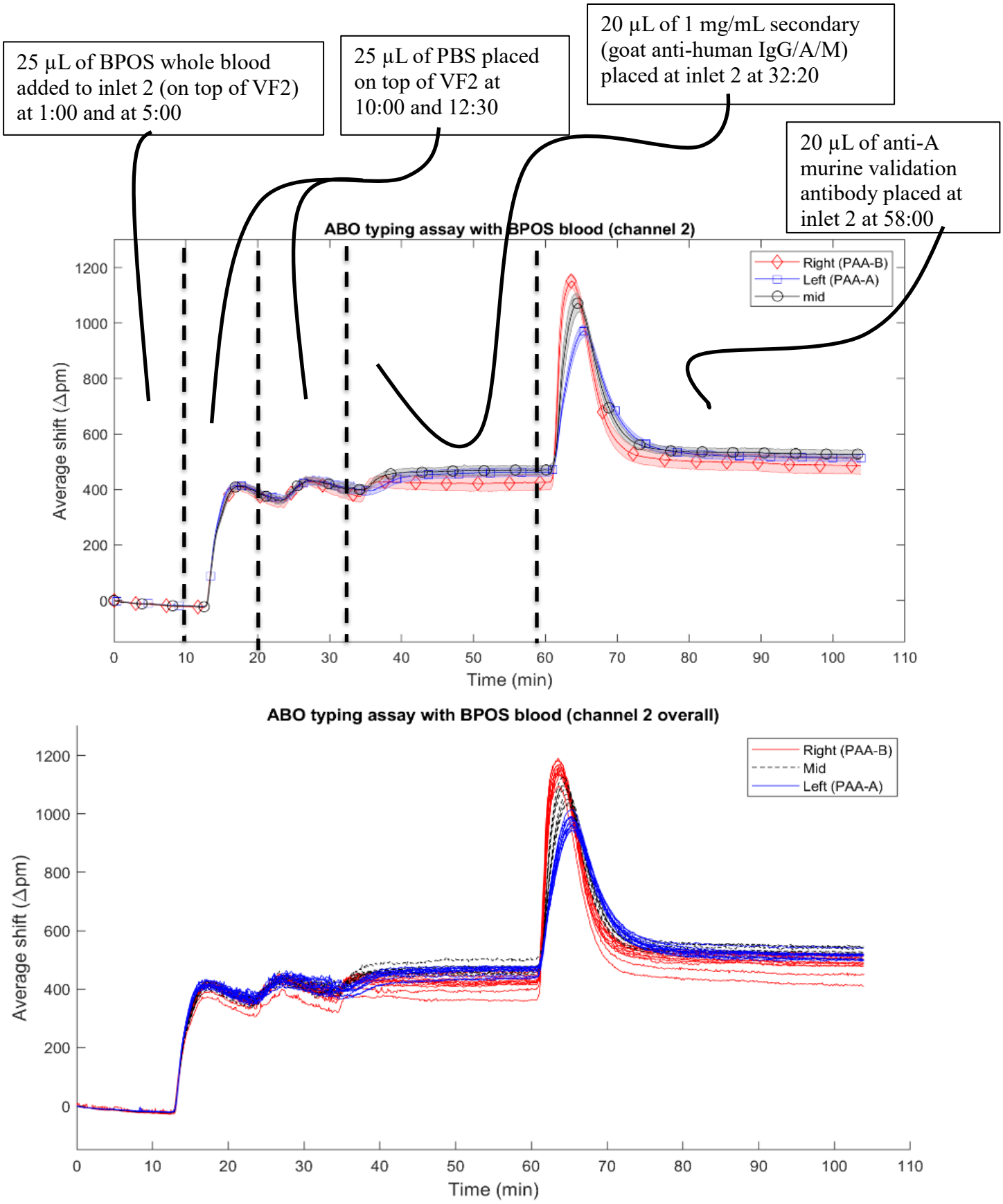

Figure 48: ABO reverse typing assay with BPOS whole blood (replicate 2)

Chapter 6. CONCLUSION AND FUTURE WORK

6.1 ASSESSMENT OF ACCOMPLISHMENTS AND COMPARISON TO PAST WORK

At the conclusion of my thesis, we met most of our engineering design goals. These specifications include:

1) The mount/gaskets were integrated and reusable for our OEM silicon photonic platform (Genalyte)
2) The gaskets included area for plasma separation membrane
3) The gaskets minimized leaking and produced a uniform flow profile

We did demonstrate efficient plasma separation with our system as shown in 5.2. We concede that we did not optimize or consistently demonstrate a convincing ABO typing assay using whole blood separation. When we tried to separate volumes of whole blood higher than 50 µL there was much fouling and heme/cell leakage and we found that this potentially prevented a robust response from the amplification antibody. This separation can be optimized by increasing the area of the VF2 membrane and the size of the inlet window by length (5 by 5 mm to 5 by x mm where x is greater than 5 and lengthwise) to achieve a high enough antibody titer to successfully perform an ABO reverse typing assay. Follow-up optimization is required to determine the impact of heme and cell leakage ABO typing assay as we could not determine if it was the poor separation (i.e. we did not push out enough plasma from the membrane) or the fouling of the chip that caused the failure.

In our previous work integrating paper fluidic reagent delivery on our custom silicon photonic platform, we successfully demonstrated an ABO reverse typing assay with human plasma. We were able to demonstrate the same typing results using the previous assay protocol

with our paper fluidic mount on the Genalyte and we illustrated similar fluid dynamic capabilities. On our system, we improved the clamp on the absorbent pad with an acyclic piece with screws threaded so that we can have an even pressure on top of the pad. We also included gaskets that can accommodate vertical paper-based plasma separation and demonstrated successful plasma separation within our system.

6.2 INNOVATION IN THE SHORT TERM

There are various design and assembly changes this system and project would benefit from, these alterations include:

1) Permanently bond gaskets together and create a bottom gasket that permanently levels the chip on the mount
2) Design gaskets that can accommodate a larger area of separation membrane and gaskets that can implement horizontal separation
3) Increase with width of the nitrocellulose membrane to observe the upper flow rate limit and increase the overall speed of the assays

In order to bond the gaskets together, we can use silicon glue or consider fabricating them from a more rigid and watertight material. To increase the volume of blood used in the separation design we can utilize Ahlstrom horizontal plasma separators that are treated with agglutination agents. Other than changing the dimensions and plasma separation membrane we can implement a way to have the separation membrane separate while dry and then have a step incorporating it into the glass fiber. This design will require careful engineering but is also something to consider as the separation membranes operate best when not pre-wet.

6.3 ABO TYPING ASSAY AND BEYOND

The system we designed focuses on reverse ABO blood typing, but we would like to include a way to forward type with our paper fluidic adaptation. In this project, we demonstrated that cell/heme leakage into the network from the separation membrane does not stop the flow in the system. With this knowledge, it is conceivable that we could optimize our separation such that the right amount of plasma and cells with surface antigens would pass over the surface of the chip to run a reverse and forward ABO typing assay while preventing excess fouling.

The Ratner lab leverages silicon photonic biosensors mostly for ABO blood typing but there are many other serologic assays that can be run with the platform as described in chapter 2. Our system was validated with the reverse ABO typing assay, but we would like to demonstrate the generalizability of the mount potentially with an assay detecting bloodborne pathogens/proteins like Chagas, malaria or prostate-specific antigen. These assays can integrate with the whole blood separation step but would first be validated with spun down plasma.

This project was the culmination of 2 years my own work facilitated by previous work done in the Ratner lab. With this thesis, we successfully integrated paper fluidic reagent delivery into our OEM silicon photonic platform and demonstrated that paper-based plasma separation was possible within the system. With validated the system with a reverse ABO typing assay with human plasma and integrated plasma separation. We have not yet demonstrated a reverse ABO typing assay with whole blood. However, with further optimization, we can produce a more robust proof-of-concept. After the completion of this thesis, we have a foundation of paper fluidic mounts and adaptation designs for the OEM Genalyte silicon photonic platform of which we can build off for future work in the lab.

As diagnostic tests become more point-of-care, continuous and quantitative silicon photonic biosensors are likely to play a larger role in the clinical diagnostic infrastructure. However, the technology will only fill this role if the costs and complexity of the systems are decreased. We hope that this thesis and auxiliary work in the Ratner lab will bring the technology closer to the clinic and towards a more lab-on-a-chip idealization.

BIBLIOGRAPHY

1. Esteva, A.; Kuprel, B.; Novoa, R. A.; Ko, J.; Swetter, S. M.; Blau, H. M.; Thrun, S., Dermatologist-level classification of skin cancer with deep neural networks. *Nature* **2017,** *542* (7639), 115.
2. McClatchey, K. D., *Clinical laboratory medicine*. Lippincott Williams & Wilkins: 2002.
3. Lodwig, V.; Heinemann, L., Continuous glucose monitoring with glucose sensors: calibration and assessment criteria. *Diabetes technology & therapeutics* **2003,** *5* (4), 572-586.
4. Baker, B. R.; Lai, R. Y.; Wood, M. S.; Doctor, E. H.; Heeger, A. J.; Plaxco, K. W., An electronic, aptamer-based small-molecule sensor for the rapid, label-free detection of cocaine in adulterated samples and biological fluids. *Journal of the American Chemical Society* **2006,** *128* (10), 3138-3139.
5. Bogaerts, W.; De Heyn, P.; Van Vaerenbergh, T.; De Vos, K.; Kumar Selvaraja, S.; Claes, T.; Dumon, P.; Bienstman, P.; Van Thourhout, D.; Baets, R., Silicon microring resonators. *Laser & Photonics Reviews* **2012,** *6* (1), 47-73.
6. Bailey, R. C.; Washburn, A. L.; Qavi, A. J.; Iqbal, M.; Gleeson, M.; Tybor, F.; Gunn, L. C. In *A robust silicon photonic platform for multiparameter biological analysis*, Silicon Photonics IV, International Society for Optics and Photonics: 2009; p 72200N.
7. Kirk, J. T.; Fridley, G. E.; Chamberlain, J. W.; Christensen, E. D.; Hochberg, M.; Ratner, D. M., Multiplexed inkjet functionalization of silicon photonic biosensors. *Lab on a Chip* **2011,** *11* (7), 1372-1377.
8. Rivet, C.; Lee, H.; Hirsch, A.; Hamilton, S.; Lu, H., Microfluidics for medical diagnostics and biosensors. *Chemical Engineering Science* **2011,** *66* (7), 1490-1507.
9. Iqbal, M.; Gleeson, M. A.; Spaugh, B.; Tybor, F.; Gunn, W. G.; Hochberg, M.; Baehr-Jones, T.; Bailey, R. C.; Gunn, L. C., Label-free biosensor arrays based on silicon ring resonators and high-speed optical scanning instrumentation. *IEEE Journal of Selected Topics in Quantum Electronics* **2010,** *16* (3), 654-661.
10. Jokerst, N. M.; Luan, L.; Palit, S.; Royal, M.; Dhar, S.; Brooke, M.; Tyler II, T., Progress in chip-scale photonic sensing. *IEEE transactions on biomedical circuits and systems* **2009,** *3* (4), 202-211.
11. Heck, M. J.; Bauters, J. F.; Davenport, M. L.; Doylend, J. K.; Jain, S.; Kurczveil, G.; Srinivasan, S.; Tang, Y.; Bowers, J. E., Hybrid silicon photonic integrated circuit technology. *IEEE J. Sel. Top. Quantum Electron* **2013,** *19* (4), 6100117.
12. Fard, S. T.; Donzella, V.; Schmidt, S. A.; Flueckiger, J.; Grist, S. M.; Fard, P. T.; Wu, Y.; Bojko, R. J.; Kwok, E.; Jaeger, N. A., Performance of ultra-thin SOI-based resonators for sensing applications. *Optics express* **2014,** *22* (12), 14166-14179.
13. Schmidt, S. Enhancing the performance of silicon photonic biosensors for clinical applications. 2017.
14. Kirk, J. T.; Lannert, K. W.; Ratner, D. M.; Johnsen, J. M., Serologic and Phenotypic Analysis of Blood Types Via Silicon Nanophotonics. *Blood* **2014,** *124* (21), 1565-1565.
15. Williams, D. F.; Lyman, D., *Blood compatibility*. CRC press Boca Raton, FL: 1987; Vol. 1.
16. Storry, J.; Olsson, M. L., The ABO blood group system revisited: a review and update. *Immunohematology* **2009,** *25* (2), 48.
17. Mujahid, A.; Dickert, F., Blood group typing: From classical strategies to the application of synthetic antibodies generated by molecular imprinting. *Sensors* **2016,** *16* (1), 51.
18. Kim, D. S.; Lee, S. H.; Ahn, C. H.; Lee, J. Y.; Kwon, T. H., Disposable integrated microfluidic biochip for blood typing by plastic microinjection moulding. *Lab on a Chip* **2006,** *6* (6), 794-802.
19. Goodnough, L. T.; Brecher, M. E.; Kanter, M. H.; AuBuchon, J. P., Transfusion medicine—blood transfusion. *New England Journal of Medicine* **1999,** *340* (6), 438-447.
20. Gordon, R. D.; Iwatsuki, S.; Esquivel, C. O.; Tzakis, A.; Todo, S.; Starzl, T. E., Liver transplantation across ABO blood groups. *Surgery* **1986,** *100* (2), 342-348.
21. Kalra, J., Medical errors: impact on clinical laboratories and other critical areas. *Clinical biochemistry* **2004,** *37* (12), 1052-1062.
22. Bonini, P.; Plebani, M.; Ceriotti, F.; Rubboli, F., Errors in laboratory medicine. *Clinical chemistry* **2002,** *48* (5), 691-698.
23. Linden, J.; Paul, B.; Dressler, K., A report of 104 transfusion errors in New York State. *Transfusion* **1992,** *32* (7), 601-606.
24. Linden, J. V.; Wagner, K.; Voytovich, A. E.; Sheehan, J., Transfusion errors in New York State: an analysis of 10 years' experience. *Transfusion* **2000,** *40* (10), 1207-1213.
25. Washburn, A. L.; Bailey, R. C., Photonics-on-a-chip: recent advances in integrated waveguides as enabling detection elements for real-world, lab-on-a-chip biosensing applications. *Analyst* **2011,** *136* (2), 227-236.
26. Luchansky, M. S.; Bailey, R. C., Silicon photonic microring resonators for quantitative cytokine detection and T-cell secretion analysis. *Analytical chemistry* **2010,** *82* (5), 1975-1981.
27. Vollmer, F.; Arnold, S.; Keng, D., Single virus detection from the reactive shift of a whispering-gallery mode. *Proceedings of the National Academy of Sciences* **2008,** *105* (52), 20701-20704.
28. Shang, J.; Cheng, F.; Dubey, M.; Kaplan, J. M.; Rawal, M.; Jiang, X.; Newburg, D. S.; Sullivan, P. A.; Andrade, R. B.; Ratner, D. M., An organophosphonate strategy for functionalizing silicon photonic biosensors. *Langmuir* **2012,** *28* (6), 3338-3344.
29. Heideman, R.; Hoekman, M.; Schreuder, E., TriPleX-based integrated optical ring resonators for lab-on-a-chip and environmental detection. *IEEE Journal of Selected topics in quantum electronics* **2012,** *18* (5), 1583-1596.
30. Chrostowski, L.; Hochberg, M., *Silicon photonics design: from devices to systems*. Cambridge University Press: 2015.
31. De Vos, K.; Bartolozzi, I.; Schacht, E.; Bienstman, P.; Baets, R., Silicon-on-Insulator microring resonator for sensitive and label-free biosensing. *Optics express* **2007,** *15* (12), 7610-7615.
32. Morrow, N. R., Physics and thermodynamics of capillary action in porous media. *Industrial & Engineering Chemistry* **1970,** *62* (6), 32-56.
33. Roselli, R. J.; Diller, K. R., *Biotransport: principles and applications*. Springer Science & Business Media: 2011.
34. Araújo, A.; Andrade Jr, J. S.; Herrmann, H. J., Critical role of gravity in filters. *Physical review letters* **2006,** *97* (13), 138001.
35. Fu, E.; Ramsey, S. A.; Kauffman, P.; Lutz, B.; Yager, P., Transport in two-dimensional paper networks. *Microfluidics and nanofluidics* **2011,** *10* (1), 29-35.
36. Lutz, B. R.; Trinh, P.; Ball, C.; Fu, E.; Yager, P., Two-dimensional paper networks: programmable fluidic disconnects for multi-step processes in shaped paper. *Lab on a Chip* **2011,** *11* (24), 4274-4278.

37. Sajid, M.; Kawde, A.-N.; Daud, M., Designs, formats and applications of lateral flow assay: A literature review. *Journal of Saudi Chemical Society* **2015,** *19* (6), 689-705.
38. Ngom, B.; Guo, Y.; Wang, X.; Bi, D., Development and application of lateral flow test strip technology for detection of infectious agents and chemical contaminants: a review. *Analytical and bioanalytical chemistry* **2010,** *397* (3), 1113-1135.
39. Posthuma-Trumpie, G. A.; Korf, J.; van Amerongen, A., Lateral flow (immuno) assay: its strengths, weaknesses, opportunities and threats. A literature survey. *Analytical and bioanalytical chemistry* **2009,** *393* (2), 569-582.
40. Anfossi, L.; Baggiani, C.; Giovannoli, C.; D'Arco, G.; Giraudi, G., Lateral-flow immunoassays for mycotoxins and phycotoxins: a review. *Analytical and bioanalytical chemistry* **2013,** *405* (2-3), 467-480.
41. Martinez, A. W.; Phillips, S. T.; Whitesides, G. M.; Carrilho, E., Diagnostics for the developing world: microfluidic paper-based analytical devices. ACS Publications: 2009.
42. Jung, W.; Han, J.; Choi, J.-W.; Ahn, C. H., Point-of-care testing (POCT) diagnostic systems using microfluidic lab-on-a-chip technologies. *Microelectronic Engineering* **2015,** *132*, 46-57.
43. Clark, T. J.; McPherson, P. H.; Buechler, K. F., The triage cardiac panel: Cardiac markers for the triage system. *Point of Care* **2002,** *1* (1), 42-46.
44. Ge, L.; Yan, J.; Song, X.; Yan, M.; Ge, S.; Yu, J., Three-dimensional paper-based electrochemiluminescence immunodevice for multiplexed measurement of biomarkers and point-of-care testing. *Biomaterials* **2012,** *33* (4), 1024-1031.
45. Lin, L.; Guthrie, J., Preparation and characterisation of novel, blood-plasma-separation membranes for use in biosensors. *Journal of Membrane Science* **2000,** *173* (1), 73-85.
46. Yang, X.; Forouzan, O.; Brown, T. P.; Shevkoplyas, S. S., Integrated separation of blood plasma from whole blood for microfluidic paper-based analytical devices. *Lab on a Chip* **2012,** *12* (2), 274-280.
47. Liana, D. D.; Raguse, B.; Gooding, J. J.; Chow, E., Recent advances in paper-based sensors. *Sensors* **2012,** *12* (9), 11505-11526.
48. Songjaroen, T.; Dungchai, W.; Chailapakul, O.; Henry, C. S.; Laiwattanapaisal, W., Blood separation on microfluidic paper-based analytical devices. *Lab on a Chip* **2012,** *12* (18), 3392-3398.
49. Chrostowski, L.; Grist, S.; Flueckiger, J.; Shi, W.; Wang, X.; Ouellet, E.; Yun, H.; Webb, M.; Nie, B.; Liang, Z. In *Silicon photonic resonator sensors and devices*, Laser Resonators, Microresonators, and Beam Control XIV, International Society for Optics and Photonics: 2012; p 823620.
50. Ratner, D. M.; Johnsen, J. M.; Kirk, J. T.; López, J. A.; Brault, N. D.; Jiang, S., Photonic blood typing. Google Patents: 2017.
51. Suter, J. D.; White, I. M.; Zhu, H.; Shi, H.; Caldwell, C. W.; Fan, X., Label-free quantitative DNA detection using the liquid core optical ring resonator. *Biosensors and Bioelectronics* **2008,** *23* (7), 1003-1009.
52. Vollmer, F.; Braun, D.; Libchaber, A.; Khoshsima, M.; Teraoka, I.; Arnold, S., Protein detection by optical shift of a resonant microcavity. *Applied physics letters* **2002,** *80* (21), 4057-4059.
53. Ramachandran, A.; Wang, S.; Clarke, J.; Ja, S.; Goad, D.; Wald, L.; Flood, E.; Knobbe, E.; Hryniewicz, J.; Chu, S., A universal biosensing platform based on optical micro-ring resonators. *Biosensors and Bioelectronics* **2008,** *23* (7), 939-944.
54. Khumwan, P. Simultaneous Serologic and Phenotypic Analyses of Blood on Silicon Photonics. University of Washington, University of Washington digital library, 2018.

APPENDIX

Flow rate replicates:

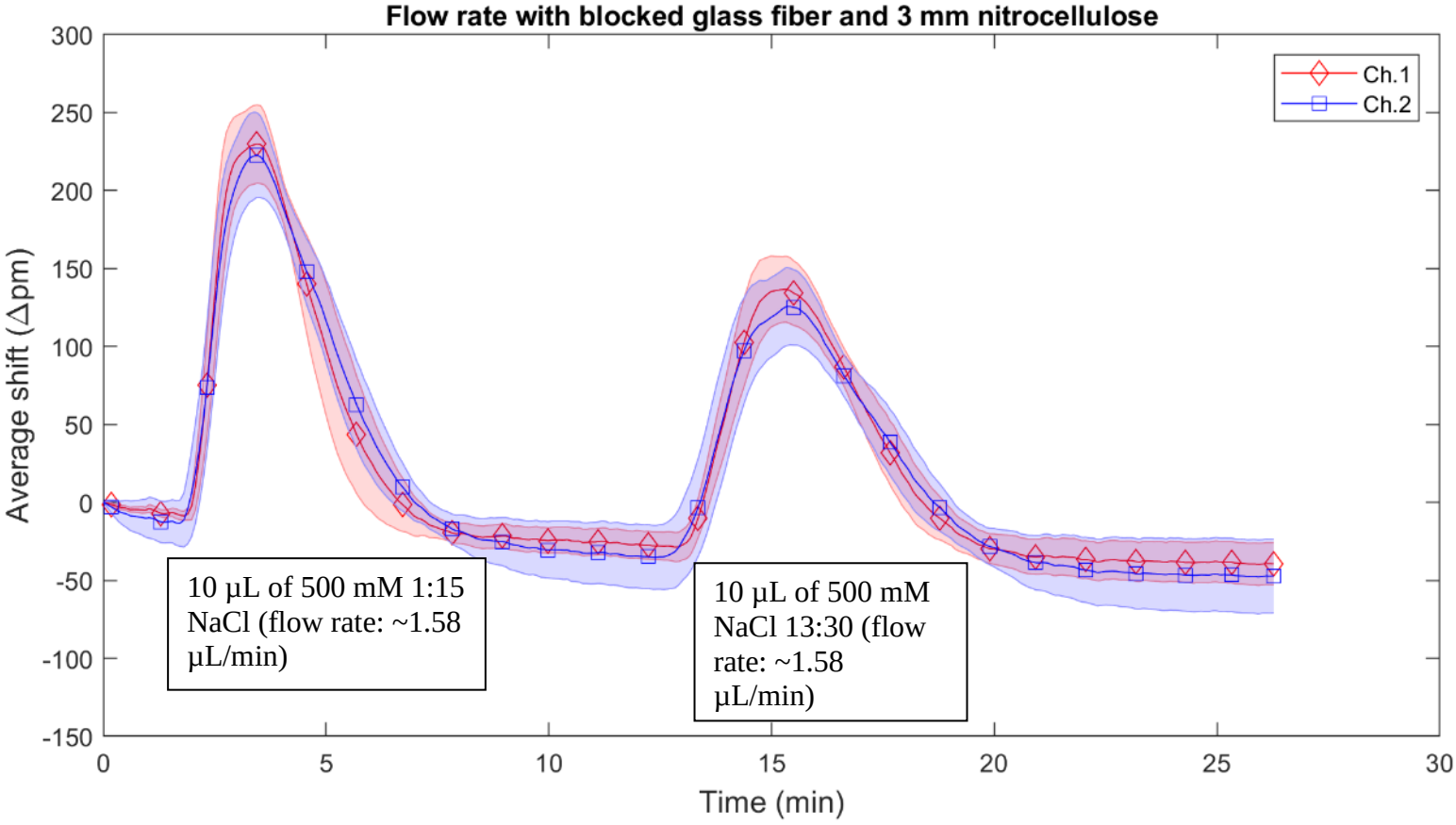

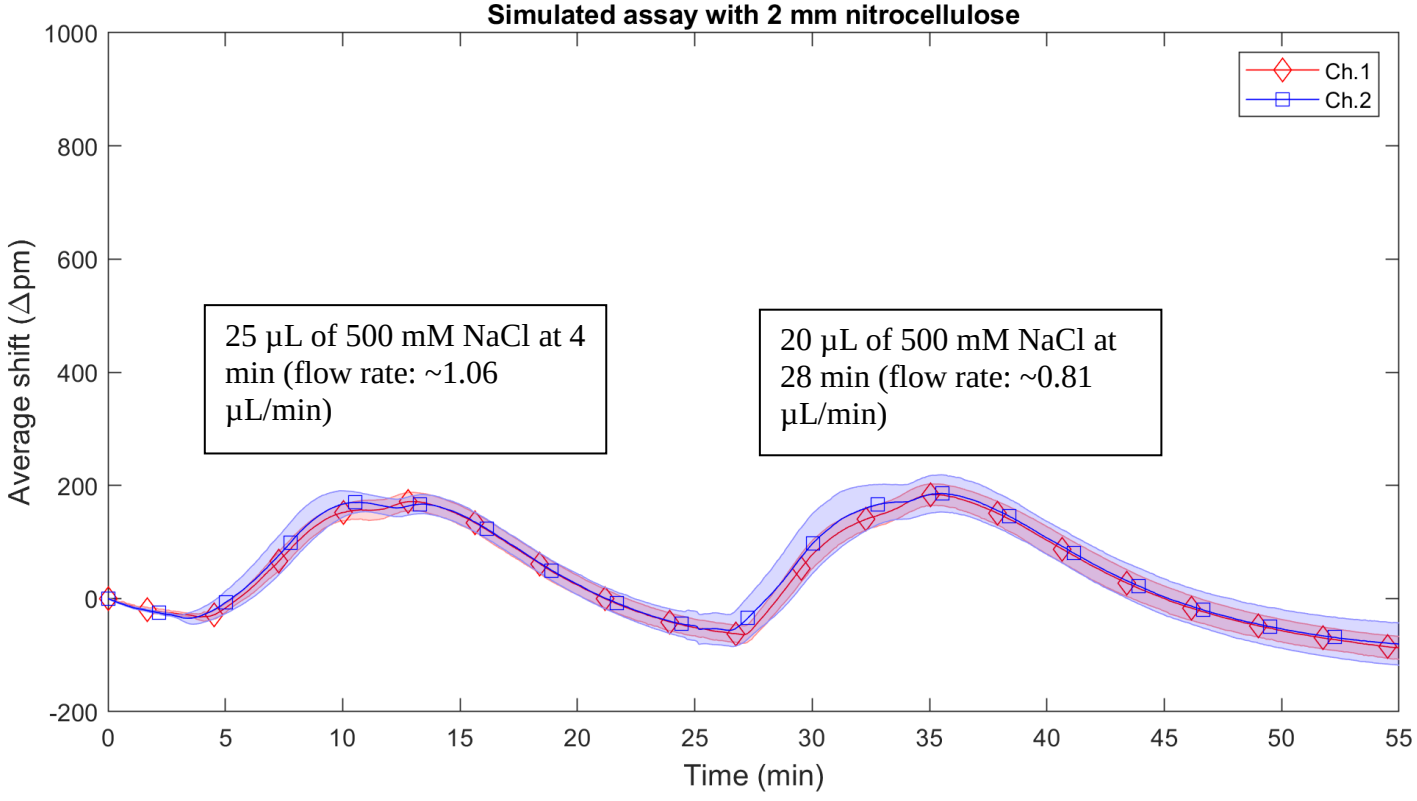

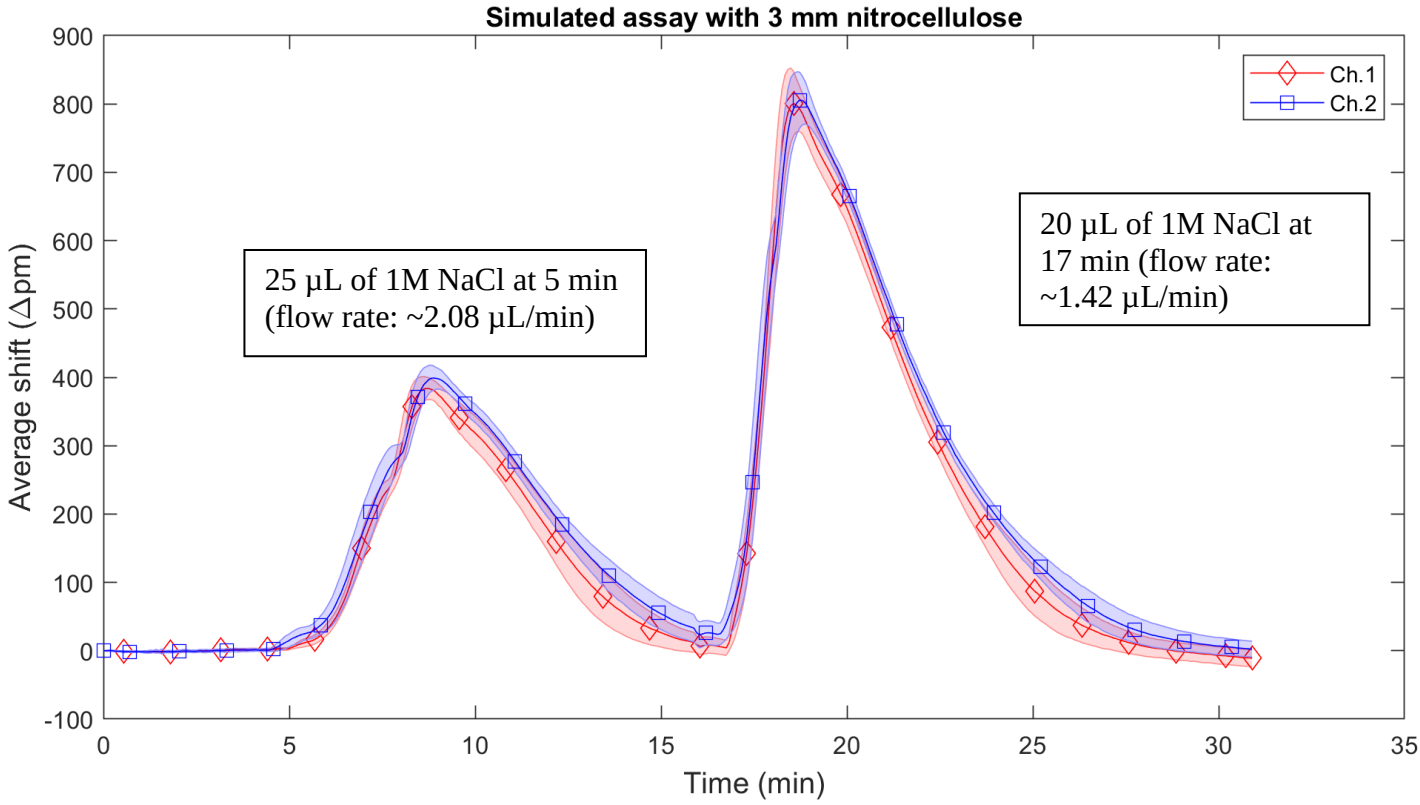
Simulated assay with 3 mm nitrocellulose
Ch.1
Ch.2
25 µL of 1M NaCl at 5 min (flow rate: ~2.08 µL/min)
20 µL of 1M NaCl at 17 min (flow rate: ~1.42 µL/min)
Average shift (Δpm)
Time (min)

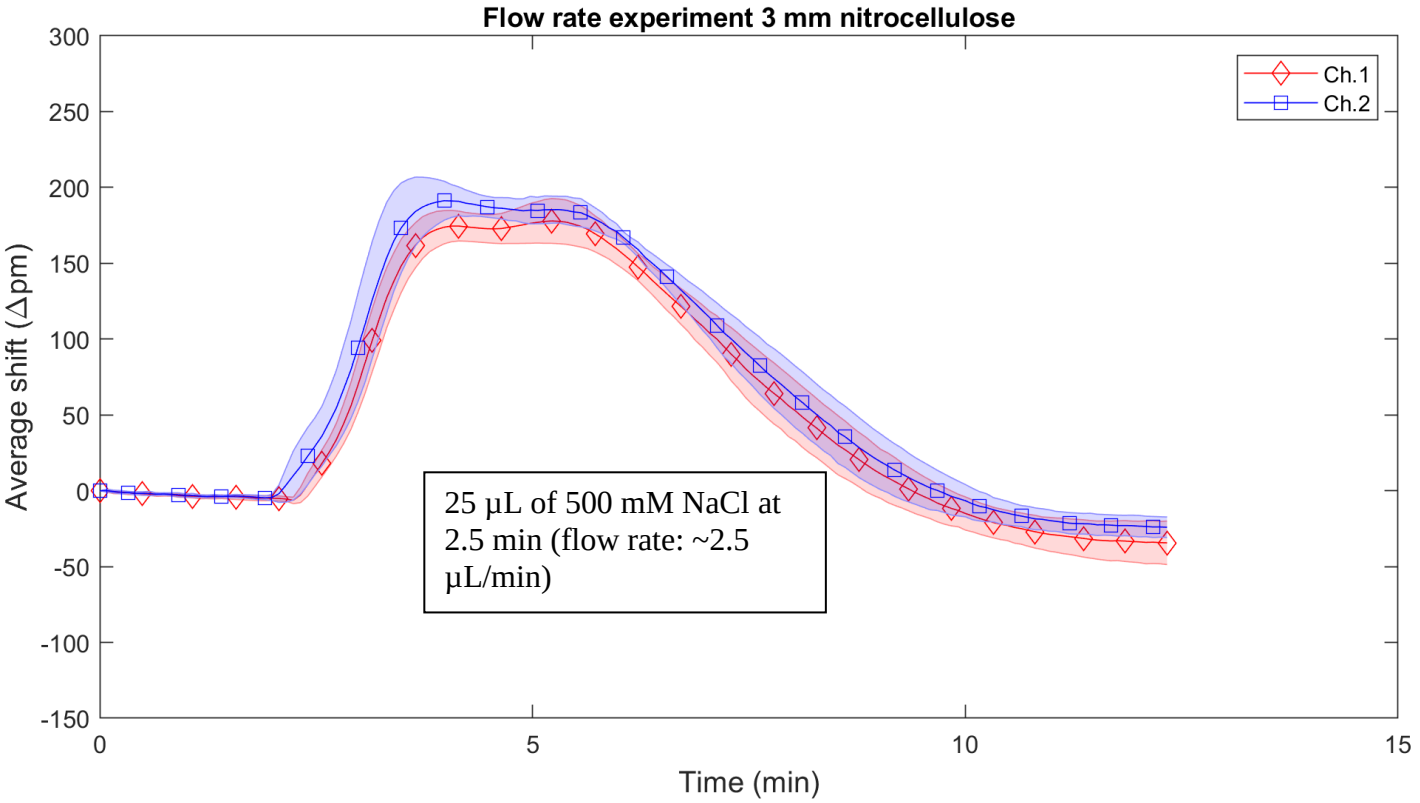
Flow rate experiment 3 mm nitrocellulose
Ch.1
Ch.2
25 µL of 500 mM NaCl at 2.5 min (flow rate: ~2.5 µL/min)
Average shift (Δpm)
Time (min)

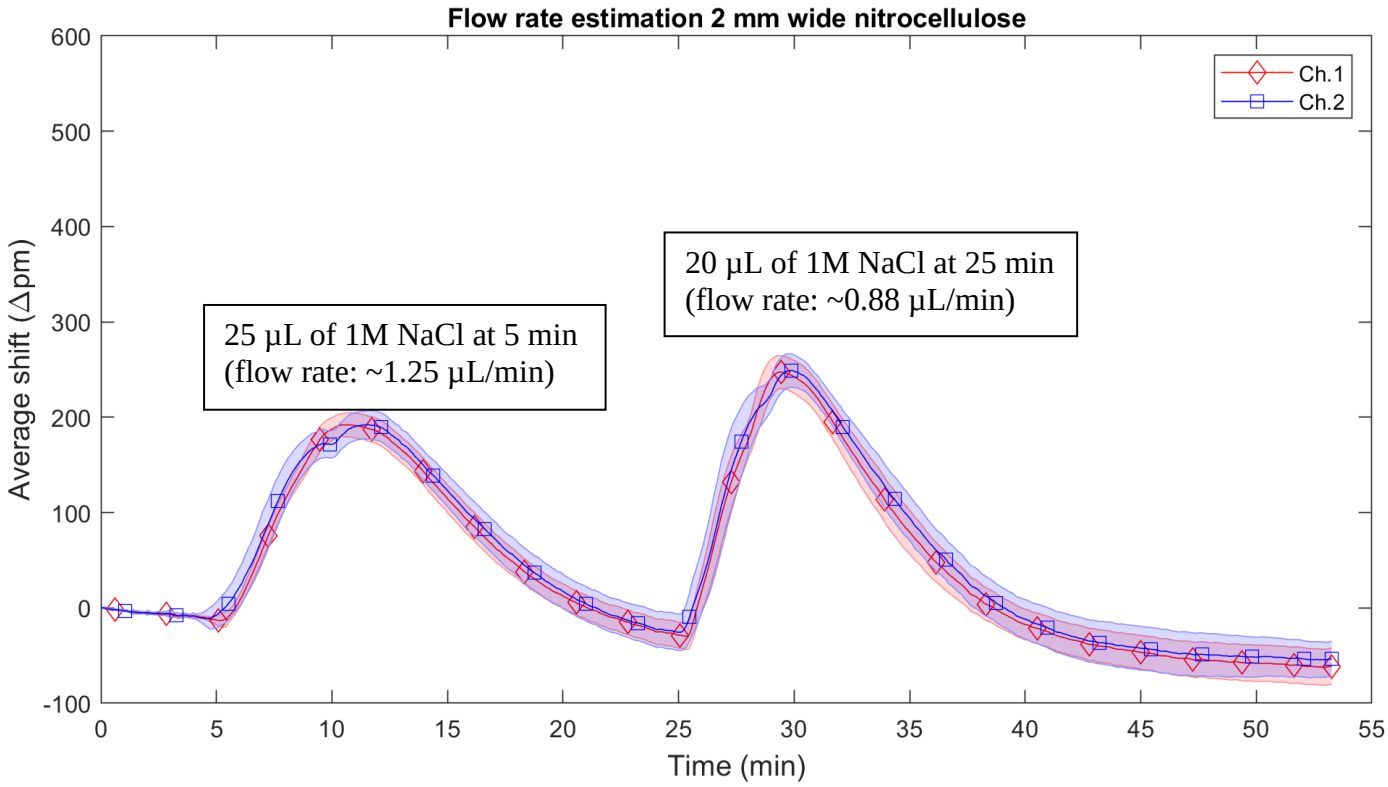
Flow rate estimation 2 mm wide nitrocellulose
Ch.1
Ch.2
25 µL of 1M NaCl at 5 min (flow rate: ~1.25 µL/min)
20 µL of 1M NaCl at 25 min (flow rate: ~0.88 µL/min)
Average shift (Δpm)
Time (min)

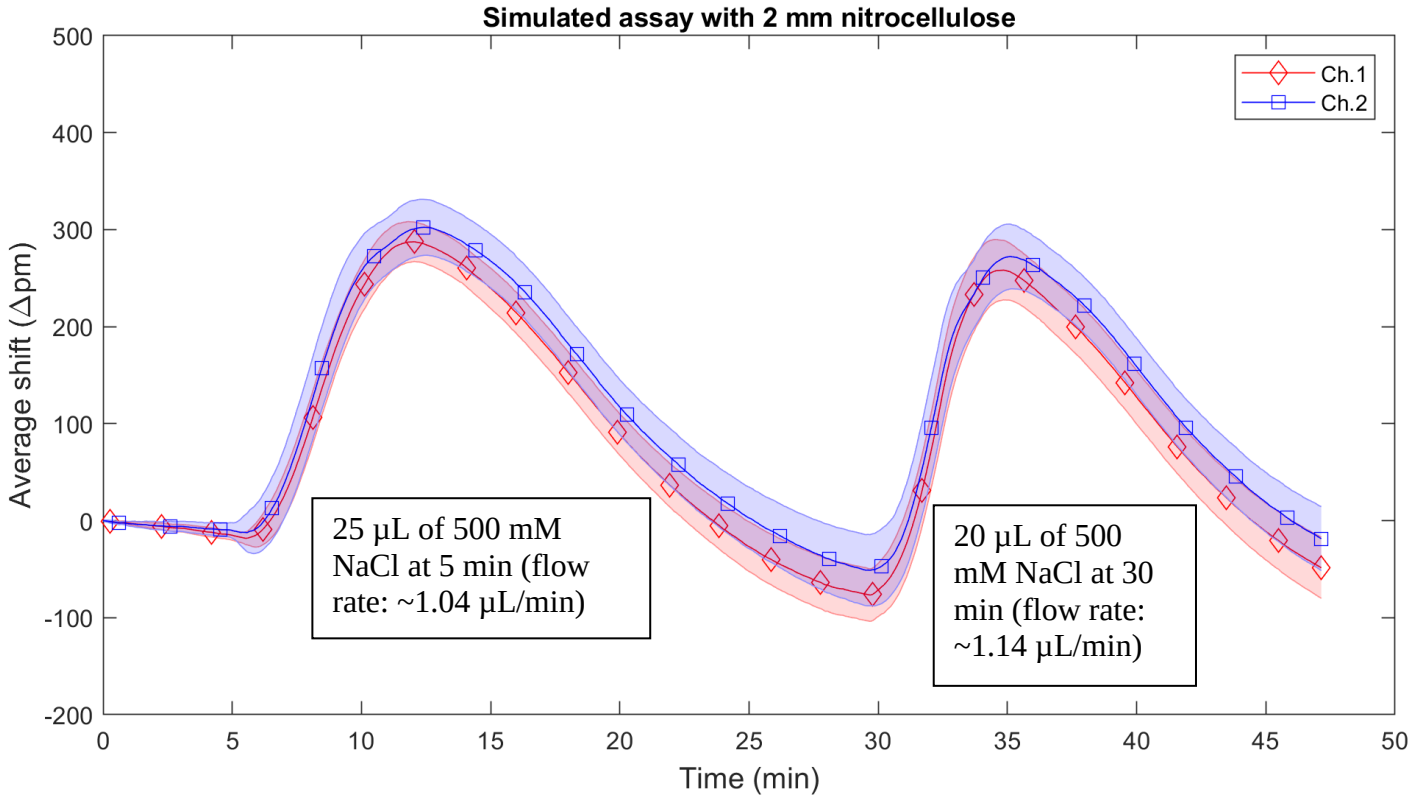
Simulated assay with 2 mm nitrocellulose
Ch.1
Ch.2
25 µL of 500 mM NaCl at 5 min (flow rate: ~1.04 µL/min)
20 µL of 500 mM NaCl at 30 min (flow rate: ~1.14 µL/min)
Average shift (Δpm)
Time (min)

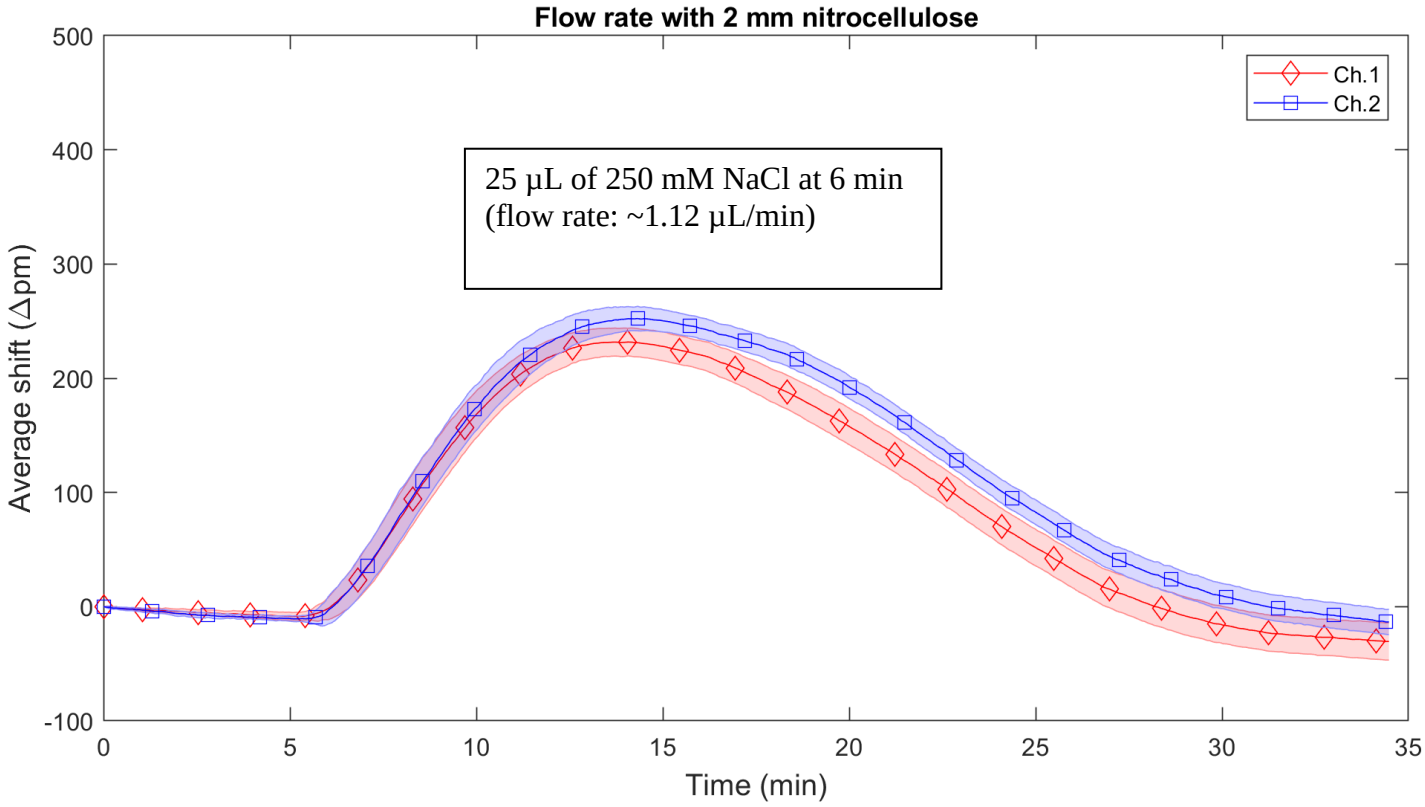
Flow rate with 2 mm nitrocellulose
25 µL of 250 mM NaCl at 6 min
(flow rate: ~1.12 µL/min)
Ch.1
Ch.2
Average shift (Δpm)
Time (min)
500
400
300
200
100
0
-100
0
5
10
15
20
25
30
35

ABO typing assays with plasma replicates (failed):

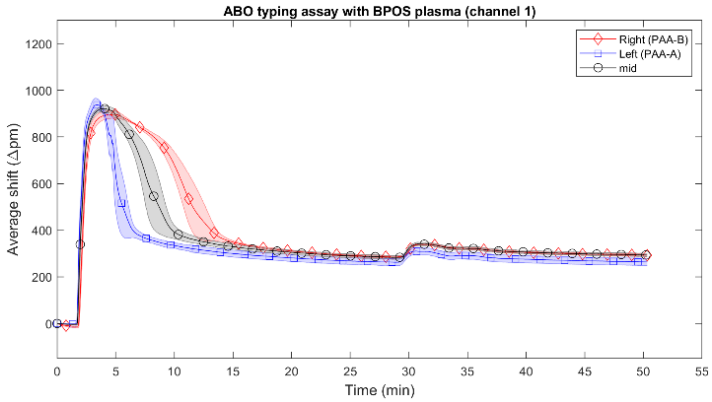

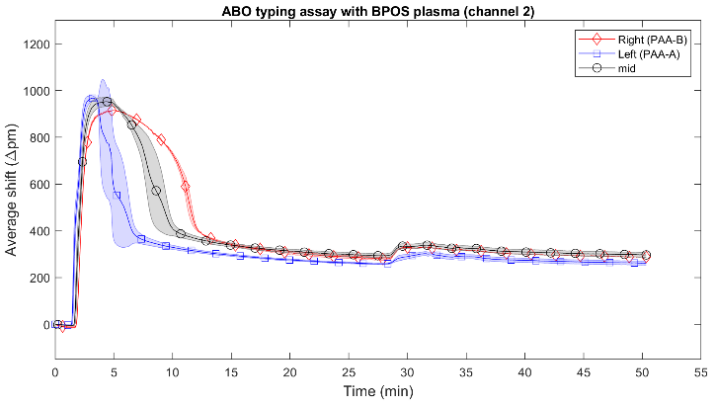

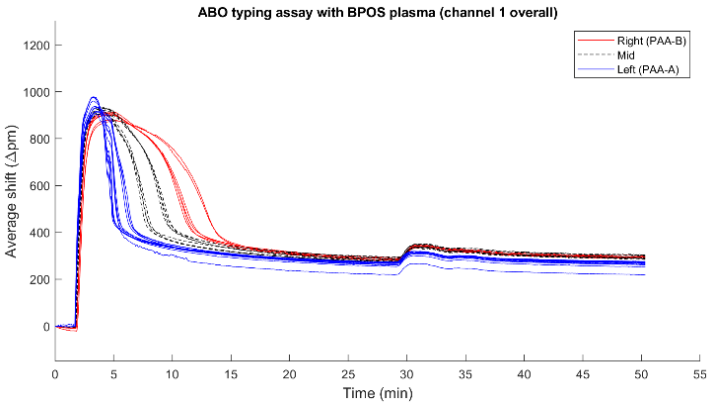

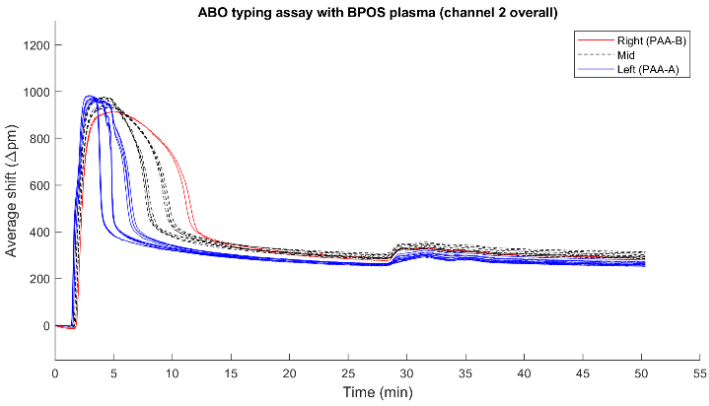

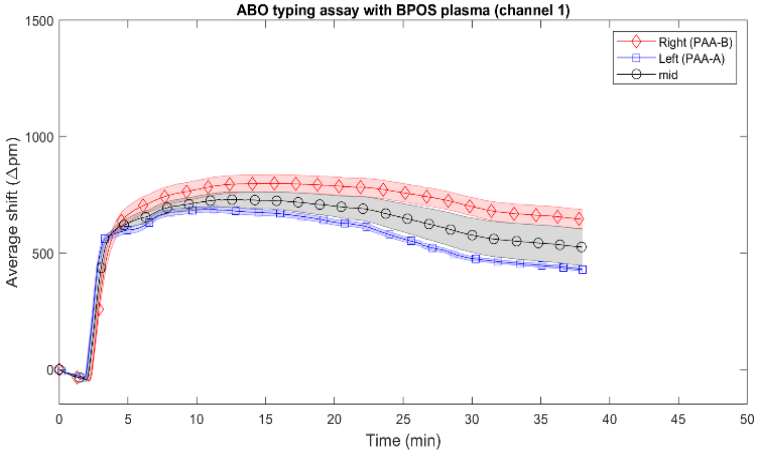
ABO typing assay with BPOS plasma (channel 1)
Right (PAA-B)
Left (PAA-A)
mid
Average shift (Δpm)
Time (min)

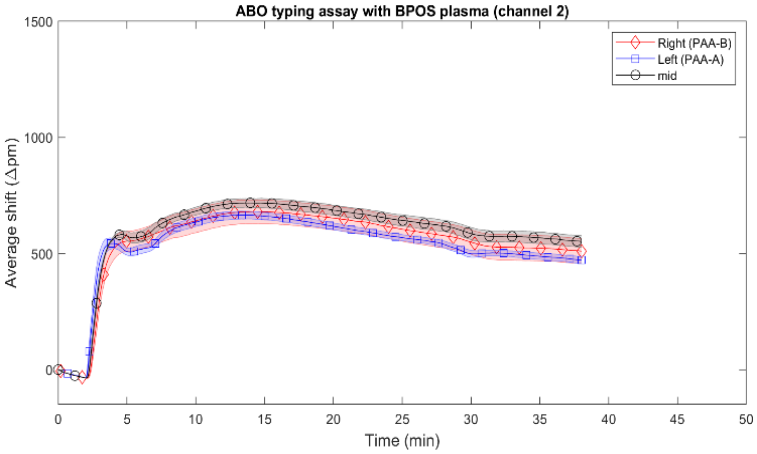
ABO typing assay with BPOS plasma (channel 2)
Right (PAA-B)
Left (PAA-A)
mid
Average shift (Δpm)
Time (min)

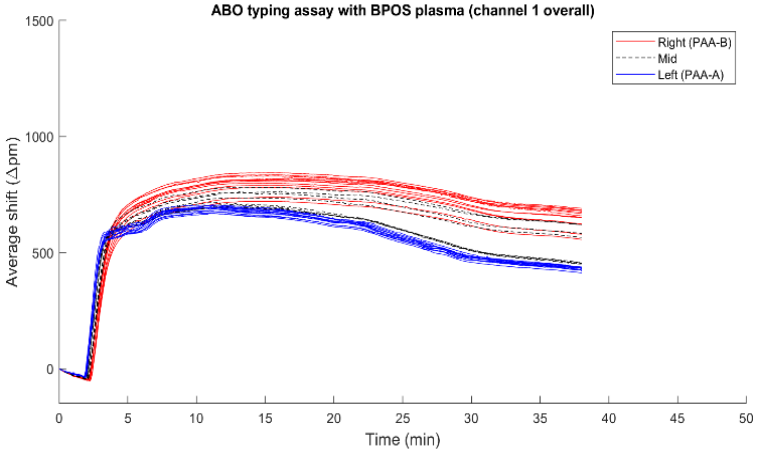
ABO typing assay with BPOS plasma (channel 1 overall)
Right (PAA-B)
Mid
Left (PAA-A)
Average shift (Δpm)
Time (min)

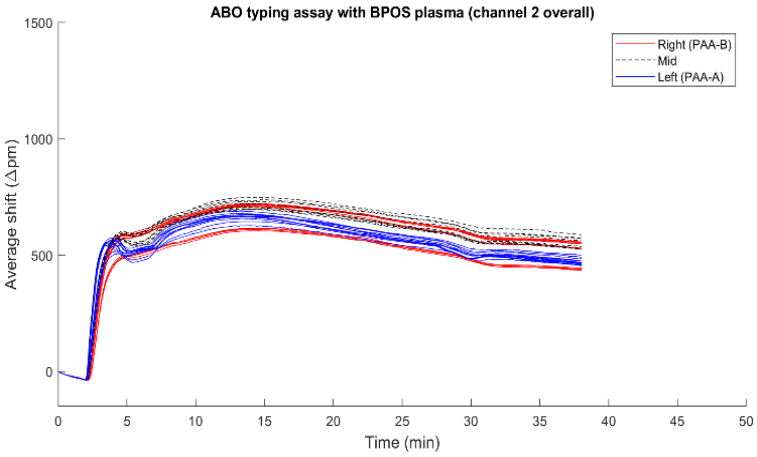
ABO typing assay with BPOS plasma (channel 2 overall)
Right (PAA-B)
Mid
Left (PAA-A)
Average shift (Δpm)
Time (min)

ABO typing assays with <50 µL of whole blood (failed):

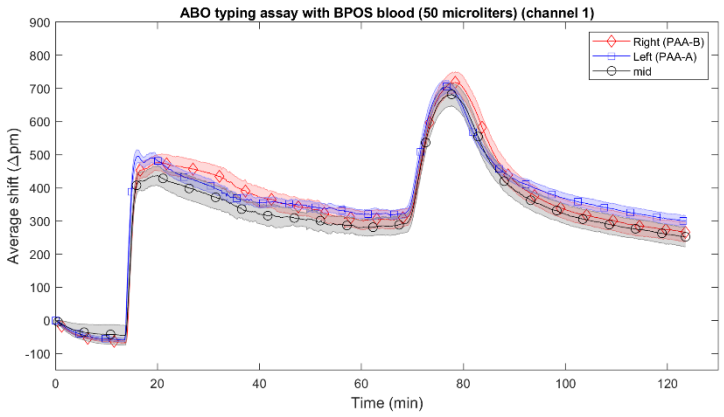

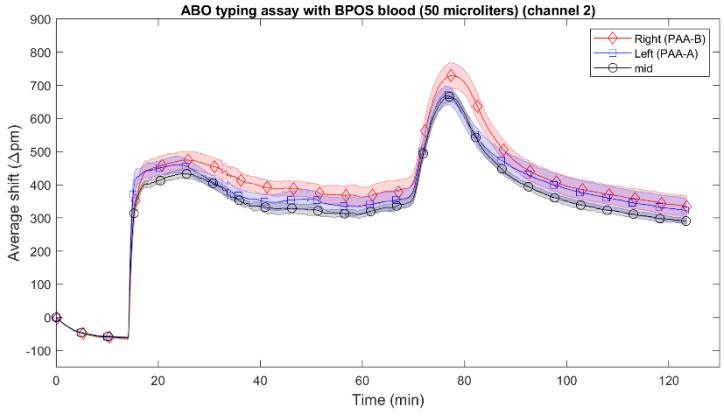

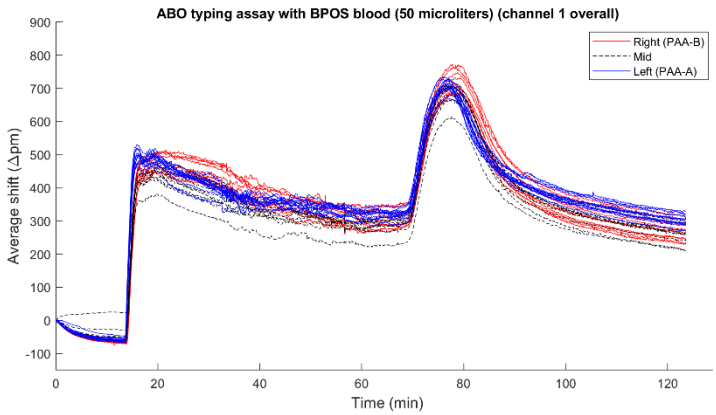

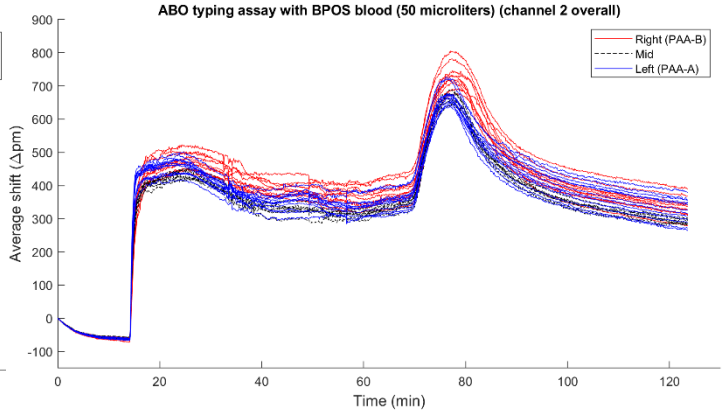

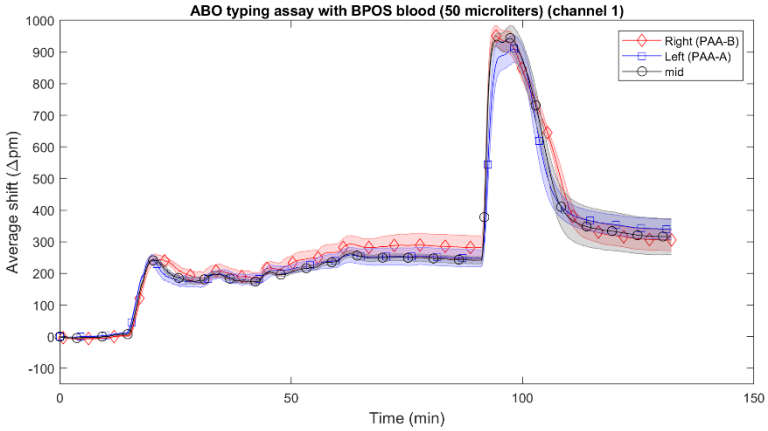
ABO typing assay with BPOS blood (50 microliters) (channel 1)
Right (PAA-B)
Left (PAA-A)
mid
Average shift (Δpm)
Time (min)

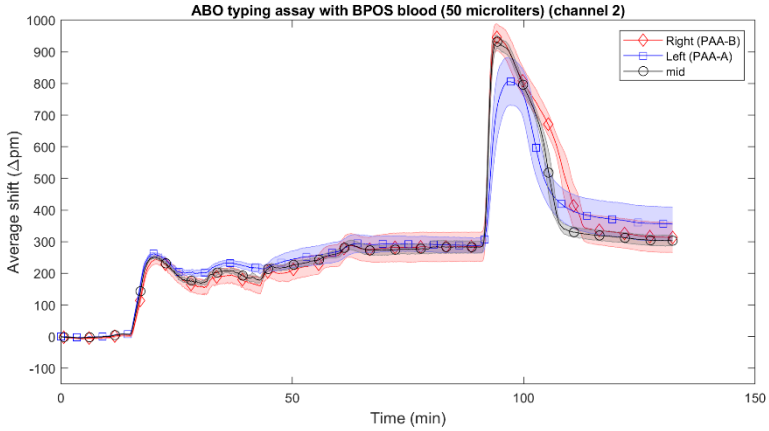
ABO typing assay with BPOS blood (50 microliters) (channel 2)
Right (PAA-B)
Left (PAA-A)
mid
Average shift (Δpm)
Time (min)

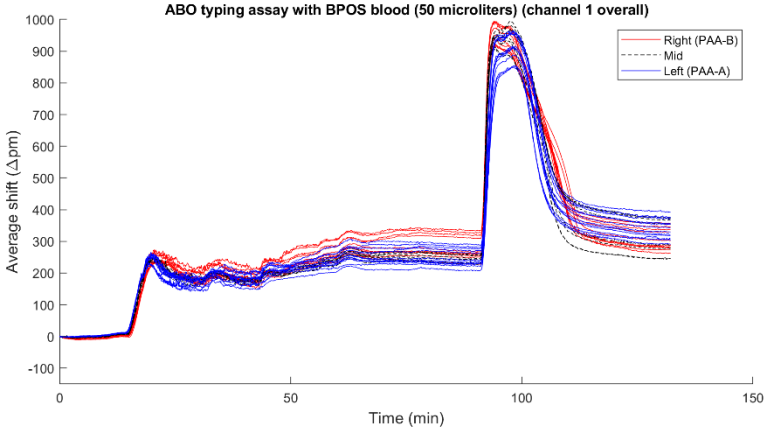
ABO typing assay with BPOS blood (50 microliters) (channel 1 overall)
Right (PAA-B)
Mid
Left (PAA-A)
Average shift (Δpm)
Time (min)

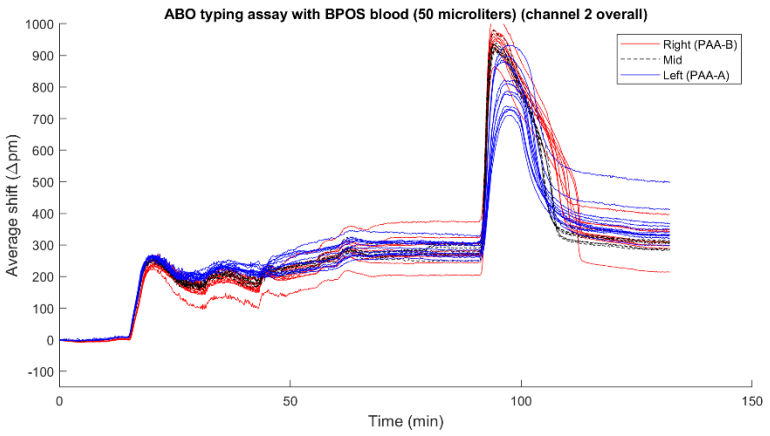
ABO typing assay with BPOS blood (50 microliters) (channel 2 overall)
Right (PAA-B)
Mid
Left (PAA-A)
Average shift (Δpm)
Time (min)

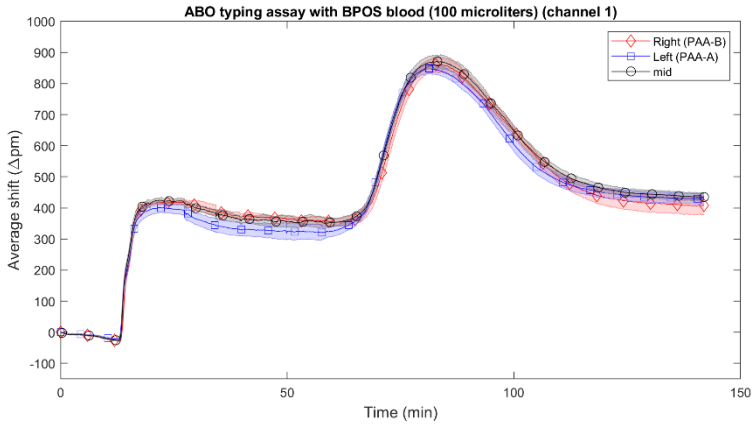
ABO typing assay with BPOS blood (100 microliters) (channel 1)
Right (PAA-B)
Left (PAA-A)
mid
Average shift (Δpm)
Time (min)

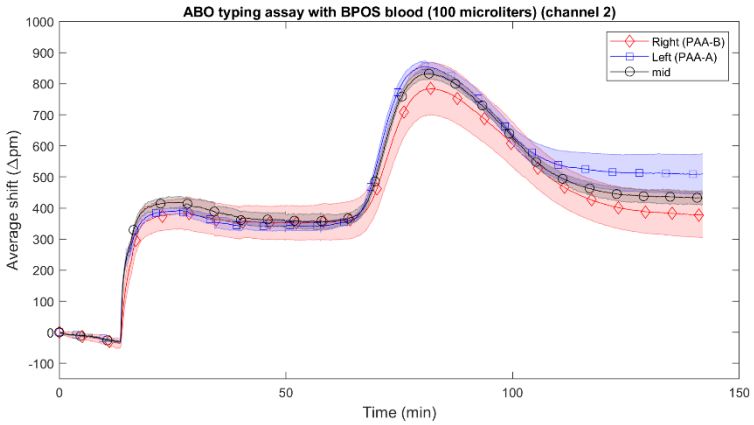
ABO typing assay with BPOS blood (100 microliters) (channel 2)
Right (PAA-B)
Left (PAA-A)
mid
Average shift (Δpm)
Time (min)

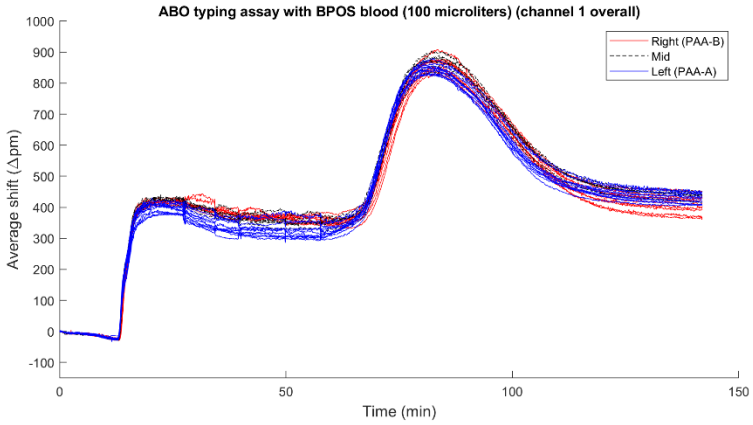
ABO typing assay with BPOS blood (100 microliters) (channel 1 overall)
Right (PAA-B)
Mid
Left (PAA-A)
Average shift (Δpm)
Time (min)

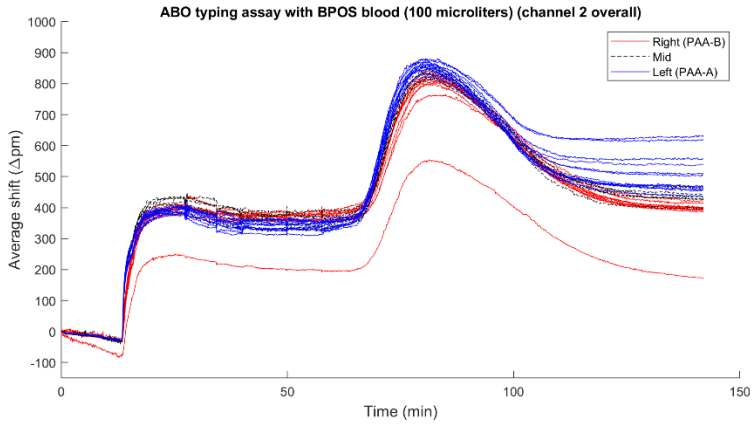
ABO typing assay with BPOS blood (100 microliters) (channel 2 overall)
Right (PAA-B)
Mid
Left (PAA-A)
Average shift (Δpm)
Time (min)

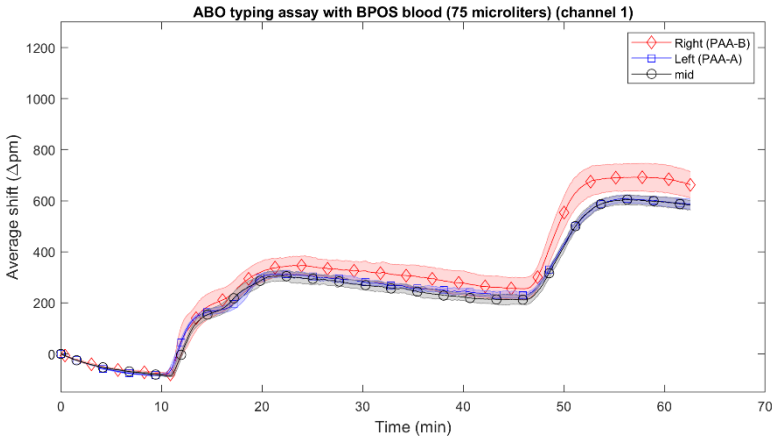
ABO typing assay with BPOS blood (75 microliters) (channel 1)
Right (PAA-B)
Left (PAA-A)
mid
Average shift (Δpm)
Time (min)

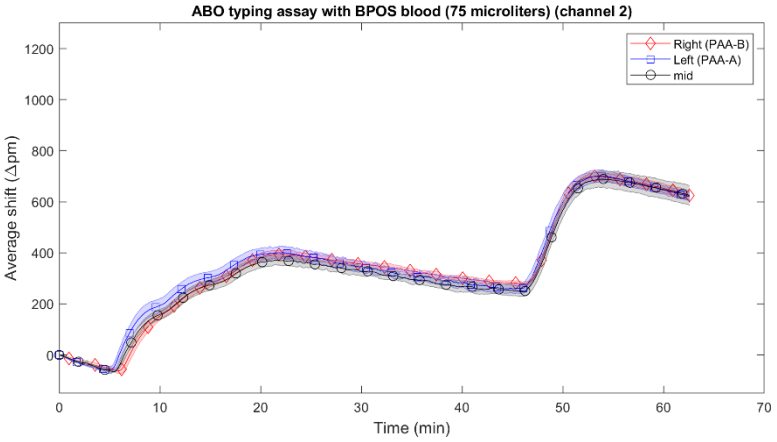
ABO typing assay with BPOS blood (75 microliters) (channel 2)
Right (PAA-B)
Left (PAA-A)
mid
Average shift (Δpm)
Time (min)

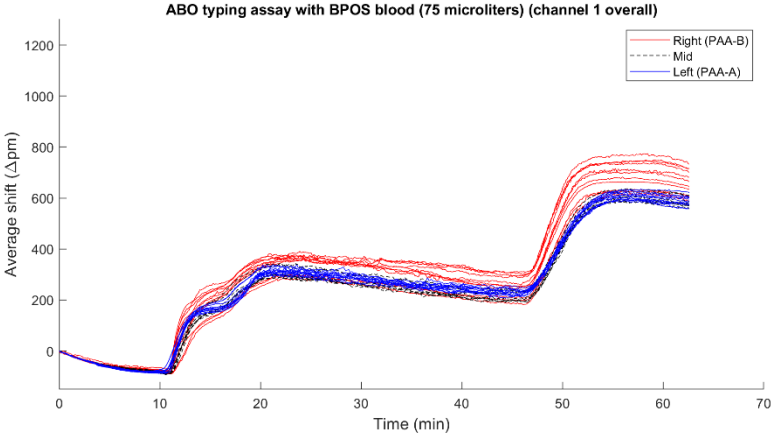
ABO typing assay with BPOS blood (75 microliters) (channel 1 overall)
Right (PAA-B)
Mid
Left (PAA-A)
Average shift (Δpm)
Time (min)

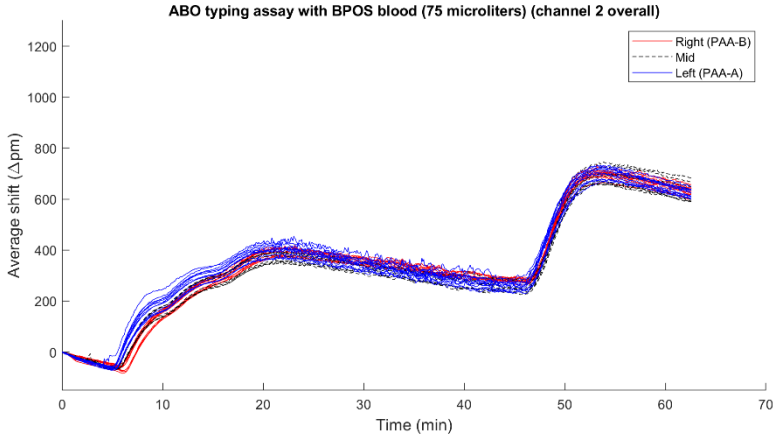
ABO typing assay with BPOS blood (75 microliters) (channel 2 overall)
Right (PAA-B)
Mid
Left (PAA-A)
Average shift (Δpm)
Time (min)